CLIMATE SYSTEM VARIABILITY BY THE PSEUDO-2D WAVELET TRANSFORMATION

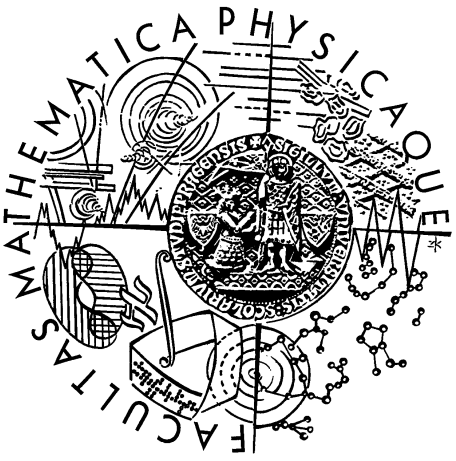

DOCTORAL THESIS

Petr Pišoft

Supervisor: doc. RNDr. Jaroslava Kalvová, CSc.
Department of Meteorology and Environment Protection
Faculty of Mathematics and Physics, Charles University in Prague

Prague 2006

Acknowledgements

My sincere thanks go to my supervisor, doc. RNDr. Jaroslava Kalvová, CSc., for her guidance, encouragement and patience during my doctoral study for the past three years, without which the completion of this work would not have been possible.

I would like to thank my close friends for their valuable comments and proof-reading of the draft of this paper. Particularly, my sincere gratitude goes to Matouš Borák, Václav Pišoft, Vera Schulmann and Jiří Sýkora.

My thanks also extend to those who helped me with the datasets processing. Special thanks go to Jiří Mrákota who helped me with the first attempt to implement the transform algorithm and to Miroslav Lenčéš who created the final efficient computation procedures.

I would also like to thank all my friends, who are too numerous to name, for their support and for all the good times in the years of my study.

And foremost, my sincere thanks go to my parents, Jitka and Václav Pišoft, who have been always supporting and encouraging me. Thank you for everything. To you I dedicate this work.

I hereby declare that this thesis is my own work and contains no material previously published or written by another person except where specifically indicated in the acknowledgements, text and bibliography. I agree with lending this paper.

Prague, 8th March 2006.

Petr Pišoft

Contents

Preface

The climate system is the environment that we live in. It is the factor that markedly influenced the evolution of human society. It is mainly because of the climate characteristics why Bordeaux is a synonym for a high quality wine or why hops from Žatec region are considered to be the best in the world. And our climate is changing. There have been observed a lot of changes in a longterm development of varied climatic quantities. Those changes are being linked to several general terms such as the greenhouse effect, global warming or the Kyoto Protocol. But what stands behind these expressions? And why is there so much excitement over the so-called greenhouse gases or some professedly melting icebergs?

Well, those are quite complicated and complex questions. Firstly, there is a group of atmospheric physics disciplines that study climate changes and related phenomena and secondly, our lives are broadly determined by those changes even if they are detected in various outlying areas. One of the first well known climate anomalies that widely influenced human development was possibly the great flood sent by God or the gods to destroy civilization as an act of divine nemesis. This may be found already in the stories of Noah and his ark in Genesis, Matsya in the Puranas scriptures of Hinduism, and Utnapishtim in the Epic of Gilgamesh. Present climate anomalies, such as droughts, floods, heat or cold waves, can cause enormous havocs and the economic and social impacts of them are colossal and far-reaching. The floods which stuck almost the whole of Europe in 2002, hurricanes which damaged the south of the United States or droughts over eastern Africa are quite good examples of possible impacts of climate variations. This does not mean that those catastrophes are clearly linked to climatic changes: they might represent the potential behaviour of the climate system which is more seesaw than it hitherto has been.

These possible impacts surely require some social responses or actions. The already mentioned Kyoto Protocol is possibly the best known example of such actions. However, there are many other projects that should either decrease anthropogenic forcing or help people get used to the changing

environment. Another consequence of the realization of the present climate system changes is the increased progress in atmospheric sciences research. That is also related to the first question, i.e. what is behind the Kyoto Protocol or what are the evidences for the global warming?

The first climatic studies are linked to simple weather observations that have been carried out since the outset of human history. Even now, the datasets acquired from the observations present the first (and often crucial) step in the analyses of the climate system. That is because it markedly helps us understand the system better and also because the cardinal element in climate changes research is climate modeling and it is necessary to compare the models results with the state of the real climate. But what could actually be obtained from analyzing the data what are the possible methods of data analysis?

A change, a variation or a transition – these are the characteristics typical for a time series which represents a climatic quantity evolution. The weather signals are just non-stationary in most cases and that requires utilization of an advance analysis algorithm. On the other hand, people always wanted to find a simple way to describe and also predict the climate system behaviour. These endeavors often resulted in almost an obsession with varied climate cycles. Yes, cycles or some periodicities would offer a clear answer as to what can be expected in the future and with them, it would surely be easier to explain various climate phenomena. However, with some exceptions, the studied processes are not periodic. It is possible to identify several quasi-periodicities and some regular cycles but even these are often instable in general.

There are several ways how the nonstationarity may be understood. Considering the purposes this paper, we will mainly operate with two conceptions of instability – frequency and spatial. The frequency nonstationarity represents a series where different frequencies occur within different time intervals. The spatial nonstationarity may represent even a frequency stationary phenomenon but with varying spatial center. This is directly linked to the choice of the analysis method, as well as to the possible type of acquired information.

The instability in frequencies of analyzed series implies utilization of a transformation which would provide the signal decomposition into the time-frequency space. Such an analysis can be made by the wavelet transform. It is a frequency analysis that has been used in meteorological studies only since the 1980s and that is, in one-dimensional form, suitable especially for the investigation of the time series that are not stationary in frequencies. The other issue is the movement in space. This usually means that the studied processes do not remain over one specific geographical

place and to describe them, it is necessary to expand the results dimension by one (or more) to catch even the evolution over the studied locations. That can be simply done by using contoured graphs or just by producing a figure for every typical time period.

Nonetheless, the real problem is to entirely analyze processes which are not stationary, both in frequencies and space. The solution is proposed by this paper that introduces and describes the pseudo-2D wavelet transform (p2D WT) – a completely new algorithm that is able to analyze a set of time series defined in a geographical grid. This analysis produces multidimensional results which describe the spatial, temporal and also frequency evolution of the studied datasets.

The main aim of this paper is to examine the capability of the pseudo-2D wavelet transform to globally analyze the climate variability. This is further divided into several minor objectives:

1. to introduce basic frequency analyses and problems connected with the time series investigation
2. to introduce the pseudo-2D wavelet transform, explain the main advantages of the procedure and show examples of its application
3. to examine NCEP/NCAR reanalysis datasets in order to gain a picture of the geographical distribution of global frequency patterns

Convention and Notation

All wavelet power spectra used and presented in this study are of the same composition in the sense that the x-axis describes time evolution and the y-axis represents periods.

- *Important conventions*

equation 3.9	refers to the ninth equation of the Chapter 3
figure 4.2	refers to the second figure of the Chapter 4
table 2.3	refers to the third table of the Chapter 2

results presented in the Appendix A are labeled as $A.x$, where x stands for the results order

- *Frequently used abbreviations*

FT	Fourier transformation
STFT	short time Fourier transformation
WT	wavelet transform
CWT	continuous wavelet transform
WPS	wavelet power spectrum
p2D WT	pseudo-2D wavelet transform
COI	cone of influence

- *Frequently used notation*

$x(t)$	time series
$X(f)$	Fourier transform of a time series x
$\psi(t)$	wavelet function
$\Psi(\omega)$	Fourier transform of a wavelet function ψ
Γ_p	set of period ranges

Chapter 1

Climate Variability and Analysis Techniques

The climate is always changing – there is no static state there. Nowadays, however, it seems that the system has been already influenced by the human activities in such a way that in the future we may be witnesses to severe climate anomalies. On the other hand, this cannot be stated before we understand the climate system well enough to be able to correctly model the possible changes. Present climatic models are already able to reproduce various system reactions with high accuracy but there are a lot of other phenomena that are simulated quite poorly. One of the reasons for this situation lies in the capabilities of current computers which are not yet able to, for example, effectively simulate the climate with high resolution. It is most likely just a matter of time to resolve that. The more serious problem, though, is the lack of our knowledge about the climate system in general. And right here a simple observation or an analysis of observations may bring new interesting information.

The following two sections introduce several striking expressions of the climate variability. The subsequent two sections are dedicated to the description of several analysis methods which are used for studying meteorological time series frequency characteristics.

1.1 Oscillatory patterns

Climate variability may also be understood in the sense of periodic motions which arise from an external forcing or which occur as a result of intrinsic dynamics. Present studies often divide such phenomena into a class of oscillatory patterns and into a class of cycles. That mostly de-

pends on the analysis methods which were used in particular studies. Frequency-oriented analyses and transformations generally identify cycles – processes that are defined in the sense of periods and frequencies. Examples of such cycles may be the quasi-biennial oscillation (QBO) or the semi-annual cycle (SAO).

The oscillatory patterns are mostly detected by a group of methods which search for patterns representing maximum amounts of, e.g., variation in the studied datasets. These are primarily represented by various types of the principal component analysis (PCA) or the canonical correlation analysis (CCA). The most distinct oscillatory patterns analyzed by those techniques are probably the El Niño/Southern Oscillation (ENSO) or the North Atlantic oscillation (NAO). A fundamental study of these oscillation pattern may be found in BARNSTON ET AL. (1987). The authors studied the 700 hPa geopotential heights field in 504 grid points at the Northern Hemisphere between 1950 and 1984. The results of the analysis of the fields were then divided into fourteen modes which represented fourteen statistically independent oscillatory systems (details in, e.g., METELKA (1997)).

Even though we are primarily interested in the variability in the sense of frequencies, it is still important to introduce the oscillatory patterns because the interpretation of the identified frequencies are often directly linked to the governing mechanism of the large oscillations like ENSO or NAO.

El Niño/Southern Oscillation (ENSO)

Possibly the best known oscillatory system is the El Niño/Southern Oscillation. Varied demonstrations of this oscillation have been observed already for hundreds of years. ENSO is an ocean-atmosphere interconnected oscillatory system which atmospheric part (Southern Oscillation) refers to an oscillation in the surface pressure between the Australian-Indonesian regions and the South-Eastern tropical Pacific. The oceanic part (El Niño) causes warming and cooling of the ocean surface and variations in the oceanic circulation in the central and Eastern Pacific. The oceanic part may be futher divided into the El Niño and La Niña episodes. These refer to the particular behaviour of the oscillations in the sea surface temperatures. El Niño in this sense stands for the warming of the ocean surface in the eastern Pacific and La Niña stands for the surface temperatures cooling. Normal (non-ENSO) conditions and El Niño situation in the Pacific Ocean and the atmosphere are also illustrated in figure 1.1.

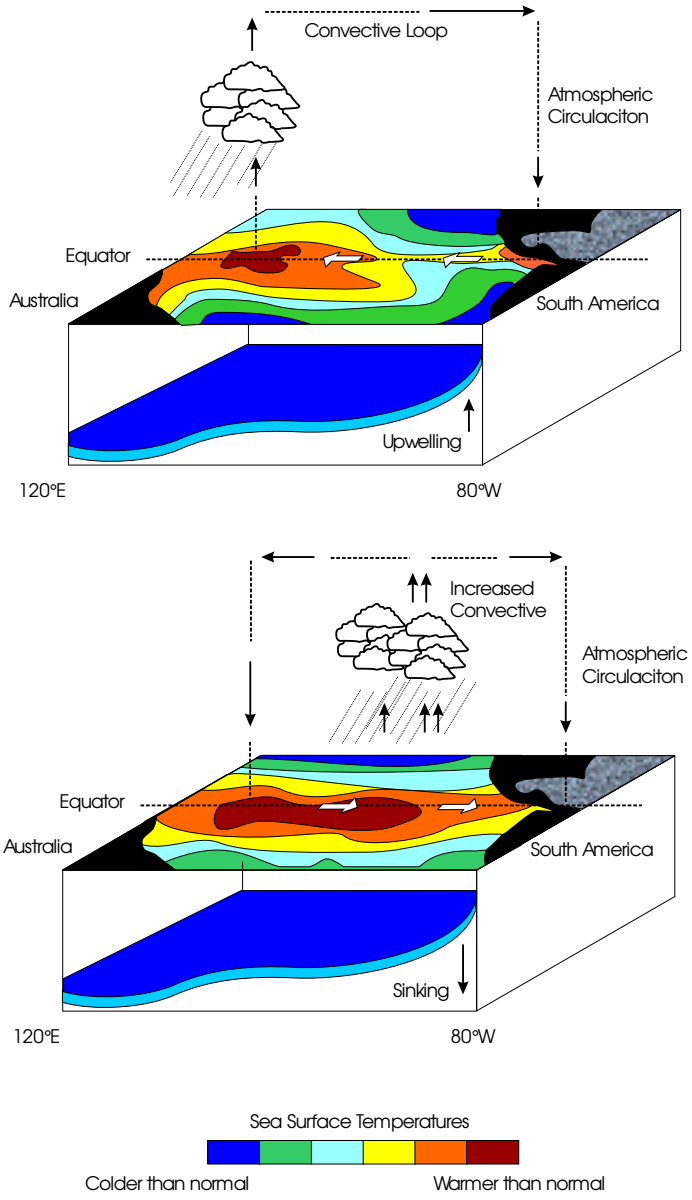

Figure 1.1: Normal (non-ENSO) conditions (top) and El Niño situation (bottom) in the Pacific Ocean and the atmosphere

North Atlantic Oscillation (NAO)

North Atlantic Oscillation (NAO) is one of the most pronounced oscillatory systems which is defined for all seasons with a maximum in the winter. The oscillation was identified by the PCA as a bipolar teleconnection

with one center of anomaly of the 700 hPa geopotential height field in the region of central latitudes of the North Atlantic between 35° and 40° north latitude, and with the second center (with a reverse sign) in the region of Iceland. Different phases result in divers conditions of zonal and meridional heat and moisture transport, and in different intensity and locations of the North Atlantic jet stream. This influences the weather conditions in the region reaching from the eastern parts of the USA to the western and partly central Europe.

1.2 Cycles and quasi-periodicities

The cycles and periodicities are in the atmospheric research mostly defined by the typical frequencies or periods of the studied phenomenon. In comparison with the oscillatory patterns, they are expressed as regular (regular in time) changes of certain climatic characteristics and they usually do not represent teleconnected systems.

The most well known climate cycle is surely the annual cycle. But there are a lot of other regular or quasi-regular periodicities which have been identified all around the world. Among these, the semi-annual, quasi-biennial, quasi-quadrennial and quasi-decal oscillations are probably the most distinct. Besides the quasi-biennial oscillation, they are introduced in the following paragraphs. The quasi-biennial oscillation is only briefly mentioned because it is expressed primarily within stratospheric levels while this paper analyzes and describes mid-tropospheric fields.

1.2.1 Annual cycle

Annual cycle is surely the climate feature that has been observed and studied for the longest time. As human societies evolved together with the development of agriculture, people started to investigate climate characteristics of the environment they lived in. And what is more noticeable than the annual variation of the surface temperature or precipitation?

The annual cycle is inseparably connected to our history and up to the present; there are numbers of studies of the climatic quantities variation during a year. In general, it is clear that no annual cycle of a climatic phenomenon can be described without an association with a specific geographical region and atmospheric level at which the cycle is to be studied. This is also presented in figure 1.2 that illustrates the annual cycles of temperature and geopotential heights at 500 hPa from three different geographical locations. It is clear that the annual cycles are completely

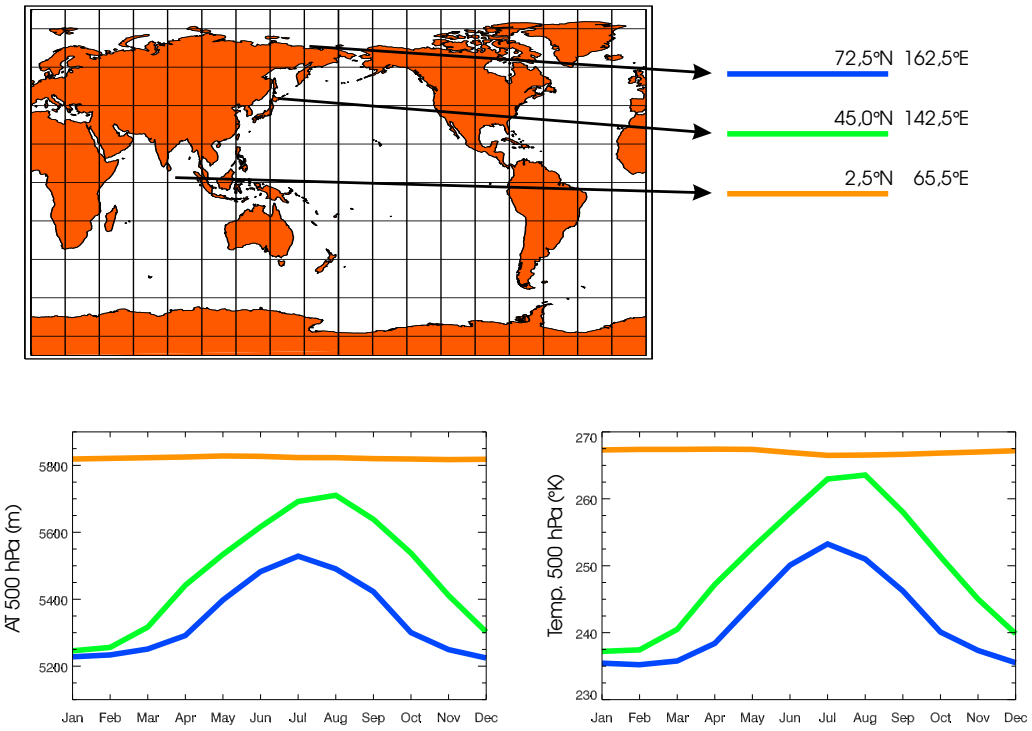

Figure 1.2: Averaged annual cycles in temperature and AT fields at 500 hPa for 1951–2000

different from each other and that is why they have to be interpreted in connection to their provenance. On the other hand, every annual periodicity may be linked to the periodic motion of the Earth around the Sun via variations in the incoming solar radiation. The problem is that the linkage is practically never so straight and it is necessary to analyze the annual cycle as a response to many interconnected climate subsystems.

The annual cycles of different quantities were also used as the determining characteristics that defined different climate zones. It is apparent that today possibly everybody has a quite a fair idea about the temperatures that can be expected during the summer or winter and about the fact that during some seasons precipitation is more frequent than during the others and so on; in other wors, the characteristic annual cycle became a *res publica*. Perhaps this is the reason why contemporary climate studies are targeted at the annual variations only in a small number of cases. Recent analyses mostly study the annual cycle in order to validate varied climate models but there are only a few studies of, e.g., the cycle frequency markedness.

HEDDINGHAUS ET AL. (1980) proposed an extensive study of different annual cycle patterns over the Northern Hemisphere. In comparison, the study differs from others mainly because of the fact that it analyzed the annual variations of several quantities at various levels, namely at 700, 500 and 300 hPa. The authors identified distinct frequency patterns with high amplitude centers over the eastern continents coasts. They concluded that the geographical structure of the annual variations of temperature as well as the 700–500 thickness fields were clearly affected by the land-sea contrasts. Quite similar patterns in the 300 hPa geopotential field were previously identified by WHITE ET AL. (1978) who suggested that at the 500 hPa level and above, the annual cycle in geopotential heights can be considered as the alternation between a distinctive wintertime pattern and a relatively flat summertime pattern. Similar results were proposed by CULLATHER ET AL. (2003). Their study is, however, focused only on the North Pole region. Here the authors stated that, in general, the concept of thermal forcing is consistent with the pressure variability over Eurasia, the lower latitudes of North America, and the Pacific and Atlantic Oceans. On the other hand, this conception is valid particularly within lower troposphere levels.

Present-day understanding of the frequency characteristics of the annual cycle can be generally summarized into several points:

- we have a good idea about the mean annual cycle properties of the majority of climatic quantities within lower atmospheric levels
- on the contrary, the annual cycle frequency patterns, in the sense of their geographical distributions together with their temporal evolutions, are mostly not so well known
- the governing processes are more explicitly linked to the thermal forcing within the lower atmospheric levels than within the upper levels
- our knowledge in general decreases with increasing altitudes; frequency patterns of the annual cycle within atmospheric upper levels are quite poorly mapped

1.2.2 The semi-annual oscillation (SAO)

The first description of the semi-annual cycle was most likely given by REUTER ET AL. (1936). The first detailed study, however, was proposed

by SCHWERDTFEGER ET AL. (1956). They showed that the semi-annual oscillation is of a significant importance to the formation of the mean annual pressure development. The authors concluded that the periodicity does not originate in the equatorial belt (connected with doubled maximum of the incoming radiation) but it should be related to higher levels in the middle and subpolar latitudes and to the different solar heating of different latitude belts.

The SAO was again more thoroughly discussed by VAN LOON (1967), who described the oscillation as a highly variable feature of the annual cycle of pressure and meridional temperature gradient that appears between mid and high latitudes of the Southern Hemisphere (SH) as two equinoctial maxima in the mid-tropospheric temperature.

Up to present day, the phenomenon has been analyzed in many papers in detail. In most cases, however, the studies are focused only on the SH regions and only a minority of the analyses describe the Northern Hemisphere (NH). On the other hand, this may be related to the fact that the SAO is highly pronounced rather over the southern polar regions and the underlying processes are different there from the governing mechanisms on the NH (WIKLE ET AL., 1996). The semi-annual cycle is then understood in two different ways: as the Southern Hemisphere and Northern Hemisphere oscillations.

The semi-annual oscillation on the Southern Hemisphere

As was mentioned already before, one of the first extensive analyses of the SAO was given by VAN LOON (1967) that proposed a study of temperatures at 500 hPa and also of the 700-300 hPa thickness. The paper suggested that the observed half-year cycle arises from the differences in the seasonal heating and cooling trends in the middle and high latitudes in combination with nearly equal annual ranges of temperature in the middle troposphere. The analysis also concluded that the variation in the meridional temperature gradient may be linked to the increased cyclonic activity in high latitudes during the equinoctial months. CHEN ET AL. (1992) and CHEN ET AL. (1996) also discussed the possibility that the semi-annual oscillation over the Southern Hemisphere is induced by the north-south shift of the local Hadley circulation. Further studies of this periodicity point to the considerable decadal variability (WALLAND ET AL., 1999) and a weakening of the semi-annual oscillation since the mid-1970s when the half-yearly pressure wave in the Southern Hemisphere became less significant (VAN DEN BROEKE, 1998B).

More specifically aimed papers of the SAO are focused on the Antarctica regions only. VAN DEN BROEKE (1998A) shows how the expanded pressure belt causes an amplification of the wave-3 structure of the circulation around Antarctica. That increases the transport of air from lower latitudes towards continental Antarctica and it directly links the SAO to the Antarctic surface temperatures (VAN DEN BROEKE, 1998A). There has also been observed a positive coupling between the amplitude of the SAO and wintertime Amundsen and Bellingshausen Seas ice extent (VAN DEN BROEKE, 2000A). Moreover the temperature trends over the Antarctica seem to be strongly associated with SAO weakening. (VAN DEN BROEKE, 2000B)

The semi-annual oscillation on the Northern Hemisphere

LANZANTE (1983) and LANZANTE (1985) proposed the first extended studies about the semi-annual cycle on the Northern Hemisphere. The studies divided the oscillation into two branches: the Asiatic region and the region stretching from northeastern Siberia to the gulf of Alaska. LANZANTE (1985) showed that the SAO is of considerable importance to the progression of heights over subtropical Asia which should be a reflection of the Asiatic monsoon. The paper also showed that the Asiatic region is out of phase with the northern regions.

The semi-annual oscillation over the Northern Hemisphere is extensivelly described and discussed by WIKLE ET AL. (1996). The study of the 500 hPa geopotential heights field over the Northern Hemisphere illustrated that the key difference with the Southern Hemisphere is that the Northern Hemisphere extratropics are dominated by the east-west land-sea contrast due to the large continental land masses in the NH, while the SH land-sea contrast reflects the north-south differential heating between Antarctica and the surrounding oceans. Futhermore, it concluded that the oscillation is generally governed by the spatio-temporal asymmetries in the seasonal variation of the Northern Hemisphere stationary eddies. The authors showed that since the land-sea differential heating contrast is less intense in the summer, the summertime eddy deviations are generally weaker than those in the winter time.

In general, the semi-annual cycle may be also classified into three general categories (CULLATHER ET AL., 2003):

1. tropical/subtropical – associated with variability in radiative forcing (SCHWERDTFEGER ET AL. (1956), VAN LOON (1967))

2. the southern high latitudes – associated with contrasts in the energy budgets of Antarctica and the Southern Ocean (VAN LOON (1967), VAN DEN BROEKE (1998A))

3. the northern high latitudes – associated with asymmetries in the seasonal variation of the Northern Hemisphere stationary edies (LANZANTE (1985), WIKLE ET AL. (1996))

1.2.3 The quasi-quadrennial oscillation (QQO)

Current studies of the El Niño/Southern Oscillation (ENSO) often deal with *quasi-quadrennial oscillation* – the QQO. It is an oscillation that has been identified in the temporal evolution of, e.g., sea surface temperatures or surface zonal winds over specific geographical areas like the equatorial regions. This quasi periodicity is regarded as the major ENSO oscillatory mode (RIBERA ET AL., 2002).

RASMUSSON ET AL. (1990) proposed one of the first studies that detected this cycle. The authors used the singular spectrum analysis (SSA) combined with conventional spectral techniques to identify a low-frequency mode in the wind and SST series. The results, however, were neither associated with ENSO nor identified as the QQO. The first extensive analysis that linked this oscillation with ENSO was given by JIANG ET AL. (1995) who proposed an analysis of the equatorial wind and sea surface temperature time series. The study identified separate frequency spectrum peaks in the equatorial wind and sea-surface temperature time series with the main peaks centered at about 52 months and 24-28 months. The first oscillatory pattern was refered to as the quasi-quadrennial oscillation (QQ mode). The second (less distinct) mode was identified as the quasi-biennial oscillation (QBO). However, it should be noted that the quasi-biennial oscillation detected in this analysis is different from the one of the best known oscillation in stratospheric studies – quasi-biennial zonal wind oscillation (for details see, e.g., REED ET AL. (1961), HOLTON ET AL. (1972), DUNKERTON ET AL. (1985), SCAIFE ET AL. (2000)).

Another study supporting such results was proposed by BRASSINGTON (1997). The authors comfirmed the existence of a remarkable quasi-quadrennial mode in the El Niño/Southern Oscillation. Moreover, they showed that the QQ mode demonstrates significant variability in frequency. MORON ET AL. (1998) specified the period of the main spectral peak to 43 months. The discrepancy between this and the period of the main peak reported by JIANG ET AL. (1995) was explained as a result of different time periods of the analyzed datasets. The analysis also showed

that the most distinct frequency shifted abruptly in the 1960s, from near-five years before to near-four years afterwards. ZHANG ET AL. (1998) illustrated that the QQO exhibits a propagation of the SST anomalies northeastward from the Philippine Sea and then eastward along 40°N, but over the tropical Pacific it behaves more like a standing wave.

YUAN (1999) stated that the QQ mode resulted from a slow baroclinic adaptation process between the atmosphere and the ocean in the Pacific basin. The study also concluded that the strength and length of period of this oscillation depend on its phase relation with the annual cycle of the eastern Pacific cold tongue.

Similarly to the above mentioned semi-annual oscillation analyses, QQO is connected to the South Pole regions climate as well. DRINKWATER ET AL. (2001) showed that fluctuations in the volume flux of sea ice correspond to the quasi-quadrennial oscillation. Moreover, the study indicated that series of quasi-quadrennial coupled oscillations, that are expressed in the form of positive and negative sea ice concentration and ice-drift anomalies, were induced by spatial variations in atmospheric sea--level pressure forcing in the Weddell Sea.

A complex analysis of NCEP/NCAR datasets variability was given by RIBERA ET AL. (2002). The analysis shows that the interannual tropospheric climate variability associated with the ENSO signal is identified in distinct quasi-biennial and quasi-quadrennial frequency ranges. These ranges changed their character over time, with the QQ peak drifting from about 3.5 to 4.5 year period over the 50-year interval. The authors further illustrated that the analysis of the evolving geopotential height anomaly pattern confirms an established close connection of the QQ frequency ranges with the Pacific North American (PNA) pattern. The study finally concluded that the only clear oscillatory interannual signal in tropospheric climate during the latter half of the 20th century is associated with the ENSO phenomenon, characterized by two distinct bands of variance – the quasi-quadrennial and the quasi-biennial oscillation.

RIBERA ET AL. (2003) presented a sequel of the previously quoted paper. They stated that the QQO in the Southern Hemisphere suggests mass transport between the Indian, Pacific and Atlantic basins. On the contrary, the evolution of the QQO in the Northern Hemisphere indicates a pattern of mass transport over the course of the cycle which is largely confined to the Pacific basin. Futhermore, the authors concluded that the associated patterns of heat and mass transport suggest a direct influence of ENSO on the equatorial Pacific and Indian oceans, and an extratropical influence on the South Atlantic ocean.

1.2.4 The quasi-decadal oscillation (QDO)

It is rather difficult to sum up the existing studies about quasi-decadal oscillations (QDO). The first problem is that there is no general agreement on the period bands within which the analyzed process should have occurred. This means that one has to set his or her own ranges. In this paper, the QD mode is delimited by range of the 8–12 years. The second problem is that the quasi-decadal oscillation studies are often connected to the 11 year solar sunspot cycle (even if it is not supported by the results) and therefore the governing processes are searched within external forcing, while internally driven dynamics is omitted. The issue is widely described and generally discussed in a contributive study proposed by GARRIC ET AL. (2003). The authors at first summarize studies that are devoted to the quasi-decadal periodicities in modern climate, to modern solar cycle driven periodicities, and to paleoclimate records of sunspot cycles. They claim that there are several intrinsic mechanisms that may be responsible for the QDO like:

- thermohaline circulation, which involves long timescales
- mechanism that relies on modulation of ENSO via the delays associated with midlatitude-tropical ocean advection timescales
- the wind-driven circulation and stochastic resonance

The main part of the study consists in experiments with a general circulation model (GCM), according to which they concluded that there is a clear evidence of the QDO in climate records (historical, as well as modern). As for the upper atmosphere levels, the oscillations are plainly driven by the sunspot cycle, but uncertainties remain in the lower (tropospheric, surface and subsurface) levels. Hence, until the modeling studies of the quasi-decadal variability are exhaustive enough, performed for most of the time periods of the Earth's history, or until the robustness of these modes is theoretically disproved, there is no basis for ascribing the variability in the QD range only to external forcing factors.

Recent studies of the QDO that do not deal with the sunspot cycle are mainly divided into analyses of regions over the Pacific Ocean and the analyses over the Atlantic Ocean. The afore-mentioned analysis given by BRASSINGTON (1997) describes, besides the QQO, the quasi-decadal periods as well. The paper shows that the quasi-decadal period modes are identified in the most recent record of both, the South Oscillation index and the El Niño region sea surface temperature time series, and also over

the North Pacific regions. These observations are linked to the deepening of the Aleutian low in the North Pacific. The authors suggest that the quasi-decadal influence is connected more directly to the western and central equatorial Pacific and the east Pacific is not the source of this mode.

The analysis of the QDO over the Atlantic was given by MIZOGUCHI ET AL. (1999) who proposed that the detected quasi-decadal oscillation mode in the North Atlantic may be explained in terms of the atmosphere--ocean interaction and the advection of temperature anomalies by mean currents. DIMA ET AL. (2001A) identified quasi-decadal patterns in the SST and SLP fields over the Atlantic basin. The authors also discussed a possible decadal cycle mechanism by perturbations in the sea surface temperature fields associated with changes in the intensity of the convection in the Intertropical Convergence Zone (ITCZ) and in the Walker and Hadley circulations. DIMA ET AL. (2001B) combined the quasi-decadal variability patterns with the interannual variability over the Tropical Pacific that resulted in definition of the quasi-bidecadal (QBD) mode of variability. DIMA ET AL. (2002) showed that the Atlantic interannual SST variability is dominated by a quasi-decadal mode that is characterized by latitudinal bands of alternating polarities that extend from the tropics to the North Atlantic. The associated atmospheric pattern is similar to the North Atlantic Oscillation (NAO). Finally, TERRAY ET AL. (2002) stated that at near-decadal timescales, there is a strong evidence of a slow propagation of the SST anomalies along the North Atlantic Current (NAC) at the boundary of the subtropical and subpolar gyres.

1.3 Time series analysis techniques

Every temporal evolution of any meteorological variable may be recorded as a time series. However, it is almost impossible to obtain any particularised information without any transformation of this primordial raw form of the datasets. The choice of the analysis technique always depends on the purposes of the studies. The aim of this paper is to analyze worldwide datasets in the sense of oscillations and periodicities. Hence this section focuses on several frequency analyses.

1.3.1 Fourier transformation

The most quoted, well-known and often used frequency analysis method is the Fourier transformation (FT). It was developed in 1822 by the French

mathematician Jean Baptiste Joseph Fourier. He discovered that any periodic function can be expressed as an infinite sum of periodic complex exponential functions. Afterwards, the original algorithm was generalized also for non-periodic functions and then for periodic and non-periodic discrete time signals (POLIKAR, 1994). The Fourier transformation $X(f)$ of a time series $x(t)$ is defined as follows:

$$x(t) = \int_{-\infty}^{\infty} X(f)\, e^{2\pi i f t}\, df \tag{1.1}$$

$$X(f) = \int_{-\infty}^{\infty} x(t)\, e^{-2\pi i f t}\, dt \tag{1.2}$$

This transformation is discussed in details in, e.g., VON STORCH ET AL. (1999) or BUTTKUS (2000). To understand why the transform is not suitable for every type of time series, it is important to take into account the way it transforms the original signal. It is apparent that FT decomposes the signal $x(t)$ into complex exponential functions of different frequencies f. Thereafter the result is integrated across all times so that the final product does not contain any information about the time domain. Figure 1.3 shows an example of a stationary and non-stationary signal that should represent, say, some temperature series for the time period of 1951–2000. These signals are composed of five different frequencies that are enumerated with the corresponding periods in table 1.1. In the first series (stationary) every frequency may be detected in every time, in the second series (non-stationary) individual frequencies occur only in some parts of the signal. Fourier transformations of these signals are presented in figure 1.4. The particular graphs in figure 1.4 are nearly the same. This fact illustrates the inability of the Fourier transform to produce any information about the time domain; therefore it is impossible to distinguish between stationary and a non-stationary signals which are composed of the same periodicities.

1.3.2 Short time Fourier transformation

There are several ways of modifying the Fourier transformation so that it is more suitable for studying non-stationary processes. The basic idea is to split the original signal into shorter parts which are studied separately. The width of those particular series must then be equal to the segment of the signal where its stationarity is valid. To divide the signal, a window

Frequency	**Period**
2	0.5
1	1
0.5	2
0.2	5
$0.\overline{09}$	11

Table 1.1: The frequencies and the periods encountered in tested signals

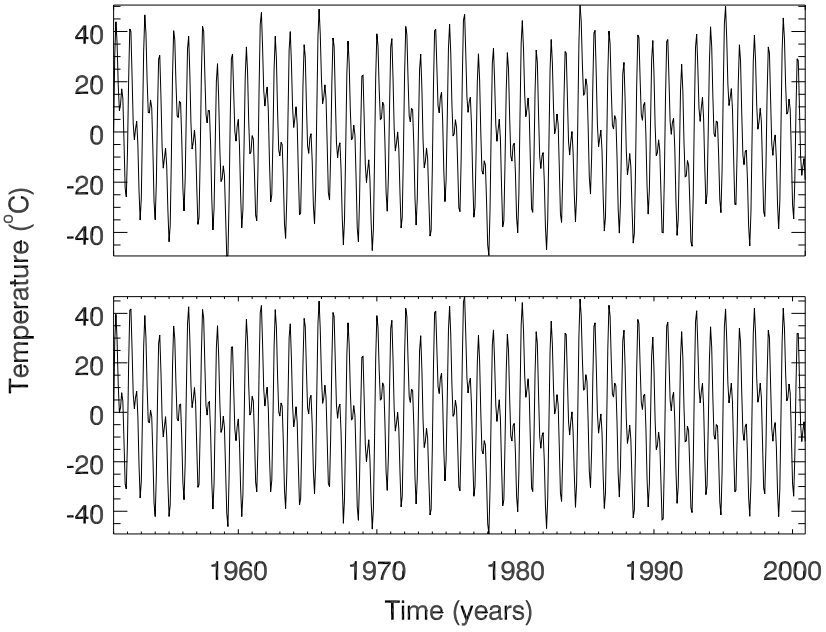

Figure 1.3: The values of the stationary (top) and the non-stationary (bottom) signal plotted against time

function is often used. An example of such an approach is represented by the short time Fourier transformation which is defined as follows:

$$STFT_X^{(\omega)}(t', f) = \int_t [x(t)\ \omega^*(t - t')]\ e^{-2\pi i f t}\, dt, \tag{1.3}$$

where the window function ω is chosen to split the series. This analysis may be also called the windowed Fourier transformation or (with some

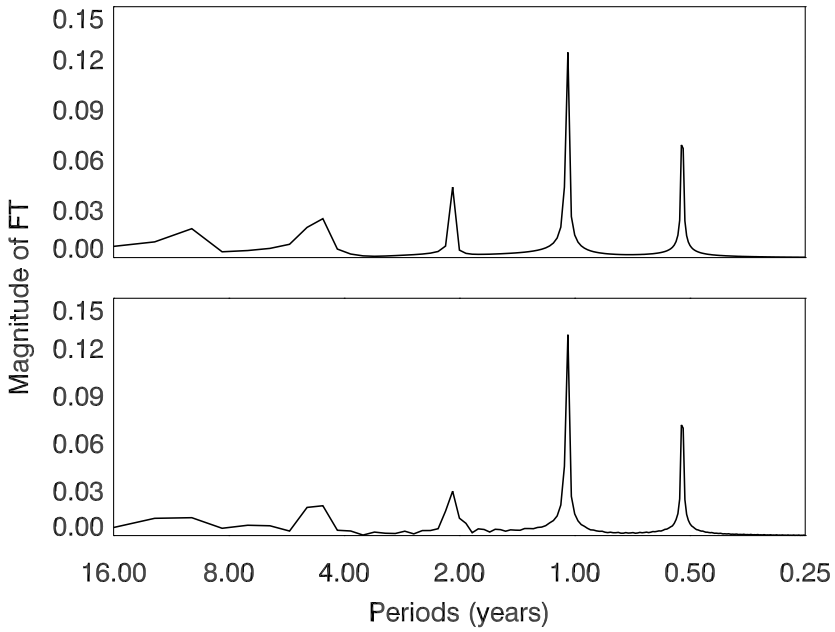

Figure 1.4: The magnitudes of the Fourier transformations of the stationary (top) and non-stationary (bottom) signal displayed in figure 1.3 plotted against the frequency

modifications) the Gabor transformation. Problems connected with this subject are discussed in detail in POLIKAR (1994) or in PIŠOFT (2002)

Nevertheless, the STFT is constrained by the resolution concerns imposed by the Heisenberg Uncertainty Principle. There is a trade-off between the temporal resolution and the spectral resolution. It is possible to gain a better time resolution by making the window function narrower but that implies worse frequency resolution and vice versa (KIJEWSKI ET AL., 2003). The problems arise from the fact that the STFT has the same resolution at all frequencies.

This means that the optimal time–frequency analysis would be an analysis with a resolution varying with frequency, effectively optimizing the Heisenberg Uncertainty Principle at all frequencies. Such an analysis is represented by the 1D continuous wavelet transform (CWT) which is described in the next section.

1.4 1D continuous wavelet transform

The problems with the analysis of non-stationary series were discussed in the previous sections. We have indicated that an ordinary transform (like the Fourier transformation) cannot distinguish between stationary and non-stationary signals in case that they are composed of the same frequencies. To study these types of series, it is possible to use the short time Fourier transformation. It is, however, only a partial solution because one encounters momentous problems with the results resolution in time or frequencies. On the other hand, we may apply the 1D continuous wavelet transform (CWT).

Wavelet transform is relatively new method of studying non-stationary signals.. The analysis combines older ideas with new mathematical results and efficient computational algorithms (PERCIVAL ET AL., 2000). It is a strong mathematical tool to transform a signal in the time domain to the time and frequency domain. Unlike STFT, the wavelet transform separates the analyzed series into different frequency components and then studies each component with a resolution matched to its scale (PIŠOFT, 2002).

1.4.1 A wavelet

The basis of the CWT is a wavelet – a function waving above and below the x-axis. It is a function similar to the STFT window function that is used to split the studied signal but now the window width is changed. A wavelet function $\psi(t)$ has to satisfy several basic conditions, such that the integral of the wavelet has to be zero and the square of the wavelet integrates to unity. The next condition, called *admissibility condition*, requires the square modulus of the wavelet's continuous Fourier transform $\Psi(\omega)$ to decay faster than $\frac{1}{\omega}$ as $x \longrightarrow \pm\infty$ and it allows the reconstruction of a signal $x(t)$ from its continuous wavelet transform (PERCIVAL ET AL., 2000). The particular conditions are defined as follows:

$$\psi \in L^1(R) \cap L^2(R) \tag{1.4}$$

$$\int_{-\infty}^{\infty} \psi(t)\, dt = 0 \tag{1.5}$$

$$\int_{-\infty}^{\infty} \psi^2(t)\, dt = 1 \tag{1.6}$$

$$0 < \int_{-\infty}^{\infty} \frac{\mid \Psi(\omega) \mid^2}{\omega} d\omega < \infty, \tag{1.7}$$

where

$$\Psi(\omega) = \int_{-\infty}^{\infty} \psi(t) e^{-2\pi i f t} \, dt \tag{1.8}$$

The conditions are also discussed in, e.g., PERCIVAL (2002).

All the wavelets depend on mother wavelets – the prototypes that generate the other window functions (the daughter wavelets). Family of the generated wavelets is formed by the scale (contraction and dilation) λ and the translation τ. An individual wavelet $\psi(t)$ can be defined by:

$$\psi^{\tau,\lambda}(t) = \frac{1}{\sqrt{\mid \lambda \mid}} \psi \left(\frac{t-\tau}{\lambda} \right) \tag{1.9}$$

Figure 1.5 shows the often used mother wavelets and table 1.2 presents their definitions. Meanings of the symbols used in table 1.2 are as follows: ω_0 stands for frequency, C is a constant (Morlet), m stands for order (Paul) or derivate (DOG) and $H(\omega)$ is the Heaviside step function (TORRENCE ET AL., 1998).

DOG	$\frac{(-1)^{m+1}}{\sqrt{\Gamma\left(m+\frac{1}{2}\right)}} \frac{d^m}{dt^m} e^{-\frac{t^2}{2}}$
Paul	$\frac{2^m i^m m!}{\sqrt{\pi(2m)!}} (1-it)^{-(m+1)}$
Morlet	$Ce^{-i\omega_0 t} \left(e^{-\frac{t^2}{2}} - \sqrt{2} e^{-\frac{\omega_0^2}{4}} e^{-t^2} \right)$

Table 1.2: The three often used wavelet basic functions (TORRENCE ET AL., 1998)

1.4.2 Continuous wavelet transform

The continuous wavelet transform of a time series $x(t)$ is defined as a convolution of the series and the wavelet:

$$W_x^{\psi}(\tau, \lambda) = \frac{1}{\sqrt{\mid \lambda \mid}} \int_{-\infty}^{\infty} x(t) \psi^* \left(\frac{t-\tau}{\lambda} \right) \, dt, \tag{1.10}$$

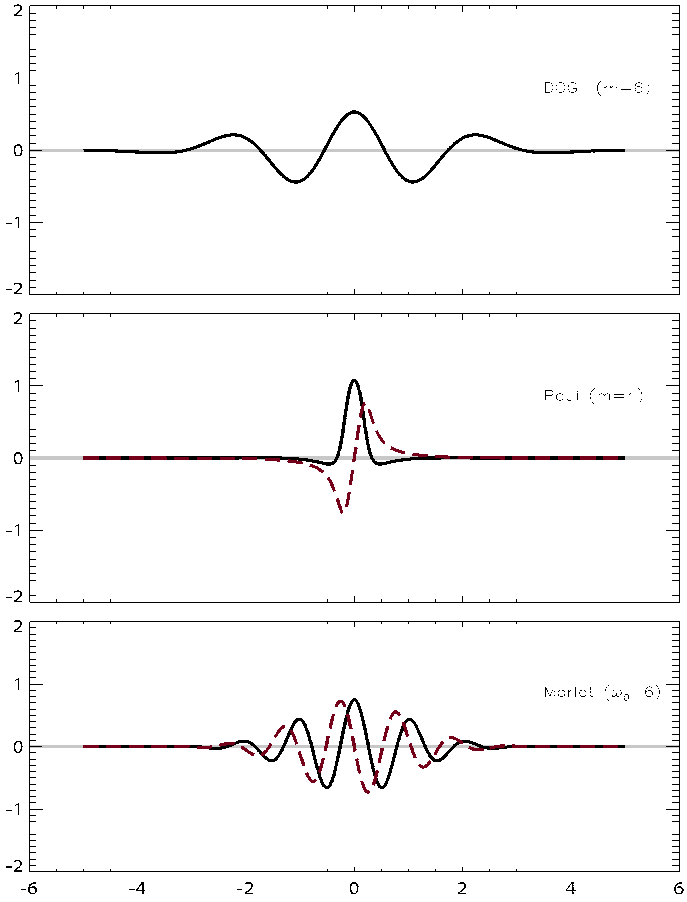

Figure 1.5: Values of the real (solid) and imaginary (dashed) parts of the mother wavelets in the time domain, meanings of particular symbols are explained in related text

where λ is the scale that plays the role of the frequency parameter and τ is the translation – an indicator of the region over which $\psi^{\tau,\lambda}(t)$ is spatially localized.

There are several ways how to handle the CWT outcomes. We may use use real $\Re\{W_x^\psi(\tau,\lambda)\}$ or imaginary $\Im\{W_x^\psi(\tau,\lambda)\}$ (in case of a complex wavelet function) parts of the wavelet transform and also phase $tan^{-1}[\Im\{W_x^\psi(\tau,\lambda)\}/\Re\{W_x^\psi(\tau,\lambda)\}]$ or amplitude $\mid W_x^\psi(\tau,\lambda) \mid$ (Torrence et al., 1998). However the most used and quoted form is the wavelet power spectrum (WPS) defined as $\mid W_x^\psi(\tau,\lambda) \mid^2$ and the global wavelet spectrum (GWS) defined as an integration of the wavelet power across

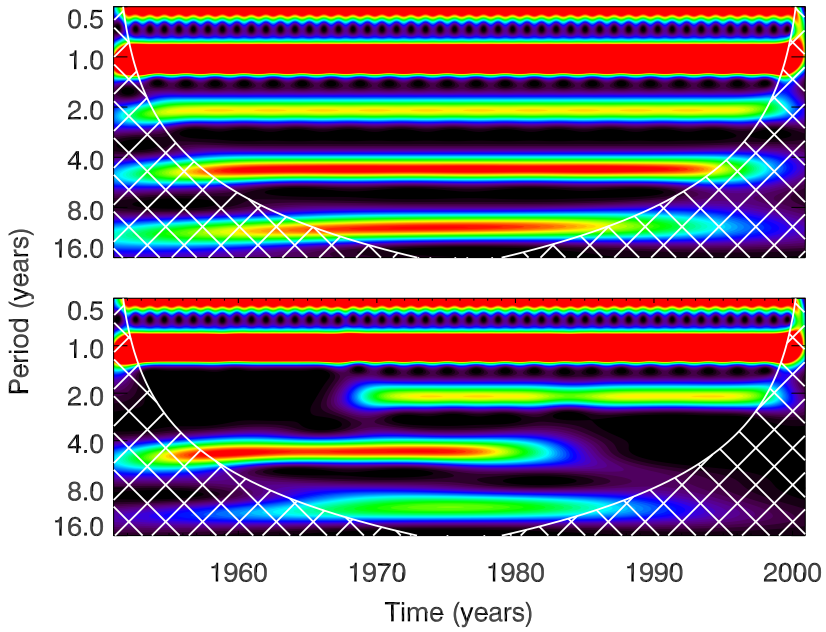

Figure 1.6: The wavelet power spectrum of the stationary (top) and non-stationary (bottom) signal – see figure 1.3

all times. Understanding the wavelet power spectrum is the key to the pseudo-2D wavelet transform and it is discussed in detail at the beginning of the next chapter.

Examples

Figure 1.6 presents the continuous wavelet transforms of the same signals that were used for the FT capabilities illustration (see figures 1.3 and 1.4). Morlet wavelet with ω_0 equal to 6 was chosen as the mother wavelet. It is obvious that now we are able to detect the frequencies (or periods) and also to identify the time period of their occurrence. The gridded region of the plots represents the *cone of influence* (COI). It is a region of the wavelet spectrum, where the edge effects (resulting from the series finite length) become important. Results inside these regions should not be taken into account.

Reconstruction

The continuous wavelet transform is a reversible transform that preserves all the information in $x(t)$. If the signal, in addition to the admissibility condition for the mother wavelet, satisfies

$$\int_{-\infty}^{\infty} x^2(t)\,dt < \infty, \tag{1.11}$$

we can recover the signal from its CWT via (PERCIVAL ET AL., 2000):

$$x(t) = W_x^{'\psi}(\tau,\lambda) = \frac{1}{C_\psi}\int_0^\infty \left[\int_{-\infty}^{\infty} W(\lambda,\tau)\frac{1}{\sqrt{\lambda}}\psi\left(\frac{t-\tau}{\lambda}\right)\,d\tau\right]\frac{d\lambda}{\lambda^2} \tag{1.12}$$

where

$$C_\psi = \int_0^\infty \frac{\mid \Psi(\omega) \mid^2}{\omega}\,d\omega \tag{1.13}$$

On the other hand, this can be also used to reconstruct only a part of the original signal – a part that is composed of only specific frequencies. Consequently, we are able to reduce the series noise and thus detect occurring trends (PIŠOFT, 2002).

Chapter 2

Pseudo-2D Wavelet Transform Fundamentals

2.1 Wavelet power spectrum

The previous section introduced the ground of the one-dimensional continuous wavelet transform. It is a time-frequency analysis that is able to expose hidden periodicities and also to identify the time period of their occurrence. However, the achieved results may describe the properties of only one time series. It means that in most cases we are able to characterize only one geographical point. Nevertheless, for large regions it is necessary to choose a method that purveys information describing the whole region.

One of the possible ways to handle this problem is to analyze datasets defined in a geographical grid by repeating the one-dimensional continuous wavelet transform of particular time series. That is also the basis of the pseudo-2D wavelet transform (p2D WT): the first step is to apply the 1D CWT and the second step is to analyze the outcome. The second step is very important, because the whole procedure produces a enormous amount of five-dimensional results and it is essential to pick up the relevant information. Even though it seems to be quite simple, this algorithm causes many difficulties and practical troubles during computation and the following interpretation. To comprehend the problems it is essential to understand what actually is the product of the applied one-dimensional wavelet transform.

One-dimensional CWT may give many different results. The most used and frequently quoted is probably the wavelet power spectrum introduced in the previous chapter. The power spectrum is simply a graph that shows the occurrence of detected frequencies in different time peri-

ods. But as a practical result, the power spectrum may be also considered merely as a matrix of numbers. All the wavelet power spectra used and presented in this study have the same composition in the sense that the x-axis describes the time evolution and the y-axis represents periods. Afterwards, individual columns represent frequency spectra for specific times and rows represent temporal development of specific periods. Realization of this conception is cardinal for understanding the way the pseudo-2D wavelet transform works. Figure 2.1 shows how this procedure can be visualized – it illustrates the decomposition of a WPS into two graphs, the first describing frequency characteristics at an exact time and the second showing how a given periodicity evolved throughout measurement. In this particular case, a non-stationary signal was analyzed. The lower (left-hand) line graph then represents frequencies occurring in the middle of

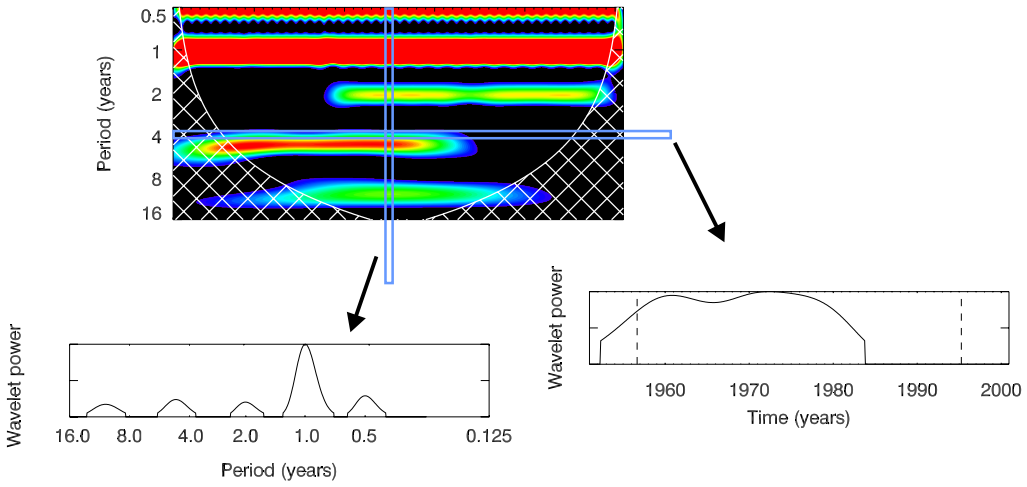

Figure 2.1: Wavelet power spectrum as a matrix decomposed into a frequency spectrum (left-hand line graph) and into a time evolution graph (right-hand line graph)

the series. And the upper (right-hand) line graph presents the temporal evolution of periods around four years. In fact, figure 2.1 illustrates the way the wavelet spectrum can be reduced by one dimension and how one can select certain information from many results. The next sections show why this is important for the pseudo-2D wavelet transform.

2.2 Pseudo-2D wavelet transform

To describe periodicity patterns over large geographical regions, it is important to choose datasets properly defined in a grid over the analyzed area. The datasets used in this study are described at the beginning of the next chapter. For now, let us imagine that the region of our interest is delineated by a set of time series specified in a geographical grid. This is generally outlined in figure 2.2. There is also shown a temporal slice (a slice that produces a picture of the dataset state at a given time) in the figure. These and similar slices are very helpful in visualization of the product of the pseudo-2D wavelet transform, because it is actually another method of reducing the dimension of the results and hence making the interpretation easier. The other slice are discussed in the next sections of this chapter.

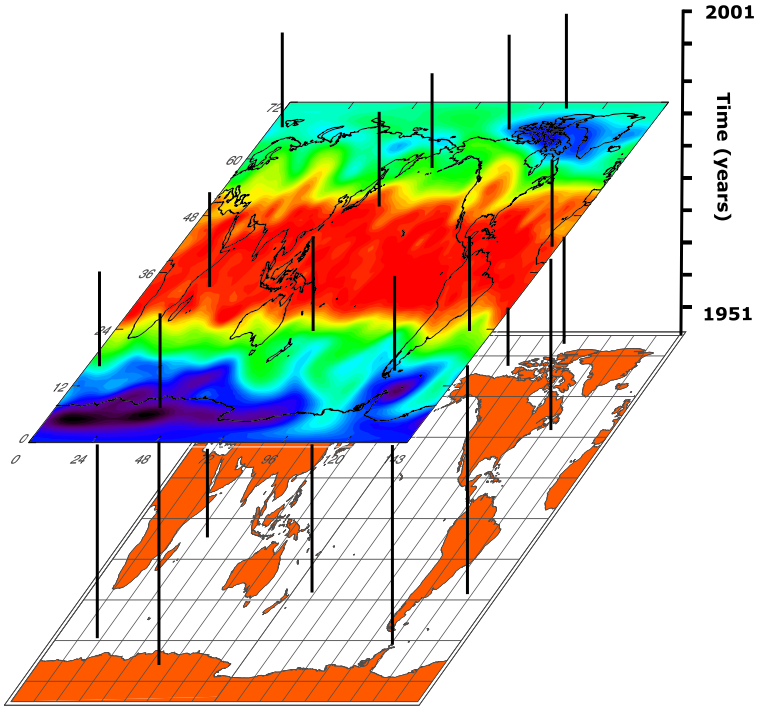

Figure 2.2: Set of time series and a temporal slice

Figure 2.2 illustrates typical climatological datasets and as we have already mentioned – one of the possibilities to analyze this is by applying the one-dimensional continuous wavelet transform on every series in the grid. This is shown in figure 2.3. Nonetheless, such a procedure produces an enormous amount of results and these results can be considered to be

up to five-dimensional data. The extents of the particular results are the following:

- geographical location (position in the grid)
- time period (specific occurrence time of an analyzed feature)
- frequency range
- wavelet power amplitude

Considering the spatial position as a two-dimensional quantity the final outcome is of five dimensions. For purpose of realization, it is necessary to make some extents constant, to make some *slices*.

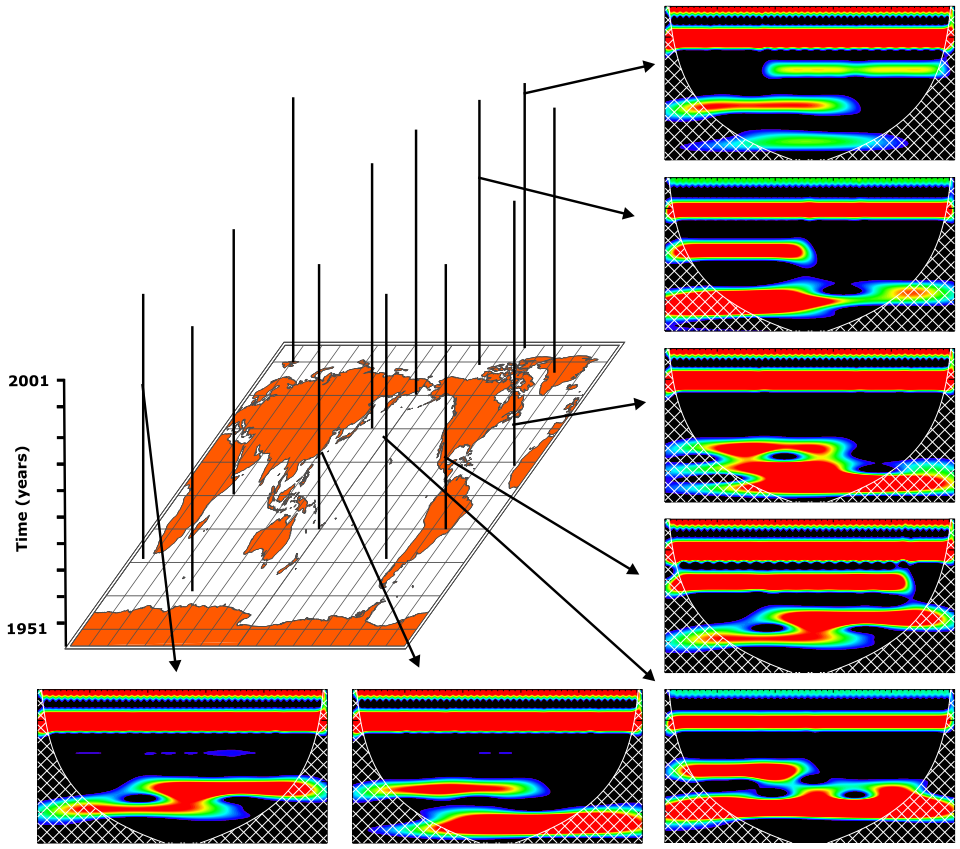

Figure 2.3: Multidimensional result after 1D CWT application

Because the purpose of the analysis is to obtain information about the whole area, the first item, spatial position, should not be reduced – the

result should describe all geographical points. However, in certain cases, we can select only some series in order to reduce the spatial dimension.

The second item in the previous enumeration is the time period. This rather a tricky object – to realize the results in three dimensions (and so make the visualisation possible), one has to choose only a certain time period. Contrary to that, the analyzed processes are rather non-stationary and it is necessary to look at the whole measurement period. The solution is to make a movie showing temporal evolution of the studied locations or to pick and display characteristic time periods under the condition of linear transition from one to another state.

The next item is the frequency range. Similarly to the time period selection, the choice of frequencies or periods range may be quite precarious. One of the reasons is the fact that the natural periodicities are not fixed by an exact value and therefore can be detected only in a range of periods.

The last result extent is the wavelet power amplitude of the identified oscillations. In most cases, one does not need to take care of these characteristics, because the final output should exceed some statistical significance over which all of the results are of more or less the same weight. The amplitude may be important in cases of studying certain distinct periods, such as annual cycles. All these objects and problems connected with them are discussed in the following sections.

2.2.1 Wavelet power spectra alteration

The pseudo-2D wavelet transform produces a great amount of results and one has to choose an algorithm that is capable of identifying any relevant information. However this can be affected already during the computation of the 1D wavelet transform. In particular cases, it is even necessary to adjust the wavelet spectra before further processing so that the p2D WT outcomes are unambiguous. This is illustrated in figure 2.1. The lower (left-hand) line graph illustrates oscillations occurring in the analyzed signal. It is apparent that the detected periods are the same periods that are listed in table 1.1. However, let us pay attention to the upper (right-hand) line graph on figure 2.1 – it represents a temporal evolution of the periods range of about four years. In the first half of the signal, we have identified a local maximum and so one could deduce that an oscillation with a period of four years has occurred there. Nevertheless, this result is at least inaccurate.

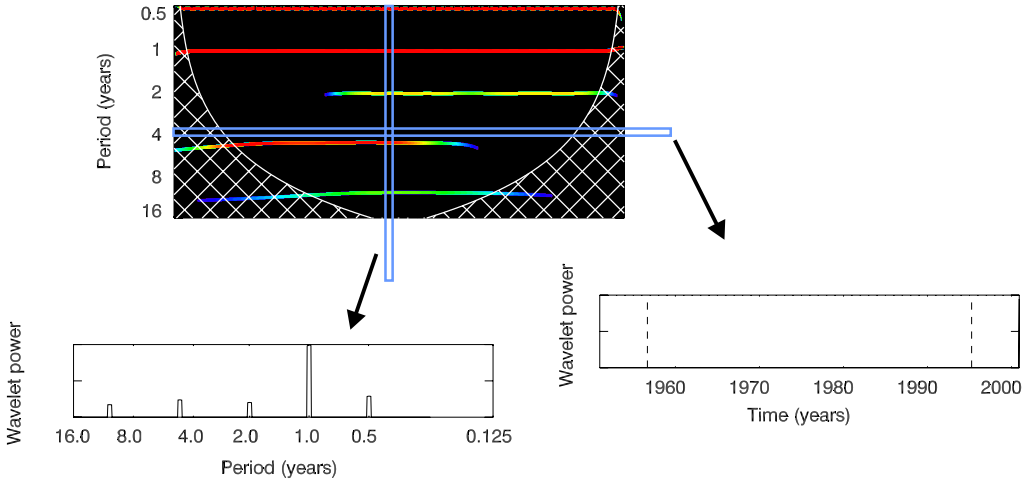

Figure 2.4: *Cleaned* wavelet power spectrum as a matrix decomposed into a frequency spectrum (left-hand line graph) and into a time evolution graph (right-hand line graph)

To avoid such an obstacle, we have to count on local frequency maxima only – this is shown in figure 2.4. This figure shows the wavelet power spectrum after being *cleaned out*. It is the same wavelet spectrum as in figure 2.1, but now only local frequency maxima were chosen. This is clearly illustrated by the line graphs – they present the same features as in the first case, but now the problems with detecting unrealistic frequencies are omitted (the period of 4 years has not been detected now at all).

On the other hand, this procedure faces problems with the choice of the proper range of periods around the detected local maximum. It is because of the fact that the analyzed processes are neither stationary nor appointed by exact and unvarying values. In practice, this can be tuned only during the computation itself, because it always depends on the analysis purpose and naturally on the type of the datasets. The values used in this study are described in the next chapter.

2.2.2 Choice of the frequency range

Troubles quite similar to those in the previous paragraph have to be solved in the next step of computation of the pseudo-2D wavelet transform. It has been already mentioned that it is necessary to make some slices after the 1D CWT is applied. The first outcomes are five-dimensional and we have to choose specific constant values of, e.g., periods to reduce the number of dimensions. Selecting only a single value, though, would yield inex-

act results. For example, a study focused on a five-years cycle would be possibly incorrect if it analyzed only periods of 5.00 years. In this case we also have to choose a certain range of values to be studied. And it is surely even more difficult than the selection of the range around the local maxima, because this choice directly influences the final results and also the interpretation. Moreover, the choice is strongly connected to the type of processes, the type of variables we are interested in and also to the geographical region over which the datasets are being analyzed. This is mostly solved only during the computation. In general, there may be only recommendations rather then rules. The following enumeration is an example of such recommendations.

- Individual ranges of periods should overlap each other to catch every value.
- Interpretation of a period range should always include results of the neighbouring ranges.
- In case of unclear results the procedure should be computed again with other ranges of periods.

In practice, the whole procedure starts with choosing the time period during which the frequency ranges should be analyzed. For example, we are

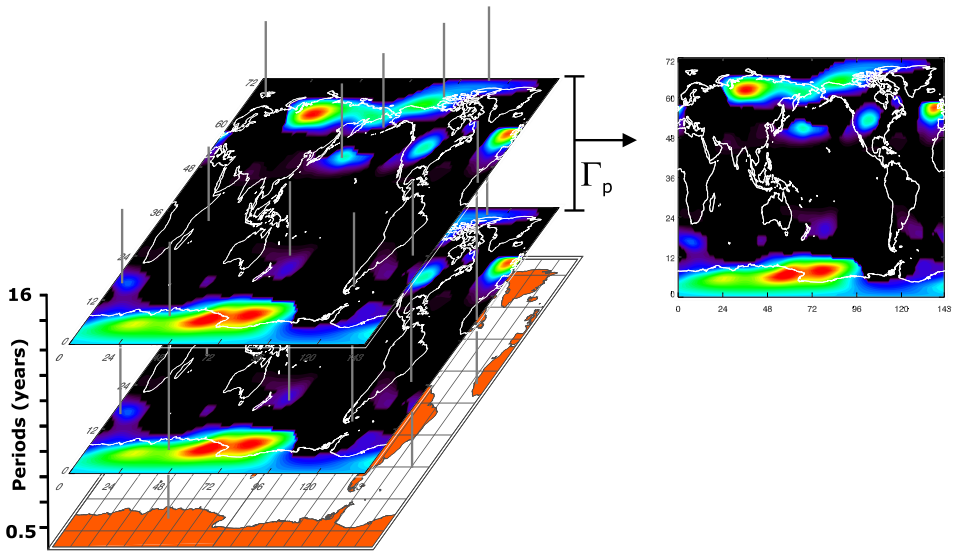

Figure 2.5: An averaging the selected range of periods (Γ_p range – see section 2.3.1)

interested in processes in the middle of the measurement period. Therefore, after the computation of the 1D CWT of every time series, we select the central column of each wavelet spectra matrix and put it back into the geographical grid. Every series in the grid then represents a frequency spectra taken in the middle of every original time series. The next step is to select several *surfaces* according to the periods ranges and for each range to make an average of all selected slices. This is shown in figure 2.5. For a range of periods Γ_p (see section 2.3.1), there are several slices selected and they are subsequently averaged into one result.

2.2.3 Time period selection

In case we are interested in only a specific range of periods and its temporal development, the procedure of the pseudo-2D wavelet transform is slightly different. Primarily, one has to select the period range. Problems connected with this topic are discussed in the previous paragraph. After that, contrary to selecting the frequency range, we pick up the relevant row in the wavelet power spectra (relevant to the time period). The following process is the same as in the previous case – the selected row is put back into the geographical grid ensued by making needful slices. In this case every series in the grid represents time evolution of the chosen period range.

2.2.4 WPS amplitude and geographical location

We have already indicated that the geographical location as well as the amplitude of the wavelet power are rather minor subjects in the theory of the pseudo-2D wavelet transform. However, in specific cases it would be interesting to choose only particular time series or to have a knowledge about regions with relatively more distinct periods.

Selecting only special geographical region does not influence the procedure itself, but it should be included in the final interpretation. The dimensions of the datasets, after the application of the 1D CWT, may naturally be reduced also by making geographical slices – on the other hand such results provide only limited information which can be useful, e.g., for some statistical purposes. In general the procedure in this case is the same as in the previous cases, only now the grid is not exactly over a geographical place, but it may describe, e.g., frequencies or time.

Because the final results should fulfil certain statistical criteria, it is mostly not contributive to study the wavelet power amplitudes in detail.

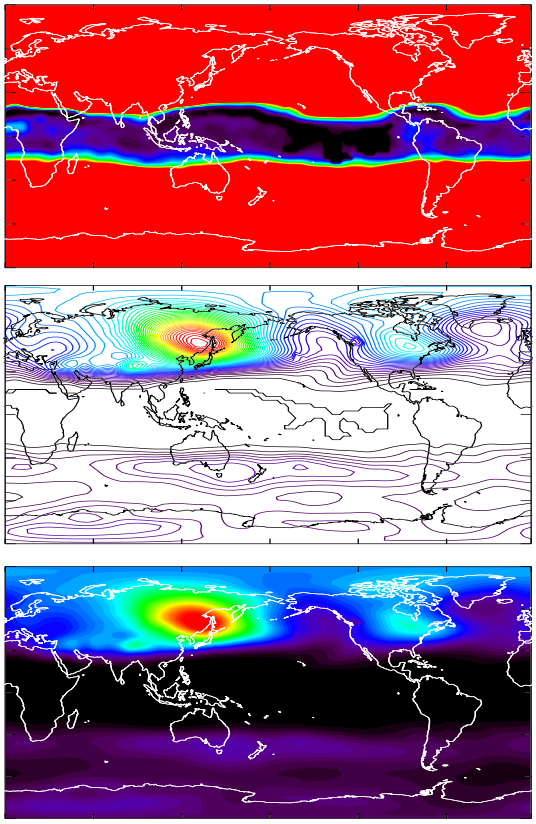

Figure 2.6: Sorting annual cycle – poor amplitude resolution (top), contoured (middle) and filled (bottom) areas

Nevertheless, in the case of striking periods such as an annual cycle, it would be interesting to know the cycle amplitude distribution. Figure 2.6 illustrates the way this can be accomplished. The selection of the right sets of the contouring boundaries here may help to identify either the regions where the annual cycle is not identified at all, or the regions where it is remarkable much more than anywhere else, or the transition between these limit values.

2.2.5 Finding interesting geographical regions

By examining worldwide data sets, the pseudo-2D wavelet transform produces many different results and it is not easy to find the relevant and important information. That is because of the fact that it is possible to find

an enormous number of periodicities in the global data sets, but only several of them occur in a significant period of time. One of the practicable approaches is to pre-examine the computed WPS to find the longest continuous parts of particular range of periods.

Latitude	**Longitude**	**1.3-2.2 years**	$\cdots$	**11.3-12.0 years**
50°05'27" N	14°25'09" W	X	$\cdots$	X
29°09'35" S	16°41'44" E	X	$\cdots$	-
$\vdots$	$\vdots$	$\vdots$	$\vdots$	$\vdots$
33°26'07" N	14°69'42" E	-	$\cdots$	X

Table 2.1: Example of the table of periods occurring in 30 years at least (the symbol X stands for the occurrence, the symbol $-$ for the non-occurrence)

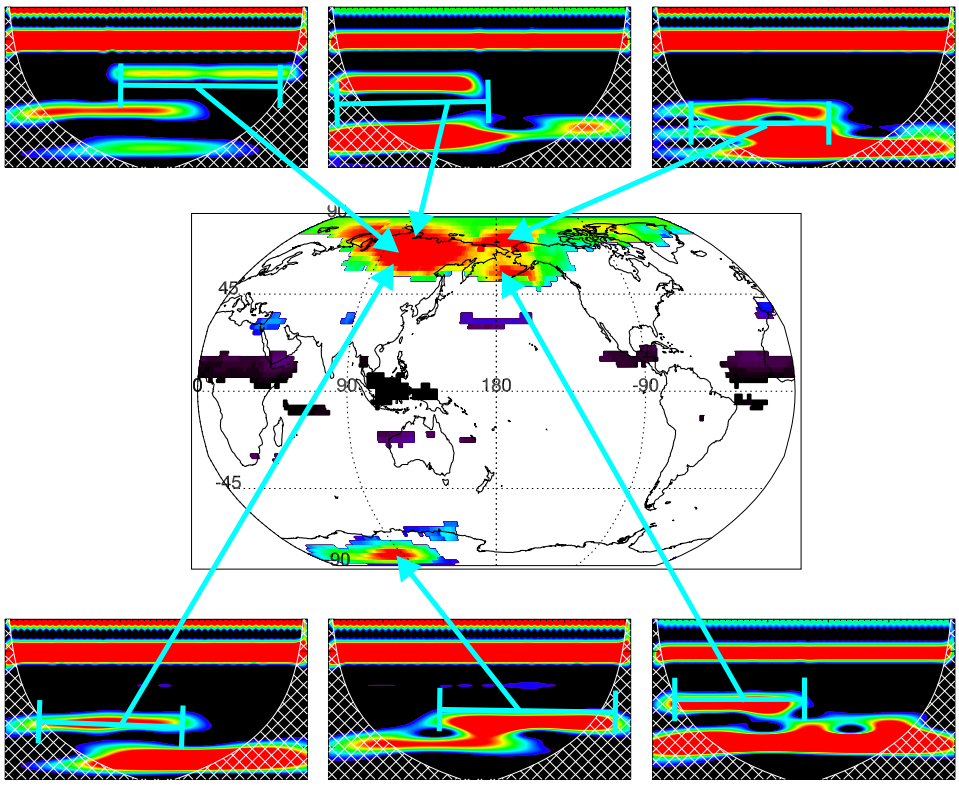

Figure 2.7: Identifying geographical regions with long-lasting periods

In practice, this means that the respective rows in the wavelet power matrix are averaged to a single series which is subsequently examined in

order to find the continuous parts. The results may be simply written down in a table and displayed in a graph. Then it is possible to identify geographical regions where a specific period have occurred for, e.g., 30 years at least. Table 2.1 and figure 2.7 illustrate the described procedures.

2.3 Mathematical description

Continuous wavelet transform is defined by the equation 1.10. Analyzing a discrete signal, however, requires also a discretation of the CWT definition. Similar problem is discussed and solved in TORRENCE ET AL. (1998). In this renowned paper, the continuous wavelet transform of a real series x_n with equal time spacing δt and $n = 0...N-1$ is defined as follows:

$$W_n(\lambda) = \sum_{n'=0}^{N-1} x_{n'} \psi^* \left[\frac{(n'-n)\delta t}{\lambda} \right] \tag{2.1}$$

This equation can be further modified by expressing the convolution by the Fourier transforms to the following form:

$$W_n(\lambda) = \sum_{k=0}^{N-1} \widehat{x}_k \widehat{\psi}^*(\lambda\omega_k) e^{i\omega_k n\delta t}, \tag{2.2}$$

where the angular frequency ω_k is defined as

$$\omega_k = \begin{cases} \frac{2\pi k}{N\delta t} & ; \quad k \leq \frac{N}{2} \\ -\frac{2\pi k}{N\delta t} & ; \quad k < \frac{N}{2}, \end{cases} \tag{2.3}$$

$\widehat{x}_k$ represents the discrete Fourier transform of x_n:

$$\widehat{x}_k = \frac{1}{N} \sum_{n=0}^{N-1} x_n e^{-2\pi ikn/N} \tag{2.4}$$

$k = 0...N-1$ is the frequency index and $\widehat{\psi}$ is the Fourier transform of the wavelet function. The wavelet power spectrum is then simply defined as $|W_n(\lambda)|^2$. This expression may be normalized – for example, normalization by $1/\sigma^2$, where σ is the variance, gives a measure of the power relative to the white noise (TORRENCE ET AL., 1998).

To describe the pseudo-2D wavelet transform in mathematical terms, let us formally express the computed wavelet spectrum as $W_\tau^\vartheta x_{k,l}$, where

$x_{k,l}$ represents a time series which is being studied (a time series from a geographical point at k degrees latitude and l degrees longitude), ϑ is the period index and τ is the time index. In other words, ϑ represents rows and τ represents columns in the wavelet power spectra matrix and k, l indicates from which location the original time series comes from. If k and l are constants, $W_\tau^\vartheta x_{k,l}$ is the common WPS. But in general, $W_\tau^\vartheta x_{k,l}$ represents a five-dimensional object – a group of geographically distributed WPSs.

2.3.1 Wavelet power spectra alteration II

To express the already discussed search for the local maxima in more precise terms, let us use the previously defined object $W_\tau^\vartheta x_{k,l}$. For this purpose let the location variables l and k be constants. The object then becomes an ordinary wavelet power spectra $W_\tau^\vartheta x$ which is only expressed in an unusual way. Let us also define a set of pairs Γ_p that determines the periods ranges and where $p = 0...M$ is the number of the ranges. The ranges and their meaning are discussed in the previous paragraphs. In general, they define the boundaries of the periods that are studied instead of an analysis of specific values of periods. An example of such a variable is presented in table 2.2.

Γ **variable index**	**Initial boundary** Γ_{p0}	**Ending boundary** Γ_{p1}
Γ_1	0.35	0.7
Γ_2	0.6	0.9
$\vdots$	$\vdots$	$\vdots$
Γ_M	15.6	16.1

Table 2.2: Example of the Γ variable – definition of the period ranges

Let us define a local maximum vicinity $\eta > 0$, which is also discussed in the previous paragraphs, and variables Θ_p and Θ_{pi} which represent the local maxima and relevant period index:

$$\Theta_p = \max(W_\tau^{\Gamma_p} x) \tag{2.5}$$

under the condition that

$$\max(W_\tau^{\Gamma_p} x) \neq \Gamma_{p0} \quad \wedge \quad \max(W_\tau^{\Gamma_p} x) \neq \Gamma_{p1} \tag{2.6}$$

The relevant period index Θ_{pi} can be then expressed as the index of the frequency where the local maximum is identified:

$$\Theta_{pi} = \vartheta \quad \longleftrightarrow \quad W_\tau^\vartheta x = \max(W_\tau^{\Gamma_p} x) \tag{2.7}$$

After that the *cleaned out* spectra $W_\tau^{'\vartheta} x$ is defined as follows:

$$\forall p, \forall \tau, \quad W_\tau^{'\vartheta} x = \begin{cases} W_\tau^{\Theta_{pi}-\eta,\ \Theta_{pi}+\eta} x & ; \quad \Theta_p \in \Gamma_p \\ \\ 0 & ; \quad \Theta_p \notin \Gamma_p \end{cases} \tag{2.8}$$

To describe application of this algorithm on the entire datasets, we would just use $\forall k, \forall l;\ W_\tau^{'\vartheta} x_{k,l}$ (instead of $W_\tau^{'\vartheta} x$).

2.3.2 Searching for the continuity

An analysis of the worldwide datasets may identify a very large spectrum of oscillations. On the other hand, only distinct periodicities last for a significant time period. Possible solution of this problem is mentioned in the previous paragraph. It is based on an algorithm that searches the WPS for the continuous regions and which can be also formally expressed using the previously defined object $W_\tau^{'\vartheta} x_{k,l}$.

Firstly, let us define a continuous region in the pseudo-2D wavelet transform context: it is simply a part of the analyzed series that does not contain any zeroes. This idea is based on the fact that the studied WPS after the cleaning procedure should contain either zeroes or relevant values. Ergo, the continuous region of a series x is defined as follows:

$$\Xi_{m,n}^x = [x(m), x(n)] \ ; \ 0 \notin [x(m), x(n)] \tag{2.9}$$

In order to examine a wavelet power spectrum, this procedure is applied on every row of the WPS matrix (period index ϑ). Using the set of period ranges Γ_p defined before, this can be expressed as:

$$\forall p, \forall \tau, \quad \Xi_{m,n}^{\Gamma_p} = W_\tau^{'\Gamma_p} x \ ; \ 0 \notin W_{m,n}^{'\Gamma_p} \tag{2.10}$$

After that it is necessary to apply a condition that every result is equal to zero if $m - n < T$, where T is the time period for which the oscillations should last (at least). In other words: only the results which describe periods that occurred longer than the time T are counted.

2.3.3 The slices

Having defined the object $W_{\tau}^{'\vartheta}x_{k,l}$, it is quite simple to express various types of the slices discussed before. In this context, a slice presents just a constant value of some of the indices ϑ, τ, k and l. For example, a variable defined as:

$$\Upsilon^{\Gamma_p} = W_{\tau}^{'\Gamma_p}x_{k,l} \;\; ; \;\; \Gamma_p = [9.9, 10.8] \tag{2.11}$$

would illustrates a temporal evolution of the geographical regions around the whole world where the periodicity of 9.9-10.8 years was distinct. Another type of slice is the time slice. Using $W_{\tau}^{'\vartheta}x_{k,l}$, a summary of occurring periods and relevant geographical regions at a specific date period D may be easily acquired by

$$\Upsilon^{\tau} = W_{\tau}^{'\Gamma_p}x_{k,l} \;\; ; \;\; \tau = D \tag{2.12}$$

Chapter 3

Practical Application and Results

The basics of the pseudo-2D wavelet transform were introduced in the previous chapter. It has been shown that the procedure starts with an application of the 1D wavelet transform on time series defined in a geographical grid. To analyze global frequency patterns in this study we have used datasets from the NCEP/NCAR reanalyses. These are described in the next section; the subsequent sections introduce the application of the pseudo-2D wavelet transform on them.

3.1 Datasets – NCEP/NCAR reanalysis

The reanalysis datasets have been created in cooperation between the National Centers for Environmental Prediction (NCEP) and the National Center for Atmospheric Research (NCAR). The product includes more than 50 years of global analyses of various atmospheric fields. The whole reanalysis process is based on the recovery of land surface, ship, aircraft, satellite, and other data whose quality was subsequently controlled. After that, the data were assimilated with a data-assimilation system kept unchanged over the reanalysis period (Kistler et al., 2001). The data-assimilation system includes the NCEP spectral model with 28 sigma vertical levels and a triangular truncation of 62 waves, equivalent to about 210-km horizontal resolution. The system is described in details in Kalnay et al. (1996).

The most often used reanalysis product are likely the gridded variables. They are divided into three classes (Kalnay et al., 1996):

- type A variables including upper air temperatures, rotational wind and geopotential height

- type B variables including moisture variables, divergent wind and surface parameters
- type C variables including surface fluxes, heating rates and precipitation

The most reliable variables are those of type A because they are generally strongly influenced by the available observations (KISTLER ET AL., 2001). The type B variables are influenced by the model and observations and are therefore less reliable. The last type of variables, type C, should be used with caution because the variables are completely determined by the model.

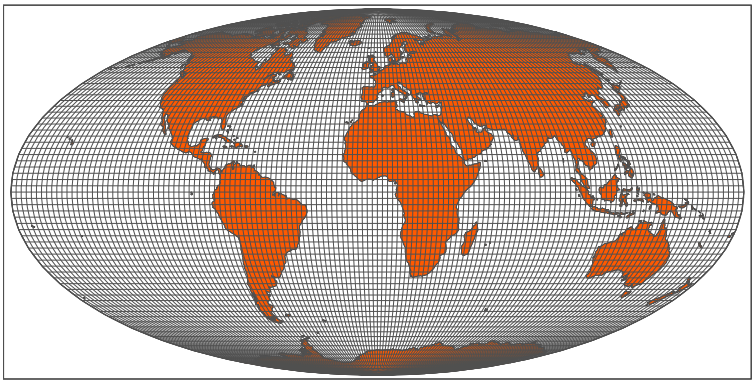

Figure 3.1: Geographical grid 2.5° × 2.5°

In this paper, we study two variables of type A: the geopotential heights field and temperature field at 500 hPa. The datasets have been analyzed in the form of monthly means for the time period of 1951-2000. The geographical grid, over which the datasets are defined, is described in table 3.1 and shown in figure 3.1.

3.2 Initial settings

We have primarily applied the 1D continuous wavelet transform defined by the equation 1.10 on the NCEP/NCAR time series describing temperature and geopotential heights fields at 500 hPa. As a mother wavelet, the

Longitude	0°E to 357.5°E	144 points	avg. res. 2.5°
Latitude	-90°N to 90°N	73 points	avg. res. 2.5°

Table 3.1: Properties of the used NCEP/NCAR geographical grid

Morlet mother wavelet (defined in the table 1.2) has been used with parameter ω_0 equal to 6. After that, the procedure which searches the WPS for the local frequency maxima (equation 2.8) was applied. The local maxima vicinity η was chosen equal to 0.2 of a year.

We have computed 90% confidence levels (according to TORRENCE ET AL. (1998)) for the wavelet power spectra of time series with removed averaged annual cycle (averaged cycle for 1951–2000). Thereafter those levels were applied on the results acquired after the cleaning procedure. The idea is based on the fact that the annual cycle is much more distinct then any other periodicity, however there may be another interesting oscillation that is not governed by the extraterestrial forces and that is not so pronounced. Besides that, removing the averaged annual cycle does not eliminate the annual periodicity from the series at all so that it is still detected. Moreover, only results that were outside the cone of influence (see the section 1.4.2) were picked out for futher computation of the pseudo-2D wavelet transform.

For the next steps of the computational procedure it is also necessary to set the period ranges Γ_p. Particular ranges used in this paper are described in table 3.2. The table defines 36 different ranges and notation used there is as follows: Γ_p is the Γ variable index, Γ_{p0} is the initial boundary and Γ_{p1} is the ending boundary. Both boundaries are expressed in years.

3.3 Pseudo-2D wavelet transform of the NCEP/NCAR reanalysis

The results of the application of the pseudo-2D wavelet transform of the NCEP/NCAR reanalysis datasets may be divided into two main categories and several other subcategories. Primarily, the results were searched for the period that lasted for a specific time T at least (all of the Γ_p ranges have been analyzed). Then the datasets were studied for the temporal evolution of particular Γ_p ranges. Analysis of the firstly acquired results, however, led to a modification of the initial settings and

Γ_p	Γ_{p0}	Γ_{p1}	Γ_p	Γ_{p0}	Γ_{p1}
Γ_1	0.10	0.70	Γ_{19}	9.15	10.15
Γ_2	0.60	1.34	Γ_{20}	9.65	10.65
Γ_3	1.15	2.15	Γ_{21}	10.15	11.15
Γ_4	1.65	2.65	Γ_{22}	10.65	11.65
Γ_5	2.15	3.15	Γ_{23}	11.15	12.15
Γ_6	2.65	3.65	Γ_{24}	11.65	12.65
Γ_7	3.15	4.15	Γ_{25}	12.15	13.15
Γ_8	3.65	4.65	Γ_{26}	12.65	13.65
Γ_9	4.15	5.15	Γ_{27}	13.15	14.15
Γ_{10}	4.65	5.65	Γ_{28}	13.65	14.65
Γ_{11}	5.15	6.15	Γ_{29}	14.15	15.15
Γ_{12}	5.65	6.65	Γ_{30}	14.65	15.65
Γ_{13}	6.15	7.15	Γ_{31}	15.15	16.15
Γ_{14}	6.65	7.65	Γ_{32}	15.65	16.65
Γ_{15}	7.15	8.15	Γ_{33}	16.15	17.15
Γ_{16}	7.65	8.65	Γ_{34}	16.65	17.65
Γ_{17}	8.15	9.15	Γ_{35}	17.15	18.15
Γ_{18}	8.65	9.65	Γ_{36}	17.65	18.65

Table 3.2: Definition of the period ranges Γ_p (all values are expressed in years)

hence to the repetition procedure. The following paragraphs describe the geographical regions of the long-lasting oscillations, the temporal evolution of individual period ranges and, also, they characterize remarkable geographical locations.

In this study, considering the length of the analyzed time period, some results (particularly the analysis of the oscillations belonging to the higher Γ_p ranges) proved to be insignificant and they are neither discussed nor shown. For that reason, the range of the analyzed datasets is always described at the beginning of the following sections.

The pseudo-2D wavelet transform produced a great number of results and only the most striking are shown in this chapter and also in the *Appendix A*. Figures of all results are included in the *AppendixB* – the attached CD.

3.3.1 The wavelet power

To express the difference between more or less striking geographical regions, we have used a colored scale of the wavelet power in the contoured graphs. The colored scale is always printed under the figures. The wavelet power is defined in the subsection *Continuous wavelet transform* of the section 1.4.1. However, the scale itself cannot be used for a mutual comparison, because it is not standardized for a specific number of studied events or for any special features.

The scale of the wavelet power has not been standardized for several reasons. In general, the reasons lie in the number of the cases, the complexity of the computing routines and the structure of the final results. The outcomes (in most cases) are represented by contoured plots describing the whole world within specific ranges of frequencies at particular time periods. This means that it is necessary to select only a limited group of values within every computed wavelet power spectrum to be plotted over the geographical grid. Subsequently, these values should be compared with each other to find an average according to which the particular values are going to be normalized. However, to compare the markedness of different period ranges, this should be done for every computed range.

This means that it would be necessary to mutually compare every achieved value of the computed wavelet power spectra and also all combinations of them in the selected ranges of periods. We have, in fact, computed the wavelet transform of time series defined in 10512 grid points; the resulted power spectra are composed of 600 columns (600 months) and 791 rows (791 specific periods). To find a normalized value or an universal computing algorithm we would have to then create a 3D matrix compounded of 1052×600×(791+N) complex values, where N stands for the number of the ranges Γ_p. That would require to investigate more then $5{\cdot}10^9$ complex values. Moreover, this procedure should reflect that over majority of the studied locations the annual cycle is x-times more distinct than any other oscillation. So counting the cycle in would result in an impaired possibility of identifying other periods.

The conclusion is that the colored scale represents only a relative strength of the interesting regions. So the particular figures cannot be compared to each other only on the grounds of the scale. Individual locations then illustrate the relatively more or less striking regions of the wavelet power.

3.3.2 Regions of long-lasting oscillations

The problems with an enormous number of results were described in the previous chapter. One way of solving this discrepancy is to pre-examine the datasets in order to find regions of long-lasting oscillations. Equation 2.10 defines this procedure in more precise terms and figure 2.7 shows the algorithm outcomes. This pre-examining procedure has also been applied in this study. The specific time for which the identified oscillations should last at least was firstly set to 10 years, then to 15, and in the last case to 20 years.

The results are shown in figures A.1-A.9 for the temperature field at 500 hPa and in figures A.10-A.18 for the geopotential heights field included in the *Appendix A*. The figures represent the geographical regions where different oscillations have been detected for the specific time T at least. Under these graphs there are also presented the colored scales describing used range of the wavelet power which is discussed in the section 3.3.1.

The datasets have been analyzed for the period ranges (listed in table 3.2) Γ_1-Γ_{24}. The most regions have been naturally detected for shorter period ranges Γ_p using the shortest time interval T equal to 10 years. The procedure using T equal to 15 and 20 years has identified markedly fewer regions. That is partly caused by the length of the studied time series and the previously discussed cone of influence.

Not surprisingly the most pronounced regions are the regions of the annual cycle (Γ_2 range). The second most marked oscillations are the periods in the Γ_1 range – semi-annual cycle. The findings are valid for the temperature field as well as for the geopotential heights field. The differ-

Γ'_p	Γ'_{p0}	Γ'_{p1}	Γ'_p	Γ'_{p0}	Γ'_{p1}
Γ'_1	1.15	3.15	Γ'_6	9.15	11.15
Γ'_2	2.15	7.65	Γ'_7	11.15	13.15
Γ'_3	2.65	4.65	Γ'_8	11.15	16.65
Γ'_4	5.15	7.15	Γ'_9	12.65	14.65
Γ'_5	7.15	9.15	Γ'_{10}	15.15	18.65

Table 3.3: Definition of the new period ranges Γ'_p (all values are expressed in years)

ences between the variables are in the geographical distribution of these cycles (see the next paragraphs for details).

None of the other period ranges is especially distinct in itself. On the other hand, e.g., the geographical locations of the period ranges Γ_6-Γ_8 and Γ_{19}-Γ_{21} cover remarkably vast areas around the equator. Ergo, in accordance with the recommendations discussed in the section 2.2.2, we have set new ranges Γ'_p that are listed in table 3.3. The results of the analysis with the new set of ranges are presented in figures A.3, A.6 and A.9 for the temperature field and in figures A.12, A.15 and A.18 for the geopotential heights field.

3.3.3 Temporal evolution of the Γ_p ranges

The analysis of the locations, where particular oscillations lasted for the specific time T at least, points to several interesting geographical areas. On the other hand, even those regions of the long-lasting periodicities have evolved in some way. And it would be contributive to study the development of the geographical locations in time.

To analyze the time evolution of the regions, we have applied the time slices discussed in the sections 2.2.2 and 2.3.3 and defined by the equation 2.12. The specific date D was at first chosen as equal to October 1969, then to January 1976 and finally to April 1983. Those values were selected as a compromise between the intention to study the temporal development and the range of the wavelet power spectra values given by the cone of influence (see the section 1.4.2).

The outcomes are shown in figures A.19-A.24 for the temperature field and in figures A.25-A.30 for the geopotential heights field included in the *Appendix A*. These graphs are followed by the colored scale of the used range of the wavelet power. The scale is of only a descriptive significance for the same reasons which are mentioned in the section 3.3.1 and which arise from the enormous amount of the results (and consequently from the impossibility to standardize them).

In the previous section we have discussed that the pre-examination of the datasets identified several distinct and stable oscillations. The annual cycle and the semi-annual periodicity are the most striking among them. The analysis also showed that there are other oscillations belonging to several period ranges that cover remarkable areas. This lead to the modification of the period ranges Γ_p and to the definition of new ranges Γ'_p (which are listed in table 3.3). The results of the analysis of those new ranges are presented in figures A.24 (the temperature field) and A.30 (the geopotential heights field). The figures describe temporal evolution only of the ranges Γ'_3 and Γ'_6. The other ranges Γ'_p have not been selected for the

analysis, because the pre-examination shows that these ranges are either insignificant by their geographical extent or they are actually included in other ranges.

3.3.4 500 hPa geopotential heights field

The following sections introduce the analysis of the 500 hPa geopotential heights field. The results are divided into several categories according to the most pronounced oscillations.

Annual cycle

The most pronounced periodicity identified in the geopotential heights field is the annual cycle (period range Γ_2). It is the only oscillation that has been detected also in the case of T equal to 30 years. The second graph in figures A.10, A.13 and A.16 illustrates the geographical distributions of the areas where the annual cycle lasted for 10, 15 and 20 years respectively. Figure 3.2 represents the state of the geographical regions where the cycle was distinct in January 1976. The temporal evolution between October 1969 and April 1983 is shown by the second column of graphs in figure A.25.

The most pronounced locations are the north-eastern of Asia and north-eastern of North America. Whereas at most regions over the equator, the annual oscillation has not been identified at all. This geographical distribution has not been changed during the whole analyzed time period.

Semi-annual cycle

The second most pronounced oscillations detected in the geopotential heights field are the oscillations belonging to the Γ_1 range of periods – approximately the semi-annual cycle. The first graph in figures A.10, A.13 and A.16 shows the distribution of the geographical regions where the semi-annual cycle lasted for 10, 15 and 20 years respectively. The structure of the geographical regions where the cycle was noticeable in April 1980 is presented in figure 3.3. Unlike the annual cycle, the geographical distribution, as well as markedness of the regions where this cycle was striking has altered. This is illustrated by the first column of graphs in figure A.25. On the other hand, the figures showing locations of periods lasting T years at least would help to determine regions, where this cycle was stable. In this case, according to the first graph of figure A.16, we may identify regions where the semi-annual cycle is marked such as: the north

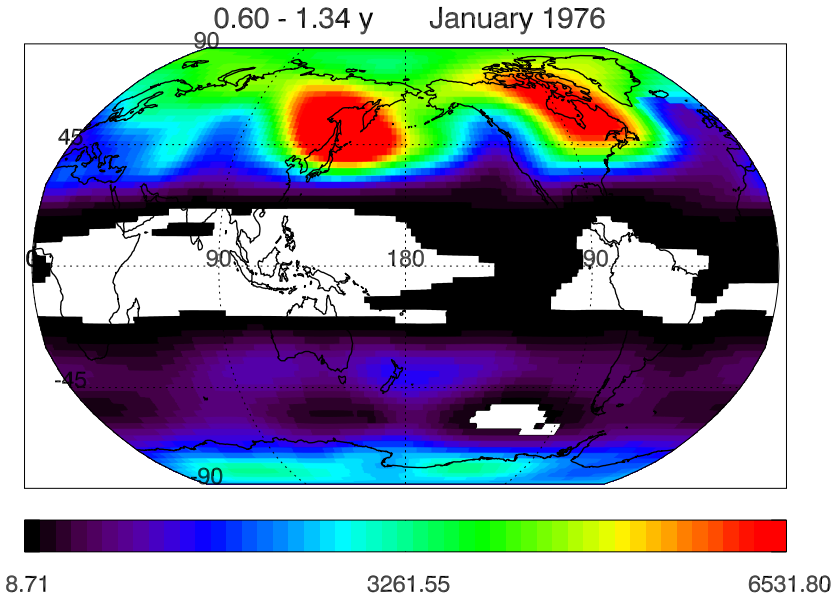

Figure 3.2: Geographical regions where oscillations in the Γ_2 range were distinct in 500 hPa geopotential heights field in January 1976 (the colored scale represents the wavelet power)

of Siberia, Alaska, the region over Himalaya range, the region over ocean east of Japan and the large area over Antarctica.

Modified Γ'_p ranges

Analysis of the other previously defined Γ_p ranges lead to the definition of the new set of ranges Γ'_p which are described in table 3.3. The reasons for this modification of the initial settings are mentioned in the setion 3.3.2. The new set comprises ten new pairs of the period boundaries. However only some of them proved to be remarkable.

The most interesting results of the analysis searching for the oscillations in the Γ'_p ranges which lasted for the specific time T at least are for the geopotential heights field presented in figures A.12, A.15 and A.18. The analysis points to several interesting events at the first sight:

- oscillations belonging to the Γ'_{10} range have not been detected at all
- Γ'_7 and Γ'_9 ranges may be included in the Γ'_8 range of periods

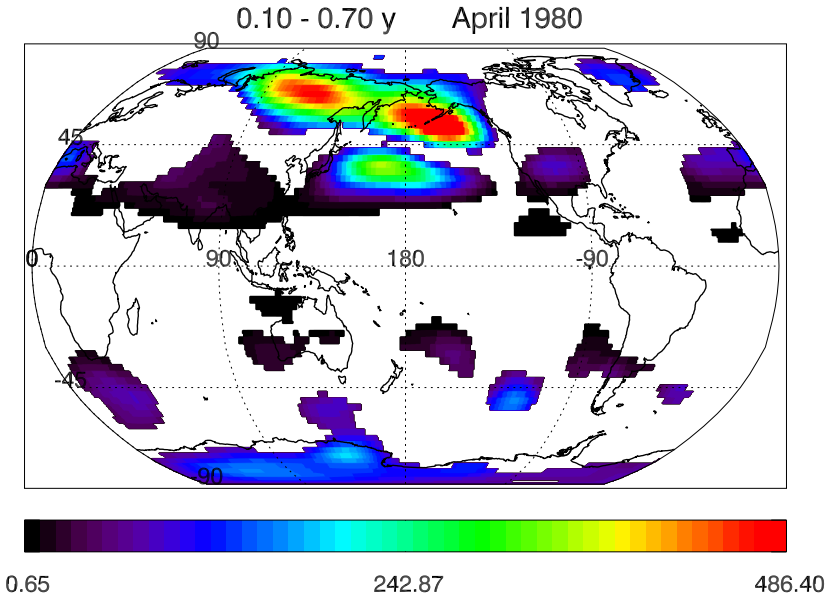

Figure 3.3: Geographical regions where oscillations in the Γ_1 range were distinct in 500 hPa geopotential heights field in April 1980 (the colored scale represents the wavelet power)

- considering the Γ'_{10} range, the Γ'_8 may be interpreted within boundaries 11.15-15.15 y
- considering the Γ'_3 range, the Γ'_2 range does not show any new results
- in comparison with other figures; the analysis within Γ'_1, Γ'_4 and Γ'_5 period ranges has not resulted in any interesting outcome
- study of the periodicities of the Γ'_6 range brought quite remarkable results

These findings lead to selection of only the Γ'_3, Γ'_6 and the Γ'_8 period ranges for futher analysis.

2.65-4.65 years periodicities

The second graph of figures $A.12$, $A.15$ and $A.18$ represents geographical regions where the oscillations of the Γ'_3 range lasted for 10, 15 and 20 years at least. The figures show that most of the areas are of a relatively small wavelet power, nevertheless they cover most of the world (especially the

regions around the equator between approximately 30°N and 30°S). The exception is the region between the Bellingshausen Sea and New Zealand where a periodicity of relatively high wavelet power has been detected. This location as well as the tropical area have been identified also in the case of the T equal to 20 years.

The temporal evolution of the Γ'_3 periods of the geopotential heights field is illustrated by the first column of graphs on the figure A.30. The analysis shows that:

- the tropical regions have not significantly evolved
- the region of high wavelet power has split into two regions over the original area and over the Wilkes Land
- a new center of relatively high wavelet power has arisen south of the Bering Sea

9.15-11.15 years periodicities

The geographical regions where the oscillations of the Γ'_6 range lasted for 10, 15 and 20 years at least are presented by the fourth graph of figures A.12, A.15 and A.18. The largest identified area is formed by a zonal belt around the equator that is on the Eastern Hemisphere limited by latitudes around 45°N and 30°S and by latitudes around 22°N and 22°S on the Western Hemisphere. The most distinct area of relatively high wavelet power is situated over the Arctic Ocean north of the Canada's Arctic islands, Alaska and Chukotka. The other (and smaller) centers of relatively higher wavelet power are situated between the Argentine Basin and the Gough Island (also called Diego Alvarez) in the South Atlantic Ocean, over the south of Greenland and a small centre located over the Kerguelen Islands. The geographical distribution of those areas is illustrated for January 1976 in figure 3.4.

The locations temporal development is illustrated by the second column of graphs in figure A.30. The particular graphs show that the main area around the equator has not noticeably changed. The evolution is evident in the changes of the wavelet power value of the minor centers. While the area east of the Argentine Basin became more striking, the most striking region over the Arctic Ocean has weakened.

11.15-16.65 years periodicities

The fifth graph of figures A.12, A.15 and A.18 represents geographical regions where the oscillations of the Γ'_8 range lasted for 10, 15 and 20 years

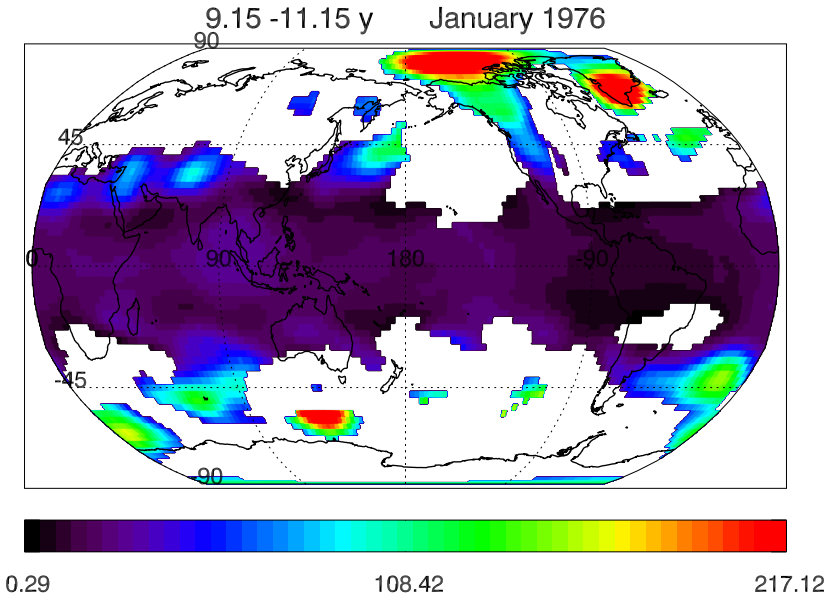

Figure 3.4: Geographical regions where oscillations in the Γ'_6 range were distinct in the 500 hPa geopotential heights field in January 1976 (the colored scale represents the wavelet power)

at least. However, for the specific time T equal to 20 years, the study has not found any periodicity. That is surely partly connected with the length of the analyzed time series and with the range of the periodicities. The most striking location is the already mentioned area between the Bellingshausen Sea and New Zealand. The next marked region is situated south of Australia.

Nonetheless, considering the length of the time series, these results do not describe the period development correctly, because most of the Γ'_8 range is inside the cone of influence of the primarily computed wavelet power spectra. Therefore the figures of the results are omitted.

3.3.5 500 hPa temperature field

The next stage of the study of the NCEP/NCAR reanalyses was to analyze the 500 hPa temperature field. The following sections describe the outcome of the analysis. In general, the results are very similar to the already discussed results of the 500 hPa geopotential heights field study. The differences may be found in the geographical distribution of the most

remarkable periodicities as well as in their temporal evolutions. Nevertheless, the main oscillations detected in the 500 hPa temperature field are the same as those identified in the 500 hPa geopotential heights field.

Results of the pseudo-2D wavelet transform of the 500 hPa temperature field are presented in figures A.1-A.9 (the analyses of the stable periods) and by A.19-A.24 (the temporal development of selected striking period ranges).

Annual cycle

The annual cycle (oscillations belonging to the Γ_2 range) is the most distinct periodicity identified in the 500 hPa temperature field. The second

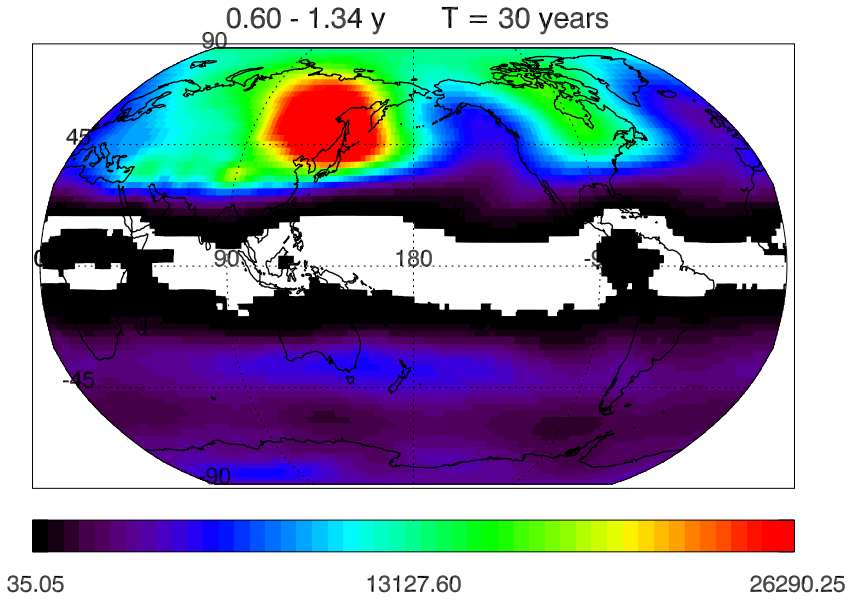

Figure 3.5: Geographical regions of distinct oscillations in the Γ_2 range (annual cycle) in the temperature field at 500 hPa lasting for 30 years at least (the colored scale represents the wavelet power)

graph in figures A.1, A.4 and A.6 illustrates the distribution of the geographical regions where the annual cycle lasted for 10, 15 and 20 years. The analysis was in this case done also with the specific time T equal to 30 years respectively. The result is shown in figure 3.5.

Similarly to the analysis using T equal to 10 or 20 years (and also to the analysis of the geopotential heights field), this study shows that the oscil-

lations of the Γ_2 period range are quite stable. The cycle has been detected for the whole analyzed time period over the whole world except for the equatorial areas. The most pronounced locations are also the north-east of Asia and north-east of North America. The differences with the geopotential heights field are primarily in the *shape* of the belt around equator, where no distinct periodicity has been detected. In case of the 500 hPa temperature field the belt is in the form of a wave of wave number equal to three. This may be distinguished from the temporal evolution between October 1969 and April 1983 that is shown by the second column of the graphs in figure A.19.

Semi-annual cycle

The second most remarkable period identified in the 500 hPa temperature field is the semi-annual cycle – the oscillations belonging to the Γ_1 range of periods (listed in table 3.2). The results of the analysis searching for the geographical areas, where this cycle lasted for 10, 15 and 20 years, are illustrated by the first graph in figures A.1, A.4 and A.6. The most striking regions here are the areas of the north of Siberia and Alaska and region over Antarctica. Unlike the geopotential heights field study, this analysis has not found any other remarkable locations.

The first column of graphs in figure A.19 shows the geographical regions development between October 1969 and April 1983. It is apparent that the marked locations have noticeably evolved. The most striking area of high wavelet power has split several times into two separated centers located over the north of Sibera and the north of North America. The process is illustrated in figure 3.6 as well.

Modified Γ'_p ranges

The analysis of the other Γ_p ranges listed in table 3.2 discovered that none of these ranges is significantly pronounced and that they are either practically included in other ranges or they are insignificant in their geographical extent. These findings lead to the definition of the new set of ranges Γ'_p which are described in table 3.3. The results of the study searching for the oscillations in the Γ'_p ranges which lasted for the specific time T at least are for the temperature field illustrated in figures A.3, A.6 and A.9. Similarly to the analysis of the geopotential heights field, the results in this case also resulted in the selection of only the Γ'_3, Γ'_6 and the Γ'_8 period ranges for futher analysis. The reasons for this choice are discussed in the subsection *Modified* Γ'_p *ranges* devoted to the analysis of the geopotential heights field.

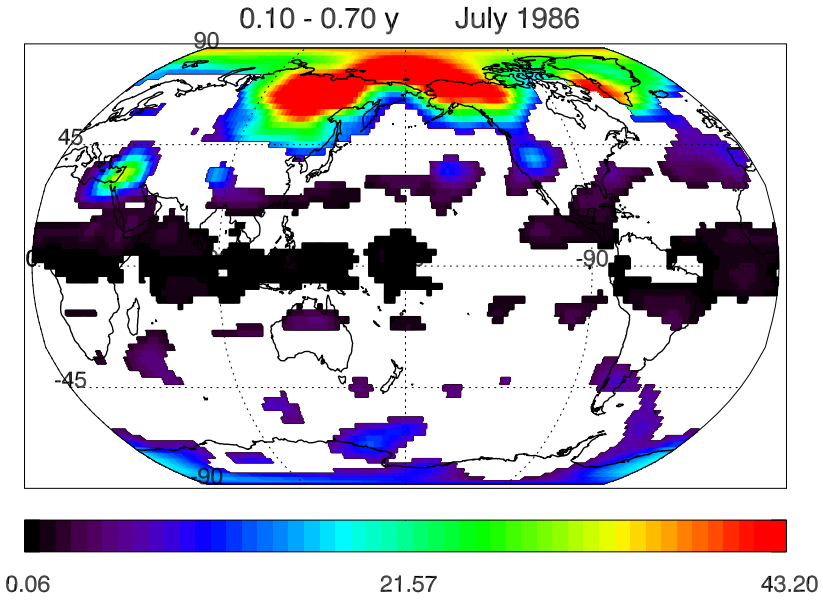

Figure 3.6: Geographical regions where oscillations in the Γ_1 range were distinct in the 500 hPa temperature field in April 1986 (the colored scale represents the wavelet power)

2.65-4.65 years periodicities

The geographical regions where the oscillations of the Γ_3' range lasted for 10, 15 and 20 years at least are illustrated by the second graph in figures $A.3$, $A.6$ and $A.9$. Despite the fact that most of the areas are of a relatively small wavelet power, they cover most of the world (especially the regions around the equator). These regions do not form as compact area as in the case of the analysis of the geopotential field, however they may be broadly delimited by the latitudes around 25°N and 25°S. The location of a relatively high wavelet power is the region between the Bellingshausen Sea and New Zealand, as well.

The regions development in time is shown in the first column of the graphs in figure $A.24$. The analysis shows that:

- the zonal belt around the equator has changed its extent especially over the Eastern Hemisphere
- two distinct centers of a relatively high wavelet power have appeared several times over the region of Tuamotus and over Hawaiian Islands

- two other regions of relatively high wavelet power have appeared several times south of the Tuamotus region and the other one north of the Hawaiian Islands centre
- these regions may be delimited by a meridional belt between the 180°W and 90°W longitudes
- there are several other striking areas that appeared approximately north of the 60°N latitude
- locations of those areas altered between the areas over the north of Europe and the regions over the north of North America and Greenland

Some of these features are also illustrated in figure 3.7.

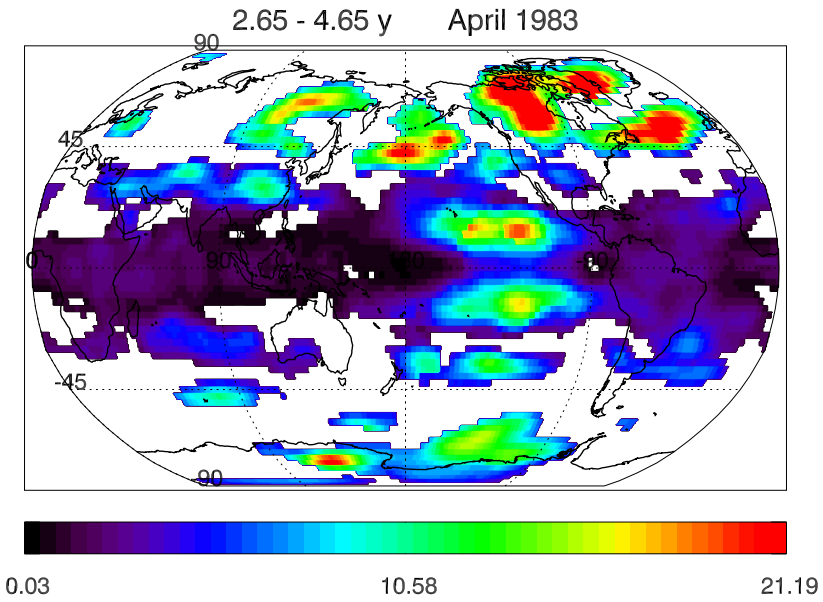

Figure 3.7: Geographical regions where oscillations in the Γ'_3 range were distinct in the 500 hPa temperature field in April 1983 (the colored scale represents the wavelet power)

9.15-11.15 years periodicities

The fourth graph of figures $A.3$, $A.6$ and $A.9$ illustrates the geographical regions where the oscillations of the Γ'_6 range lasted for 10, 15 and 20 years

at least. The largest identified area is mainly formed by a belt around the equator which is approximately limited by latitudes around 22°N and 22°S. An exception can be found in the area between the 180°W and 90°W longitudes, where the belt nearly disappears. Similarly to the analysis of the geopotential heights field, the most distinct area of relatively high wavelet power is situated over the Arctic Ocean north of the Alaska and Chukotka. The other centers of relatively higher wavelet power are situated over the south of Greenland, over the region between the Argentine Basin and the Gough Island, over the north-east of Japan, over Iran and over the Kerguelen Islands.

The temporal development of the locations is illustrated by the second column of graphs in figure A.24. The particular graphs mainly illustrate weakening of the zonal belt around the equator over the Pacific Ocean regions.

11.15-16.65 years periodicities

The geographical regions where the oscillations of the Γ'_8 range lasted for 10, 15 and 20 years at least are presented in the fifth graph of figures A.3, A.6 and A.9. Similar to the analysis of the geopotential heights field, this analysis for the specific time T equal to 20 years, has not found any periodicity. However unlike the geopotential heights study, there has not been identified any distinct center between the Bellingshausen Sea and New Zealand for the specific time T greater than 10 years. The other striking regions here are the areas over the region of the Tuamotus and over the Hawaiian Islands which were detected even with the T equal to 15 years.

Similarly to the analysis of the geopotential heights field, the results of the temporal evolution study cannot describe the period development correctly, because most of the Γ'_8 range is inside the cone of influence of the primarily computed wavelet power spectra. Therefore the figures of the results are omitted in this case as well.

3.4 The résumé

Using the pseudo-2D wavelet transform, we have studied the geopotential heights and temperature field at the 500 hPa within the time period of 1951-2000. The analyzed datasets were obtained from the NCEP/NCAR reanalysis. These are described in the section 3.1.

The reanalyses were primarily investigated in order to identify geographical regions where the periods of the Γ_p ranges lasted for the specific times T at least. The procedure and its initial settings are discussed in the section 3.3.2. The most interesting results are illustrated in figures A.1-A.9 for the temperature field and in figures A.10-A.18 for the geopotential heights field included in the $Appendix\ A$. The specific time T was chosen equal to 10, 15 and 20 years. Higher values of T proved to bring only slightly more information and only for the Γ_1 and Γ_2 period ranges. Most of the other ranges have not been detected with the higher values of T.

The analysis which was to search for the long-lasting periods has resulted into modification of the Γ_p ranges and into definition of the new set of ranges Γ'_p. The results of the procedure with the new set of ranges are shown in figures A.3, A.6 and A.9 for the temperature field and in figures A.12, A.15 and A.18 for the geopotential heights field.

In the next step of the study, we have analyzed the datesets in order to describe the temporal evolution of the previously identified interesting geographical locations of the Γ_p and Γ'_p ranges of periods. The most interesting results are illustrated in figures A.19-A.24 for the temperature field and in figures A.25-A.30 for the geopotential heights field. The procedure and its initial settings are discussed in the section 3.3.3. The previous analysis showed that only some of the Γ'_p ranges are distinct and correctly described as well: particularly the Γ'_3 and Γ'_6 range. The results of the analysis with these ranges are presented in figures A.24 (the temperature field) and A.30 (the geopotential heights field).

The particular results are described in sections 3.3.4 and 3.3.5. In general, the outcomes the analysis of the temperature field and of the geopotential heights field are quite similar. The most striking period ranges are the same in both cases. The differences may be found in the geographical regions distribution and also in their temporal development. However, these dissimilarities are slight, as well.

Chapter 4

Summary and Discussion

What can we actually obtain from the investigation of the data frequency characteristics and what are the related methods of data analysis? These are the questions that we asked in connection with the climate variability in the preface. In the first chapter, we have shown that the climate variability may be also understood in the sense of some periodic motions. Such motions may be further divided into a class of various oscillatory patterns and into a class of periodicities or cycles. The oscillatory patterns are mainly expressed as spatial oscillations of some interconnected centers. The periodicities and cycles are primarily defined in terms of typical frequencies or periods. Thereafter, we introduced some basic frequency analysis methods. It has been shown that these methods are suitable for some specific datasets, mainly those which are either stationary in frequencies or in space. To describe non-stationary natural processes in general, it is necessary to create a new algorithm that is capable of detecting an evolution of the datasets frequency characteristics both in time and space. Such an analysis is presented by the pseudo-2D wavelet transform. Its fundamentals are described in the second chapter. The algorithm is based on the 1D continuous wavelet transform and it transforms datasets defined in a grid into a multidimensional object. The result may be then interpreted by slices such as the data evolution in time, space or frequencies.

The next chapter, chapter three, introduces the application of the pseudo-2D wavelet transform on the temperature and geopotential heights fields which were acquired from the NCEP/NCAR reanalyses datasets. The analysis produced many interesting results. The most remarkable of these are presented both in the third chapter and in the *Appendix A*. All the results are included in the *Appendix B* – the attached CD. The results of the analyses of the temperature and geopotential fields are

generally quite similar, however, there are several differences mainly in the geographical distribution of the regions of distinct periodicities.

500 hPa geopotential heights field

The geopotential heights field at 500 hPa was studied for the time period of 1951-2000. The results are described in section 3.3.4 and the most interesting outcomes are presented in figures A.10-A.18 and A.25-A.30 included in the *Appendix A*.

500 hPa temperature field

The 500 hPa temperature was studied for the time period of 1951-2000, as well. The results are described in section 3.3.5 and presented in figures A.1-A.9 and A.19-A.24.

4.1 Identified cycles

The most striking periodicities, that were detected, are the same for the temperature fields as well as for the geopotential heights field. The cycles-marking in the sense of the Γ_p ranges and the period ranges exact values are listed in table 4.1. The last column in table 4.1 presents the names of the cycles that are universally used in climatological studies.

Γ_1	0.10–0.70	semi-annual oscillation (SAO)
Γ_2	0.60–1.34	annual cycle
Γ'_3	2.65–4.65	quasi-quadrennial oscillation (QQO)
Γ'_6	9.15–11.15	quasi-decadal oscillation (QDO)
Γ'_8	11.15–16.65	(higher) decadal periodicities

Table 4.1: The most striking periodicities identified in the studied datasets

Semi-annual oscillation

The semi-annual oscillation has been already detected by many studies some of which are mentioned in the first chapter. The most remarkable regions of this cycle, which we have identified in this study, are for

both analyzed fields: the north of Siberia and Alaska and the region over Antarctica. Moreover, the analysis of the geopotential heights field has also pointed to the region over the Himalaya range and the region over the Pacific Ocean east of Japan. Generally, the semi-annual oscillation is present more in the geopotential heights field than it is in the temperature field.

These results are in accordance with the majority of related studies. In the Northern Hemisphere, WIKLE ET AL. (1996) have identified in the geopotential heights fields at the 700, 500 and 300 hPa the same regions of distinct semi-annual oscillation as we have detected in this paper. The locations mainly reflect the east-west land-sea contrast and the tropical/subtropical region seems to be linked to the Asiatic monsoons (CULLATHER ET AL., 2003). WIKLE ET AL. (1996) have further concluded that the Northern Hemisphere regions are in general associated with asymmetries in the seasonal variation of stationary eddies. To test these conclusions, however, we would have to provide an extra analysis of the oscillation phase and an analysis of the field zonal asymmetries. On the other hand, the application of the pseudo-2D wavelet transform illustrated how the regions have evolved in time. These results showed a weakening of the semi-annual oscillation in the mid-1970s in contrast with the more striking regions in the late 1960s and the beginning of the 1980s.

Over the Southern Hemisphere, the pseudo-2D wavelet transform pointed to a large region over the high latitudes and mainly to the region over Antarctica. These findings are also in accordance with the most of related analyses. VAN LOON (1967) connected these oscillations to the differences in the seasonal heating and cooling trends in the middle and high latitudes. That is linked to Southern Hemisphere north-south differential heating between Antarctica and the surrounding oceans (WALLAND ET AL., 1999). Moreover, CHEN ET AL. (1996) discussed the possibility of the semi-annual oscillation over the Southern Hemisphere being induced by the north-south shift of the local Hadley circulation. However, similarly to the previously stated obstructions, it would require an extra analysis to test these results. VAN DEN BROEKE (1998B) mentioned a weakening of the semi-annual oscillation since the mid-1970s. These findings were not entirely verified by the application of the pseudo-2D wavelet transform, however, the breaking-point around the mid 1970s was also detected in this case. In general, this may indicate some decadal variability of the semi-annual oscillation (similarly to WALLAND ET AL. (1999)).

Annual cycle

The annual cycle is unsurprisingly the most distinct oscillation that has been detected in the studied datasets. The pseudo-2D wavelet transform showed that the geographical locations where the annual cycle was striking are almost the same for the temperature and geopotential heights fields. Slight differences may be found in the strength of the region over North America. Another difference is in the shape of the belt around the equator where no significant annual cycle has been detected. The most striking locations are situated over the eastern coast of Asia and their geographical distribution is identical for both of the analyzed quantities. These results also correspond to the graphs in figure 1.2, where the mean annual cycle from an equatorial location is almost not defined, however the cycle is quite striking in the series from the higher latitudes locations.

There are only a few studies that use a frequency analysis to investigate the annual cycle in the sense of the geographical distribution of the oscillation amplitude (especially at higher atmospheric levels). HEDDINGHAUS ET AL. (1980) proposed an extensive study of different annual cycle patterns over the Northern Hemisphere. The authors identified distinct frequency patterns with high amplitudes centers over the eastern continents coasts. They concluded that geographical structure of the annual variations of temperature at 500 hPa as well as 700–500 thickness fields were clearly affected by the land-sea contrasts. This is in accordance with the results acquired by this paper.

The analysis of the temporal evolution of the geographical areas where the annual cycle has been identified showed that in the temperature field the cycle has not significantly evolved, but in the geopotential heights field the study has detected changes in the markedness of the region over North America. This may also point to some decadal variability, however, it would be necessary to study datasets for a longer time period to test this hypothesis.

Quasi-quadrennial oscillation

The pseudo-2D wavelet transform of the NCEP/NCAR datasets showed that, after the annual cycle, the quasi-quadrennial oscillation is identified in most of the gridpoints. Although the analyzed regions are of a relatively small wavelet power, the locations where the QQO has been detected form a very large zonal belt around the equator that may be broadly delimited by 30°N and 30°S. The belt is less compact and slightly narrower in the case

of temperature field analysis. In addition to the areas around the equator, the pseudo-2D wavelet transform of temperature as well as geopotential fields has also detected a region of relatively high wavelet power between the Bellingshausen Sea and New Zealand.

The temporal development of the regions where the QQO has been identified is quite different for the temperature field and for the geopotential field. In general, the QQ mode is more stable in the geopotential field where the zonal belt has not significantly evolved. The only development may be seen in the southern higher latitudes. On the other hand, the analysis of the temperature field at 500 hPa showed distinct changes in the geographical distribution of the QQO regions. In comparison with the geopotential field, the transform of the temperature field detected other locations within higher northern latitudes and several fluctuating areas delimited by a meridional belt between approximately the 180°W and 90°W longitudes.

Although the quasi-quadrennial oscillation has been identified by many other studies, results presented in this paper are quite difficult to compare with some other findings. The main problem is that QQO is mostly not analyzed within higher atmospheric levels. The oscillation has been connected mainly to the ENSO phenomenon and variations in the sea surface temperatures or wind field over equatorial areas. Thefore, geographical distribution of the QQO locations is partly in accordance with the results acquired by the pseudo-2D wavelet transform. The distinct region near the South Pole was for lower levels analyzed also by Drinkwater et al. (2001). An extensive analysis was proposed by Ribera et al. (2002) who showed that interannual climate variability associated with the ENSO signal is identified in distinct quasi-quadrennial frequency range. The authors also discussed that the QQ mode in the geopotential heights field at 500 hPa is closely connected to the Pacific North American (PNA) pattern. Ribera et al. (2003) further stated that the QQO pattern in the Southern Hemisphere might indicate mass transport between the Indian, Pacific and Atlantic basins. In general, the quasi-quadrennial oscillation may be also linked to tropospheric interannual variability and planetary wave forcing (Chen et al., 2003).

Quasi-decadal oscillation

Aside from the quasi-quadrennial oscillation, the pseudo-2D wavelet transform of the NCEP/NCAR datasets has also detected a distinct quasi-decadal oscillation over the zonal belt around the equator. Even in this

case, the particular results achieved by the analyses of the temperature and geopotential heights fields are quite similar. For the geopotential field, the largest identified area is formed by a zonal belt around the equator that is on the Eastern hemisphere defined by latitudes around 45°N and 30°S and by latitudes around 22°N and 22°S on the Western hemisphere. For the temperature field, the belt is delimited approximately by latitudes around 22°N and 22°S over both hemispheres. In addition to these large areas, we have also detected smaller centers of relatively higher wavelet power over the Arctic Ocean north of Alaska and Chukotka, between the Argentine Basin and the Gough Island, over the south of Greenland, over the Kerguelen Islands and a center over the north-east of Japan.

The temporal evolution of those regions is slightly different for the temperature and the geopotential heights fields. The largest area, the zonal belt around the equator, has not noticeably changed in the case of the geopotential heights. However, in the case of the temperature field, the development in time illustrates noticeable weakening of the zonal belt, especially over the Pacific ocean. The evolution is evident also in the changes of the wavelet power value of the minor centers.

Similarly to the quasi-quadrennial oscillation, there are many studies that analyze the quasi-decadal variability of climate, but almost none of them is oriented to the middle tropospheric levels. The second problem is that the quasi-decadal oscillations are often automatically connected to the solar cycle forcing. That implies that the governing mechanism is not searched for in the intrinsic dynamics of the climate system. This is discussed in detail by Garric et al. (2003). The authors proposed several internal mechanisms that may be responsible for the QDO, such as, thermohaline circulation, modulation of the ENSO via the delays associated with the midlatitude-tropical ocean advection timescales or the winddriven circulation and stochastic resonance. Brassington (1997) proposed a study of the South Oscillation index and the El Niño region sea surface temperature time series where they detected the QQD. These results were suggested to be connected to the deepening of the Aleutian low in the North Pacific. Mizoguchi et al. (1999) studied the QDO over the Atlantic Ocean and they proposed that the detected quasi-decadal oscillation mode in the North Atlantic may be explained in terms of the atmosphere-ocean interaction and the advection of temperature anomalies by mean oceanic currents. This was partly analyzed also by Terray et al. (2002) who showed that at near-decadal timescales, there is a strong evidence of a slow propagation of SST anomalies along the North Atlantic Current (NAC) at the boundary of the subtropical and subpolar gyres.

All these findings do not disprove the results which were achieved by the pseudo-2D wavelet transform. On the other hand, the results have been neither verified nor tested because the other studies analyzed different geographical locations and different climatic quantities. To test the acquired results, i.e. whether they may arise as a consequence of the suggested mechanisms, we would have to provide a completely new study of other climatic fields like the sea surface temperatures or wind fields.

Higher decadal oscillations

The pseudo-2D wavelet transform of the NCEP/NCAR datasets has also identified a distinct variability in the period ranges of 11.15-16.65 years. The most striking location where the oscillation was detected is the area between the Bellingshausen Sea and New Zealand. Other distinct regions were identified over the equatorial Pacific Ocean. The differences between the temperature and the geopotential fields may be found especially in the geographical distribution of the distinct locations.

These findings, however, are quite difficult to be correctly discussed because the length of the original series is too short; therefore most of the computed wavelet power spectra, belonging to these period ranges, resides within the cone of influence – within the part of the spectra where the results are not reliable.

4.2 Concluding remarks

In the preface, we have specified the main aim of this paper. It was to examine the capability of the pseudo-2D wavelet transform to globally analyze the climate variability. That involved the introduction of some related frequency analysis, the introduction of the fundamentals of the pseudo-2D wavelet transform and the description of the results of application of the p2D WT on the NCEP/NCAR reanalysis datasets.

Some of the frequency analyses are described in the introduction, in the first chapter. The following chapters introduce, describe and discuss the pseudo-2D wavelet transform and its application. It has been shown that the transform is a new algorithm that was designed to describe the frequency characteristics of the studied datasets, datasets in the form of time series defined in a grid, in the sense of their evolution both in time and space. This is accomplished by the transformation of the datasets into a five-dimensional object which is subsequently interpreted through some

slices. The transform in general purveys many different types of information about the development of the studied datasets and so it is fully appropriate for studying the climate variability.

The application of the pseudo-2D wavelet transform on the NCEP/NCAR reanalysis datasets showed that the transform is able to uncover spatial centers of distinct oscillations. These findings were mostly confirmed by other studies. The contribution of this analysis is mainly in the characterization of the regions temporal evolution and also in the fact that the results describe the particular periodicities globally over the whole world.

On the other hand, when interpreting the results, it is necessary to consider the fact that we did not analyze datasets acquired only by observations but we studied reanalyzed datasets. This might have influenced the results – for example, TENNANT (2004) showed that the integration of satellite data in 1978 affected the daily circulation statistics especially for the upper tropospheric and the lower stratospheric levels. However, to test these caveats, the whole study would have to be repeated with a different type of the reanalyses datasets.

The results and their comparison with other studies also indicate futher possible applications of the pseudo-2D wavelet transform. To investigate the possible physical mechanisms standing behind the detected oscillations, the transform should be also applied on the same fields at different atmospheric levels and also on other climatic quantities, such as the sea surface temperatures. In general, the algorithm should be also supplemented by the analysis of the periodicities phase.

Appendix A

The following figures illustrate the results of the pseudo-2D wavelet transform of the geopotential heights field and the temperature field at 500 hPa. However, the study produced a great number of results and only the most striking are shown here. Figures of all results are included in the $AppendixB$ – the attached CD.

The results of the study which searches the datasets for the oscillations which lasted for the specific time T at least are presented in figures A.10-A.18 for the geopotential heights field and in figures A.1-A.9 for the temperature field. Figures A.25-A.30 illustrate the temporal evolution of the most distinct periodicities in the geopotential heights field and figures A.19-A.24 illustrate the temporal evolution of selected oscillations in the temperature field.

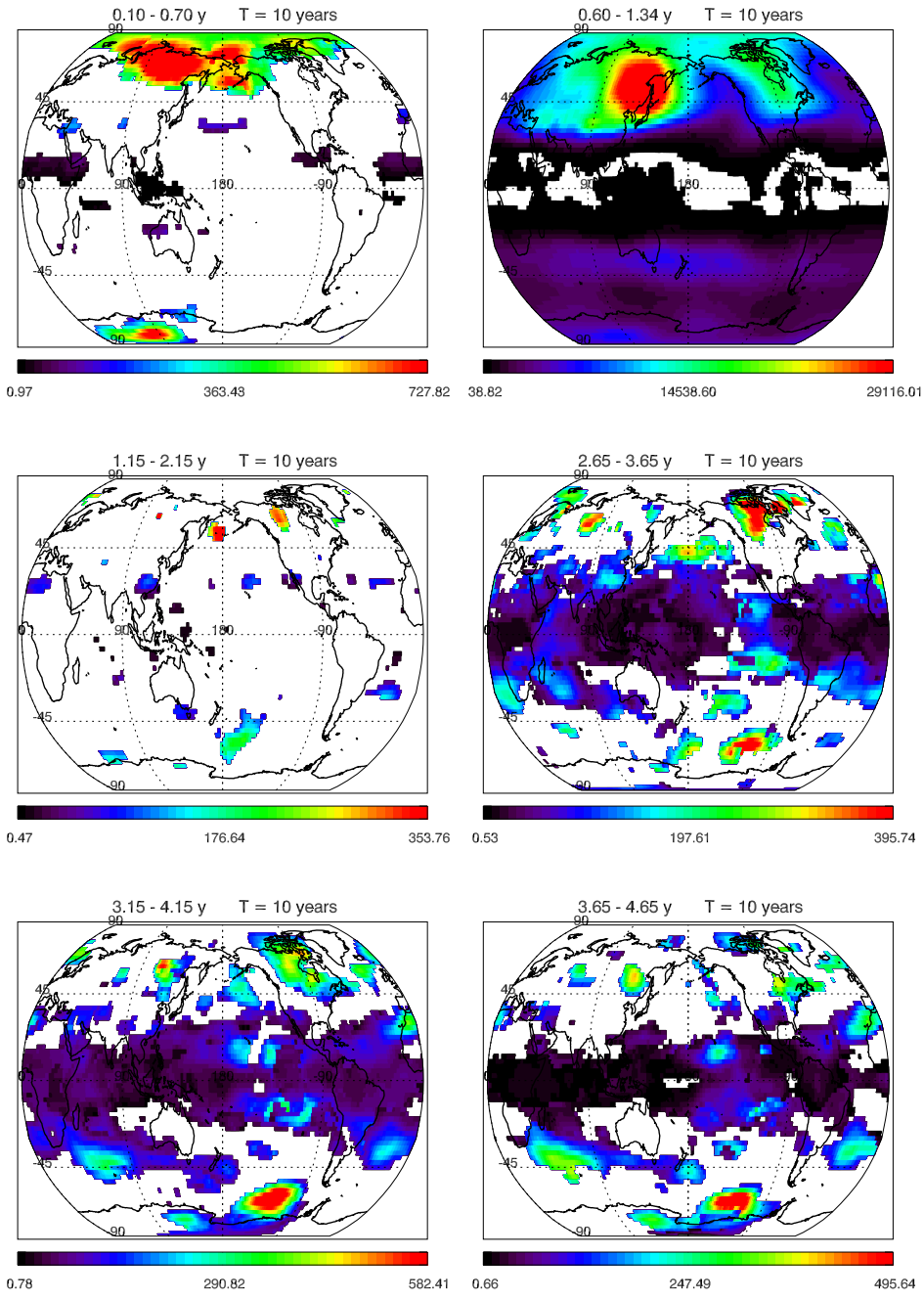

Figure *A.1:* Geographical regions of distinct oscillations in the temperature field at 500 hPa lasting 10 years at least (the colored scale represents the wavelet power)

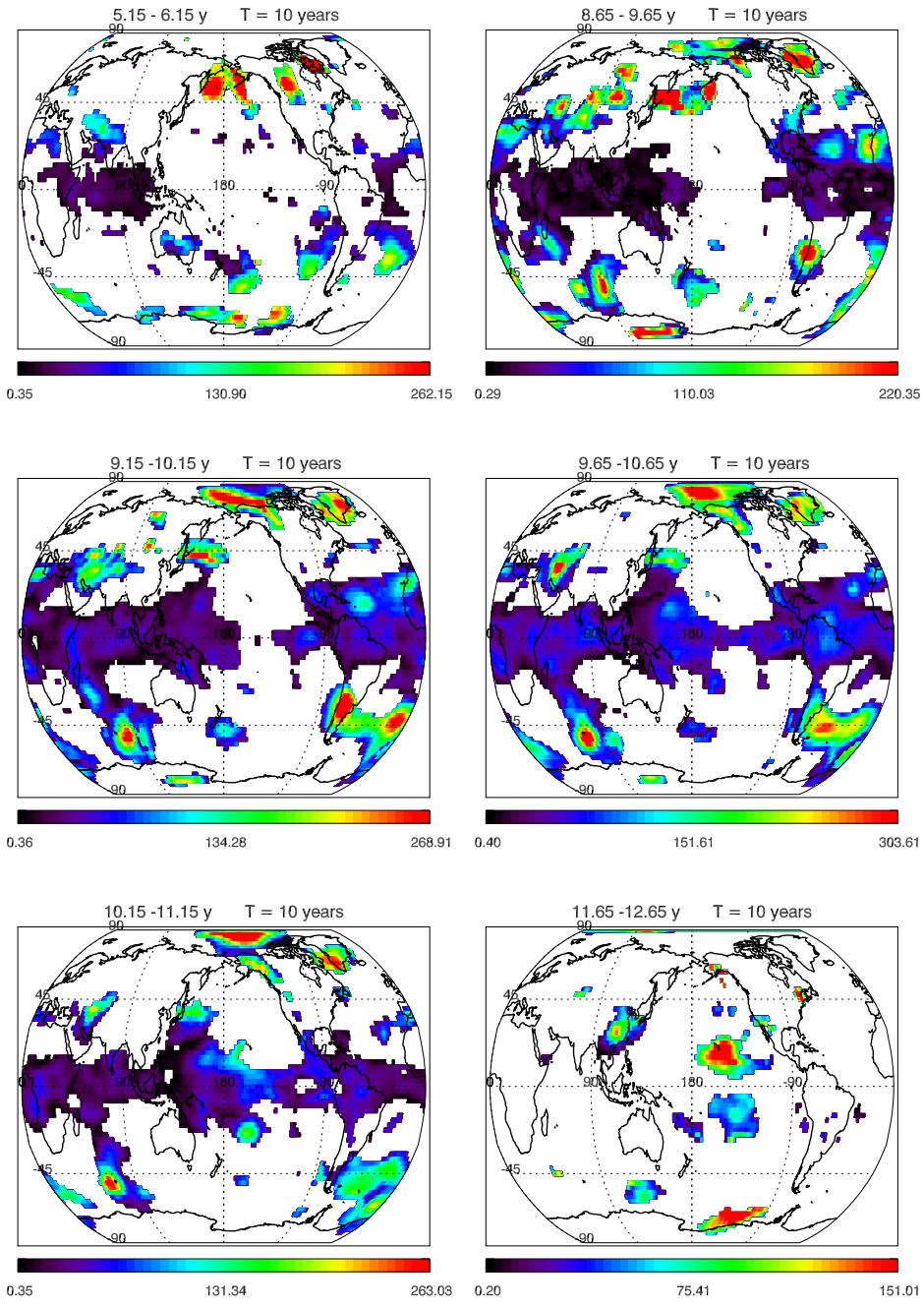

Figure *A*.**2:** Geographical regions of distinct oscillations in the temperature field at 500 hPa lasting 10 years at least (the colored scale represents the wavelet power)

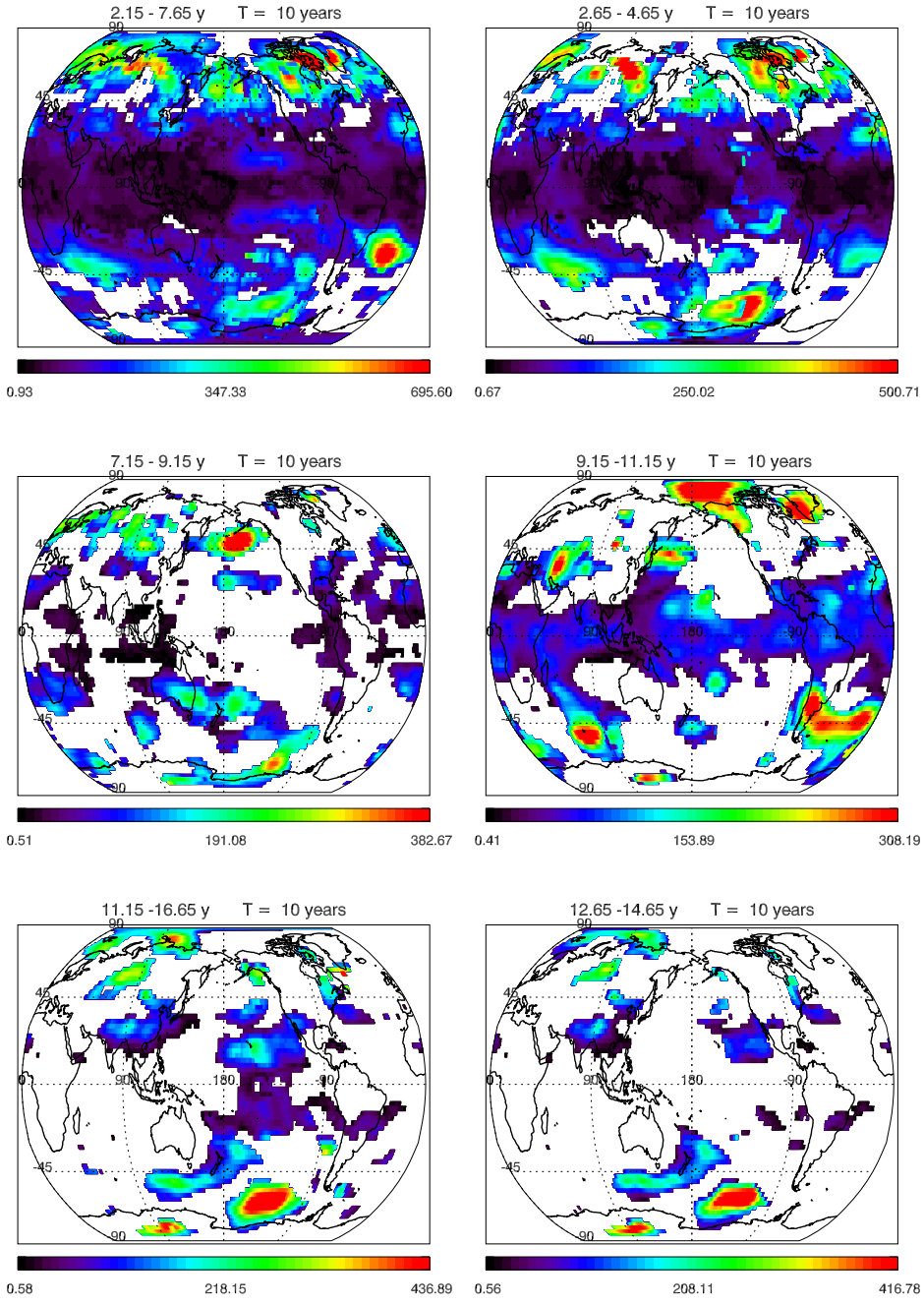

Figure *A.3:* Geographical regions of distinct oscillations in the temperature field at 500 hPa lasting 10 years at least (the colored scale represents the wavelet power)

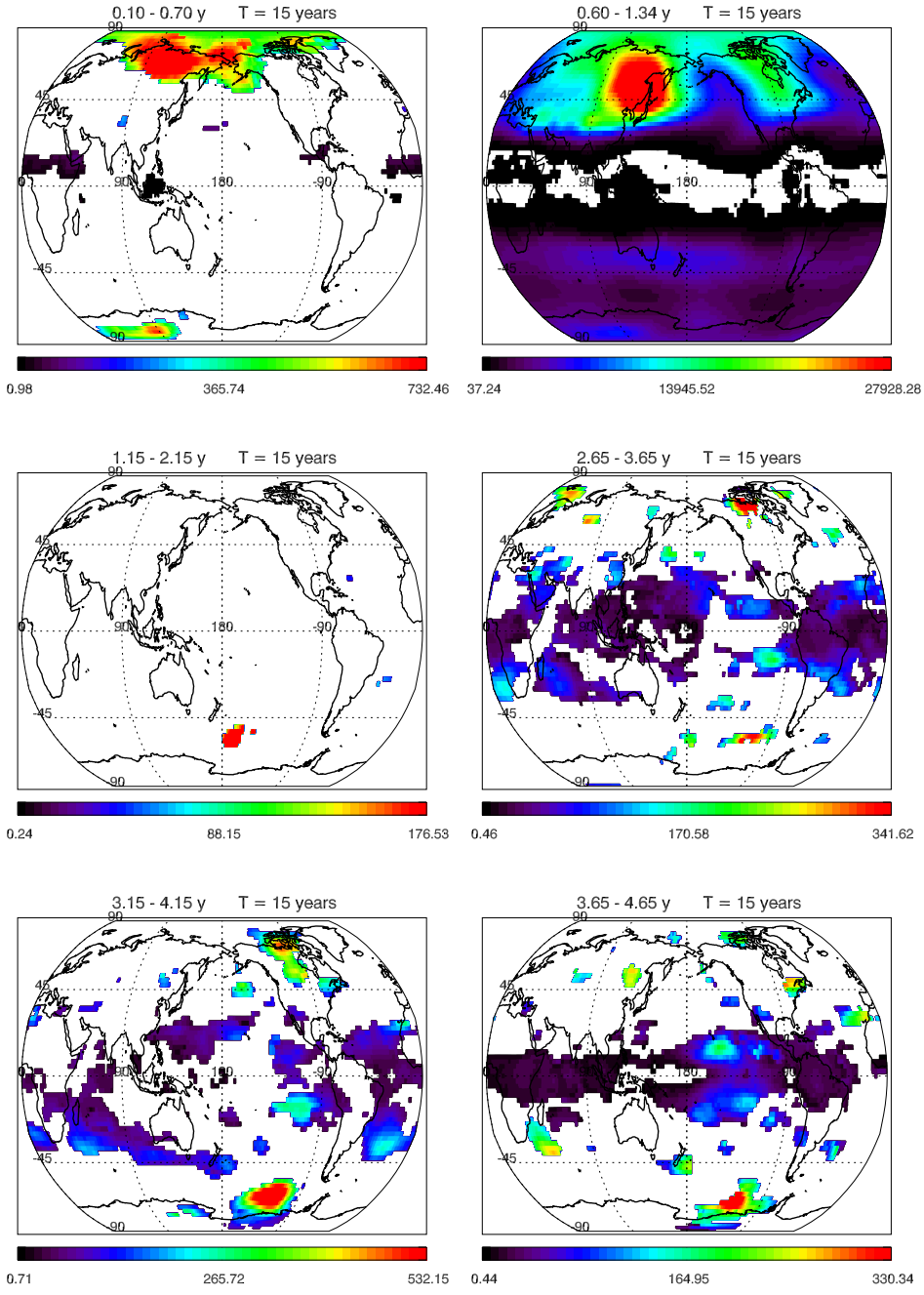

Figure *A.4:* Geographical regions of distinct oscillations in the temperature field at 500 hPa lasting 15 years at least (the colored scale represents the wavelet power)

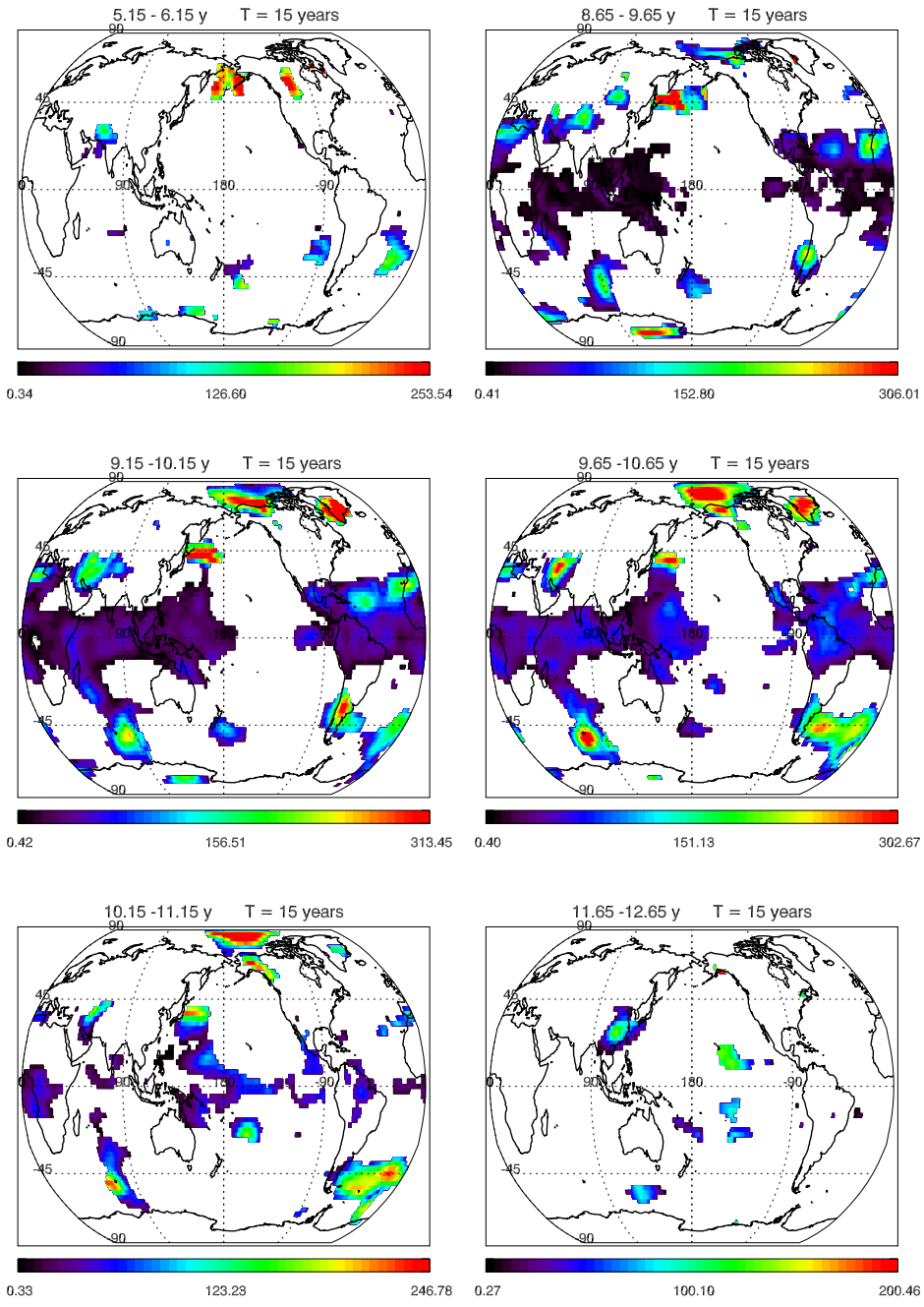

Figure *A.5:* Geographical regions of distinct oscillations in the temperature field at 500 hPa lasting 15 years at least (the colored scale represents the wavelet power)

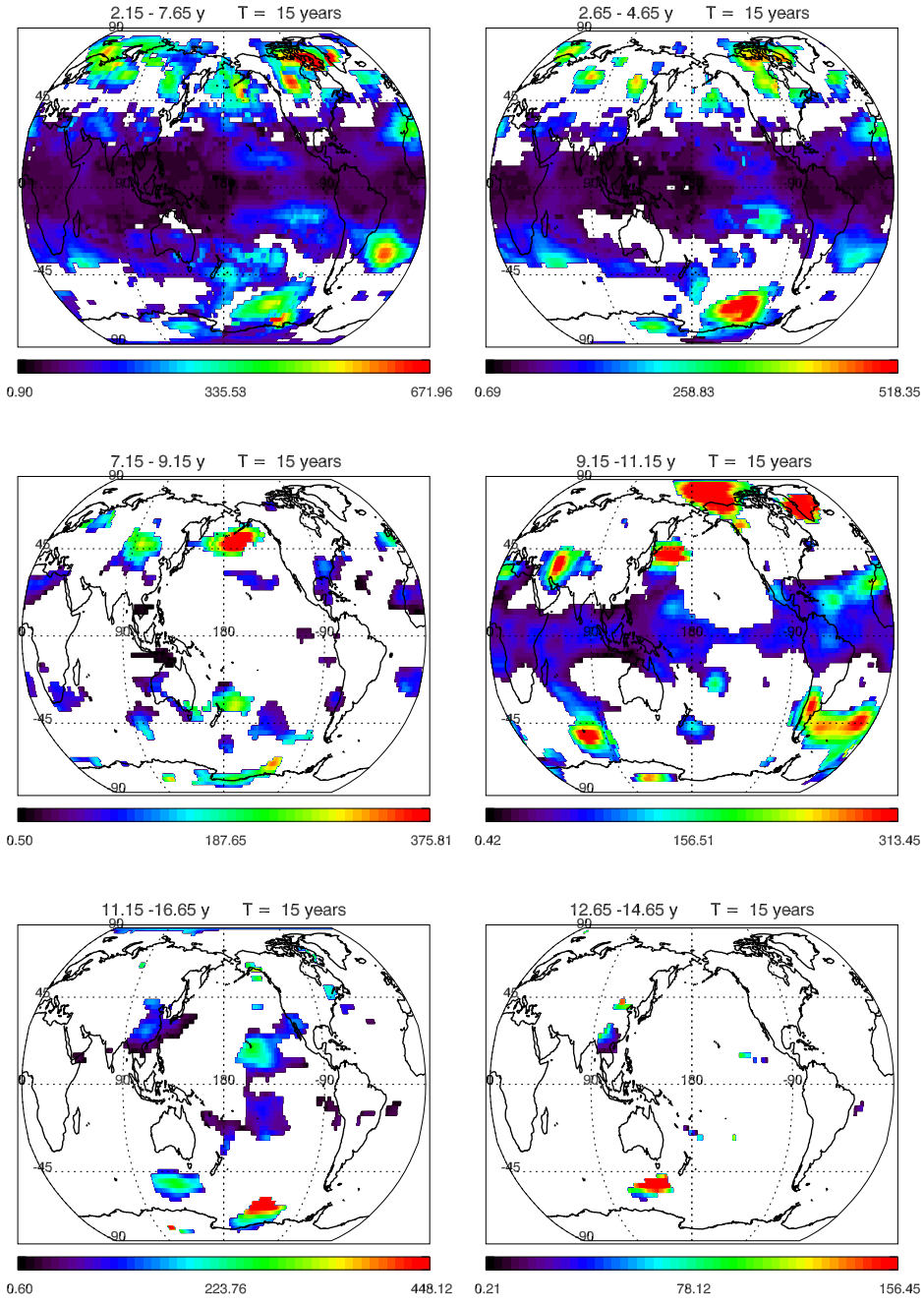

Figure *A*.**6:** Geographical regions of distinct oscillations in the temperature field at 500 hPa lasting 15 years at least (the colored scale represents the wavelet power)

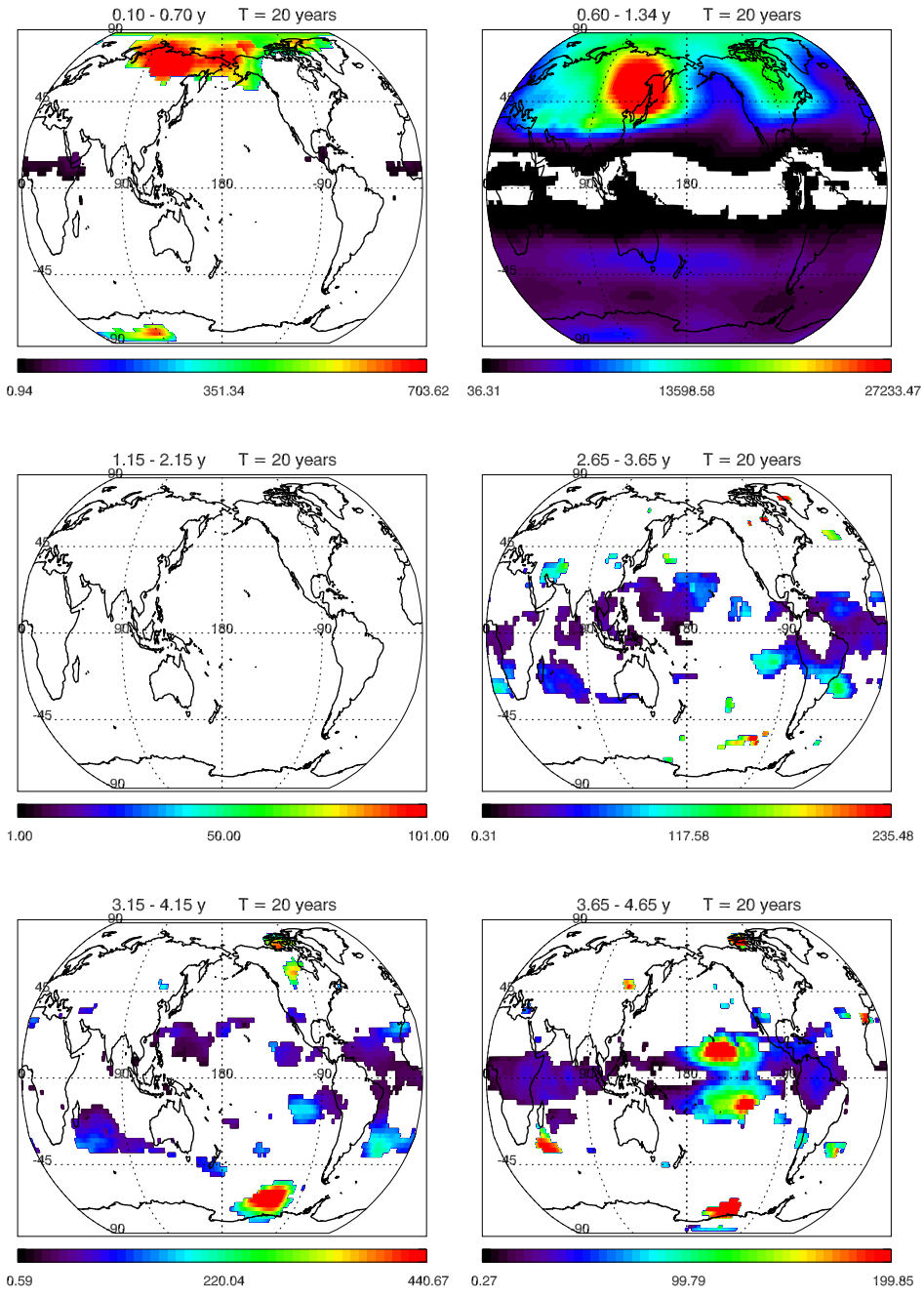

Figure *A*.**7:** Geographical regions of distinct oscillations in the temperature field at 500 hPa lasting 20 years at least (the colored scale represents the wavelet power)

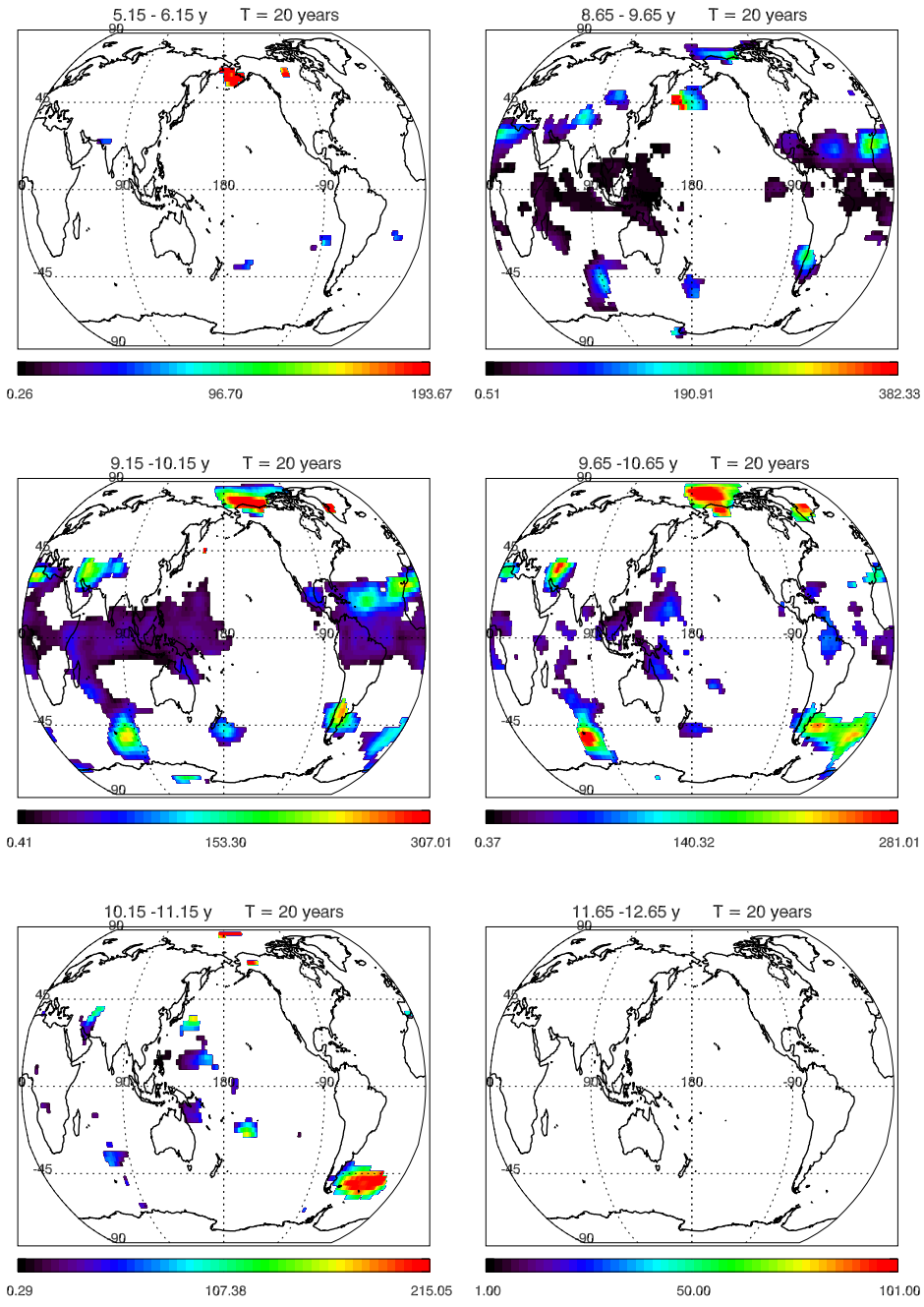

Figure *A*.**8:** Geographical regions of distinct oscillations in the temperature field at 500 hPa lasting 20 years at least (the colored scale represents the wavelet power)

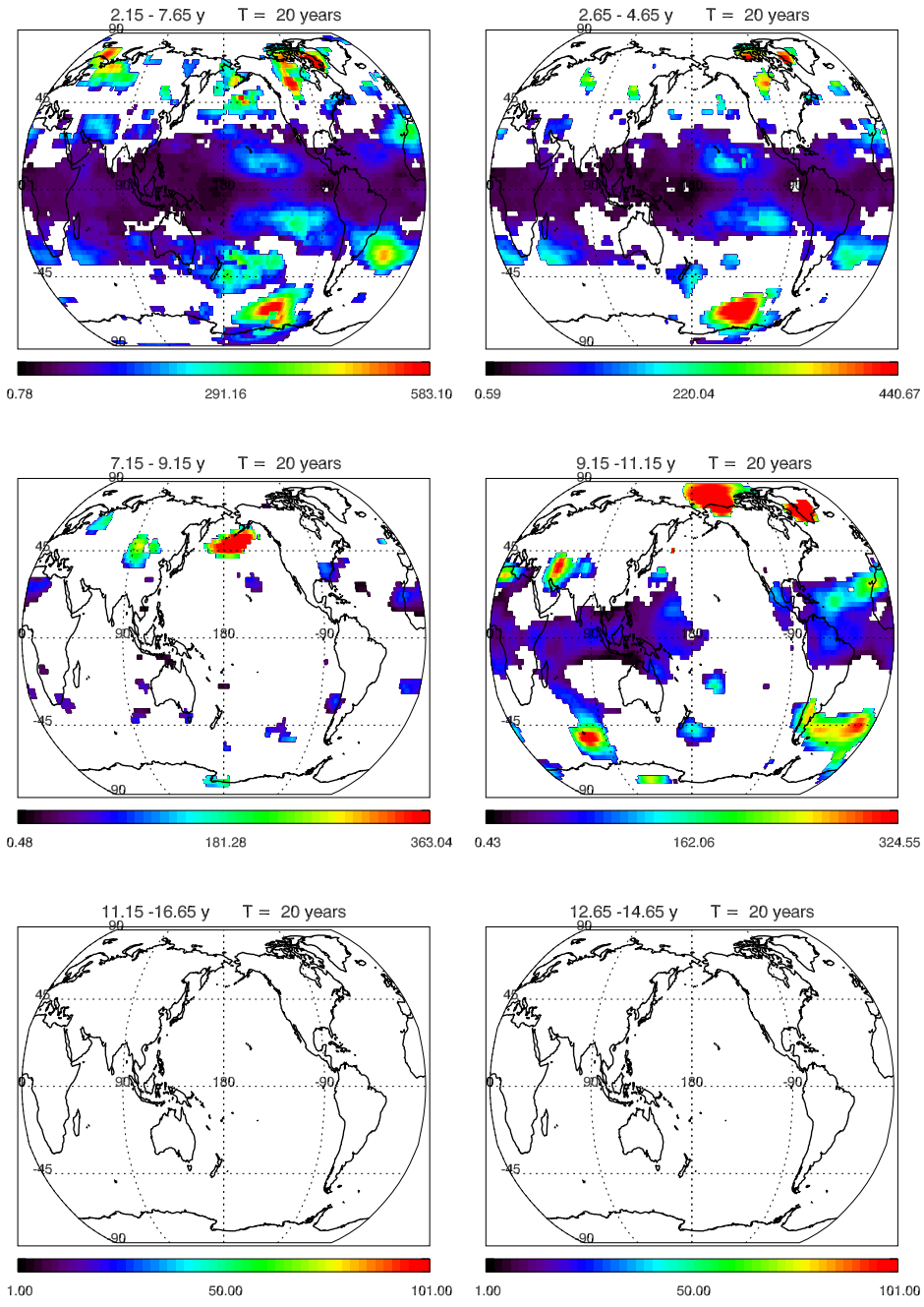

Figure *A*.**9:** Geographical regions of distinct oscillations in the temperature field at 500 hPa lasting 20 years at least (the colored scale represents the wavelet power)

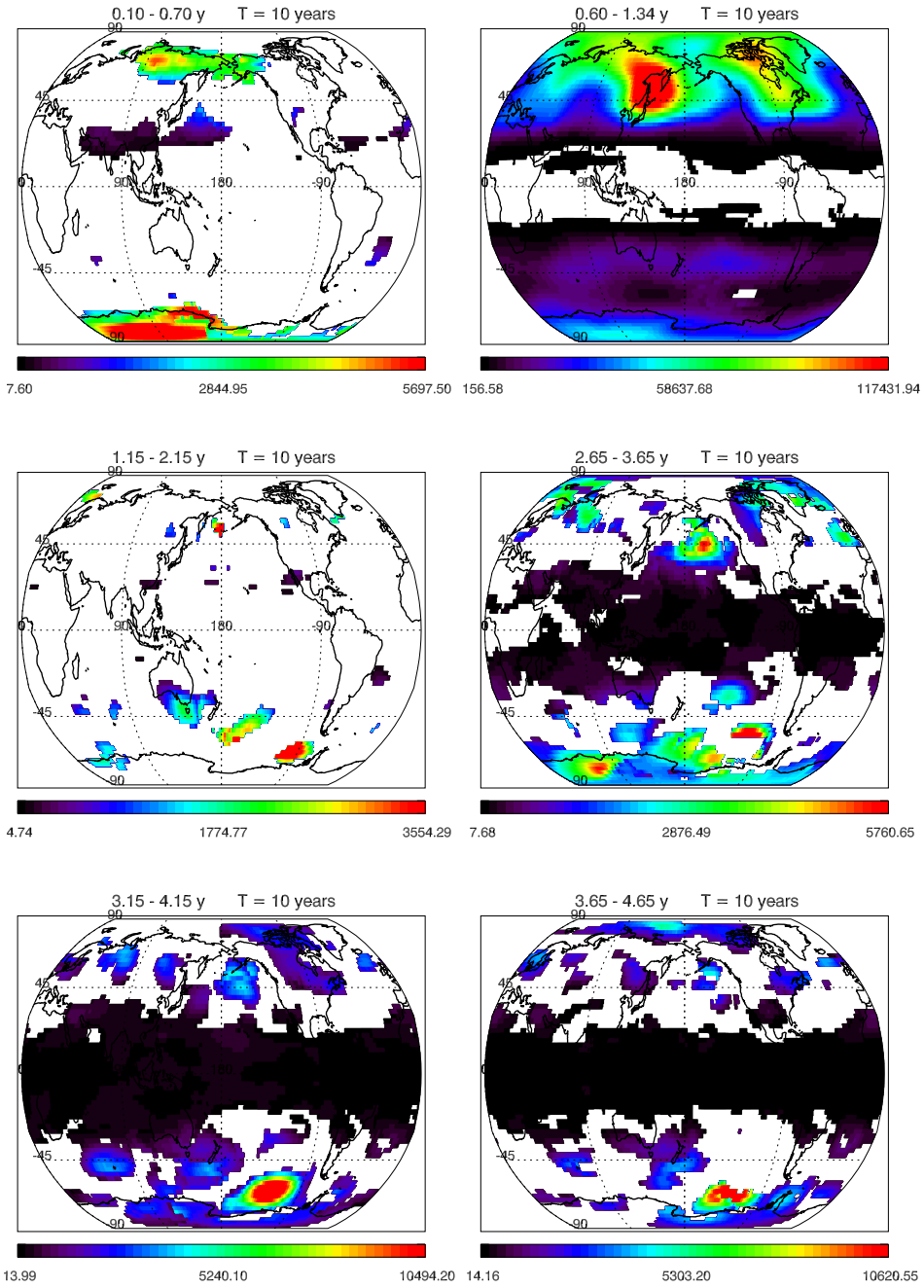

Figure *A*.**10:** Geographical regions of distinct oscillations in the geopotential heights field at 500 hPa lasting 10 years at least (the colored scale represents the wavelet power)

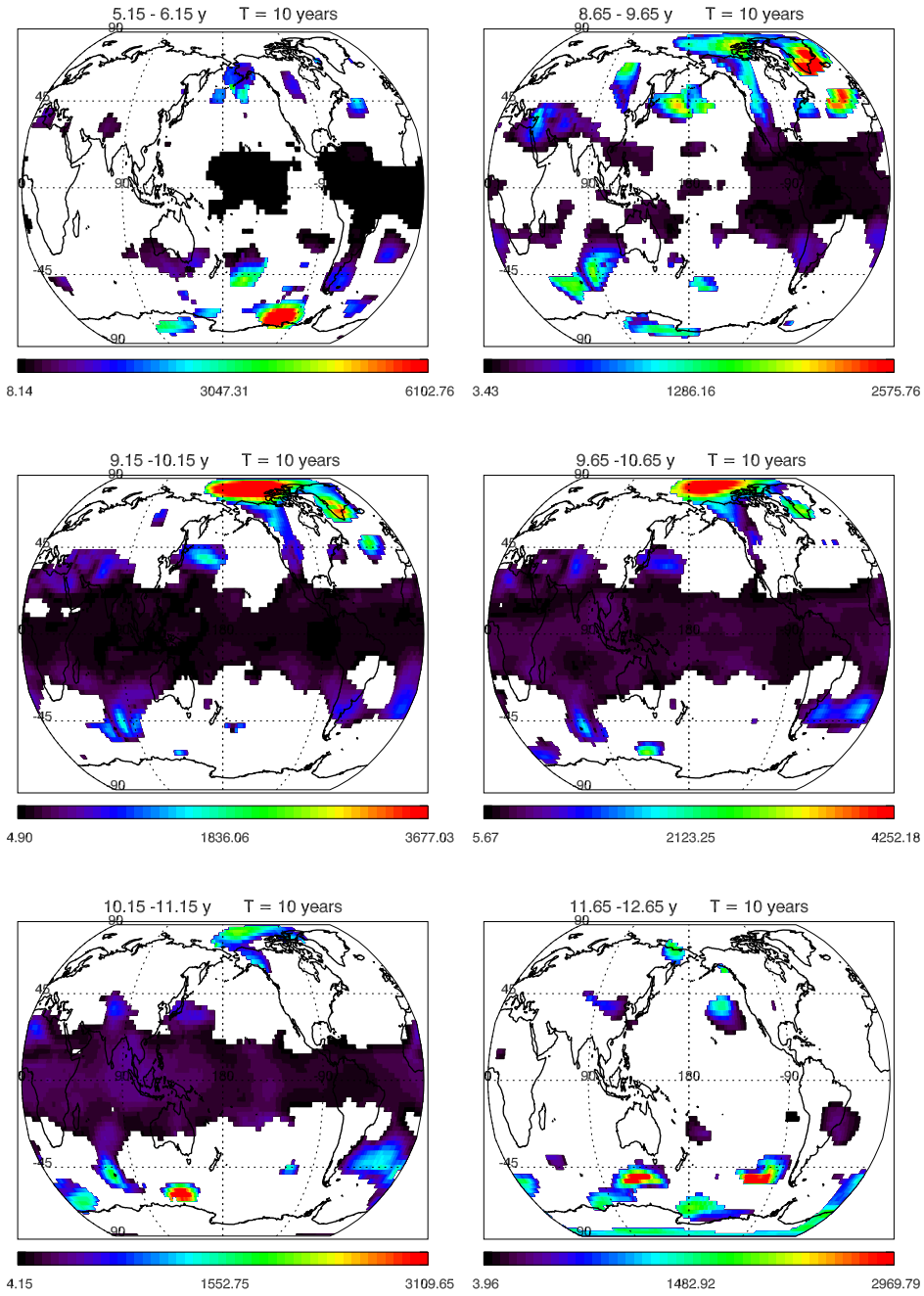

Figure *A.11:* Geographical regions of distinct oscillations in the geopotential heights field at 500 hPa lasting 10 years at least (the colored scale represents the wavelet power)

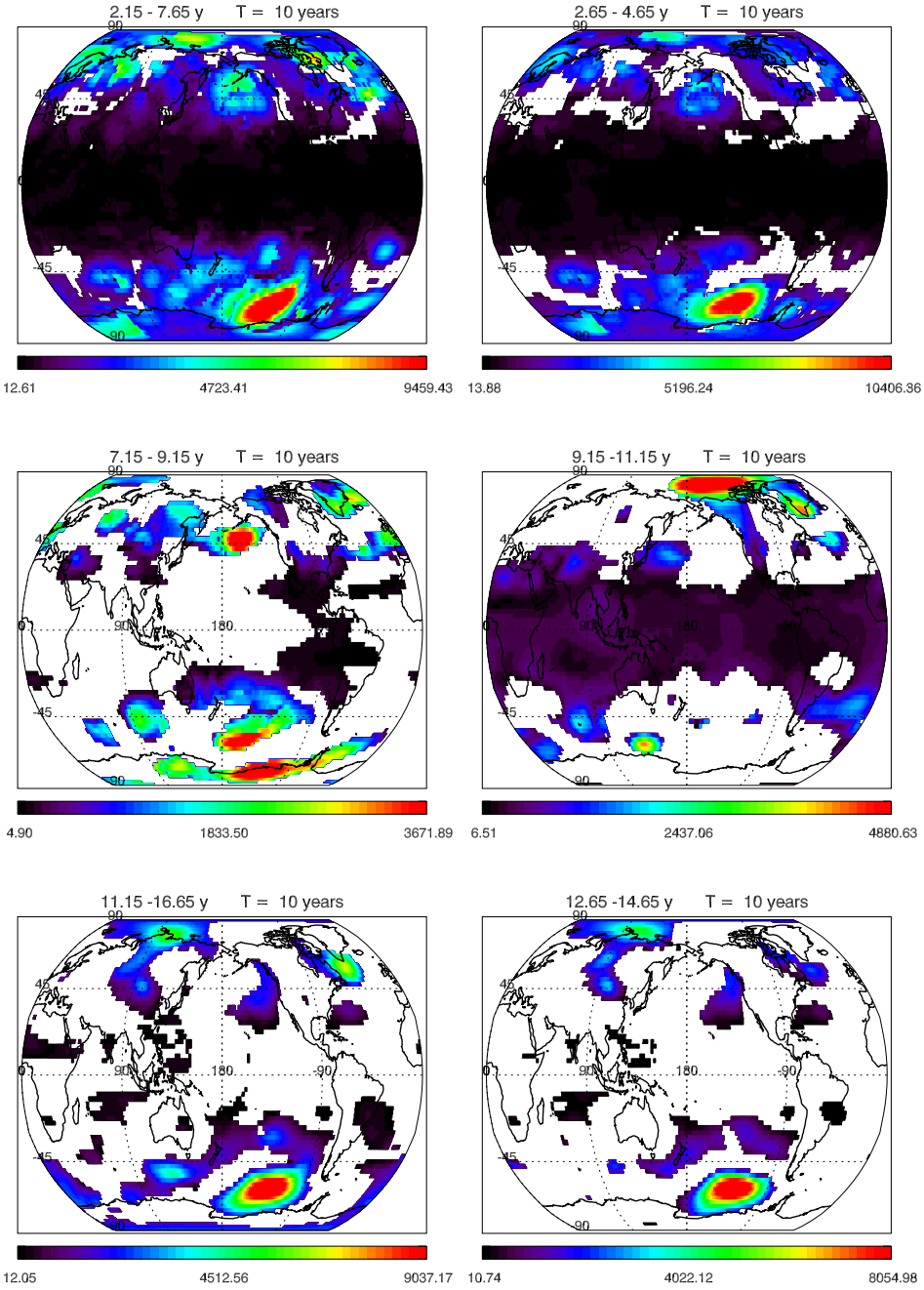

Figure *A*.**12:** Geographical regions of distinct oscillations in the geopotential heights field at 500 hPa lasting 10 years at least (the colored scale represents the wavelet power)

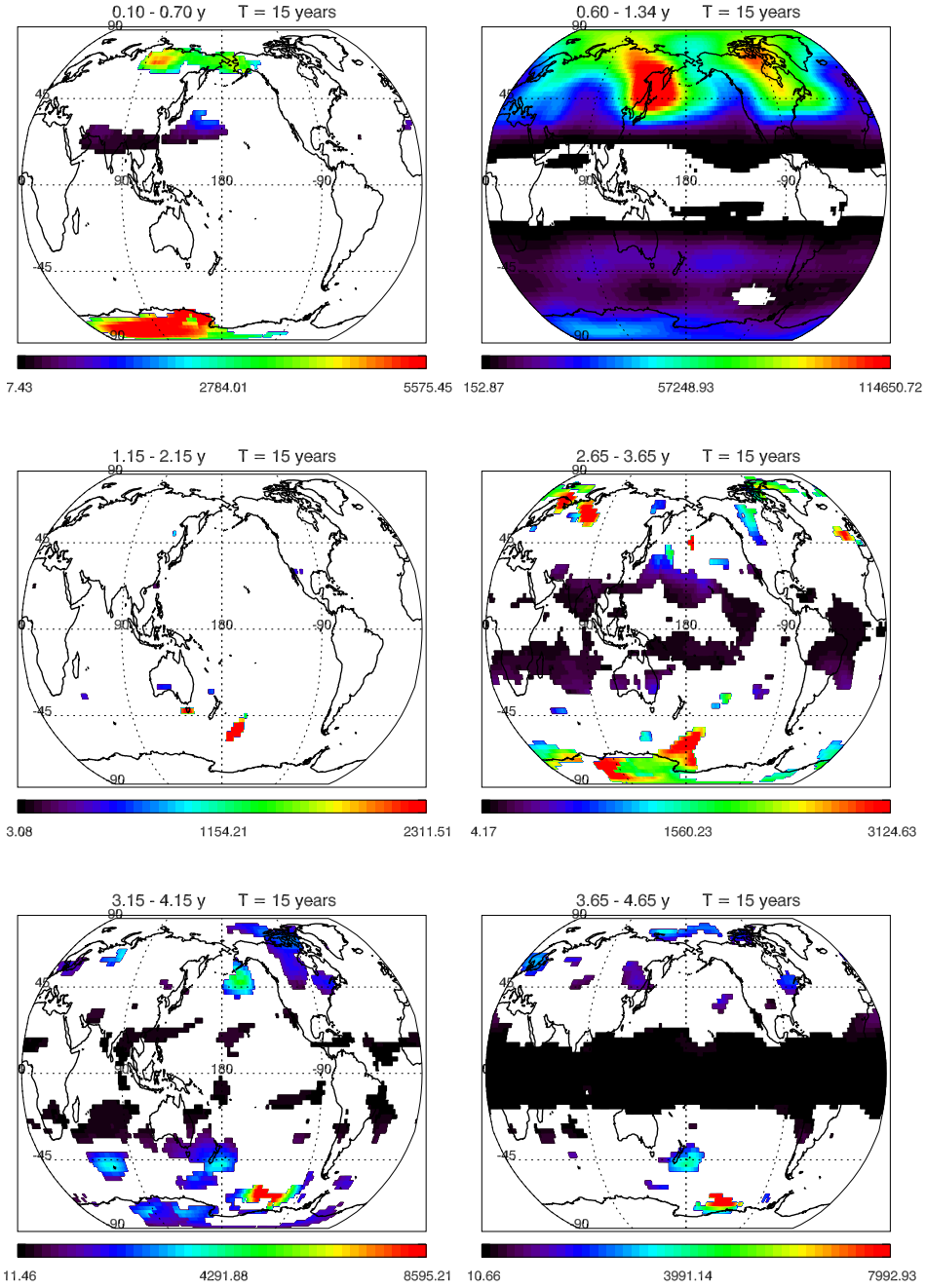

Figure *A*.**13:** Geographical regions of distinct oscillations in the geopotential heights field at 500 hPa lasting 15 years at least (the colored scale represents the wavelet power)

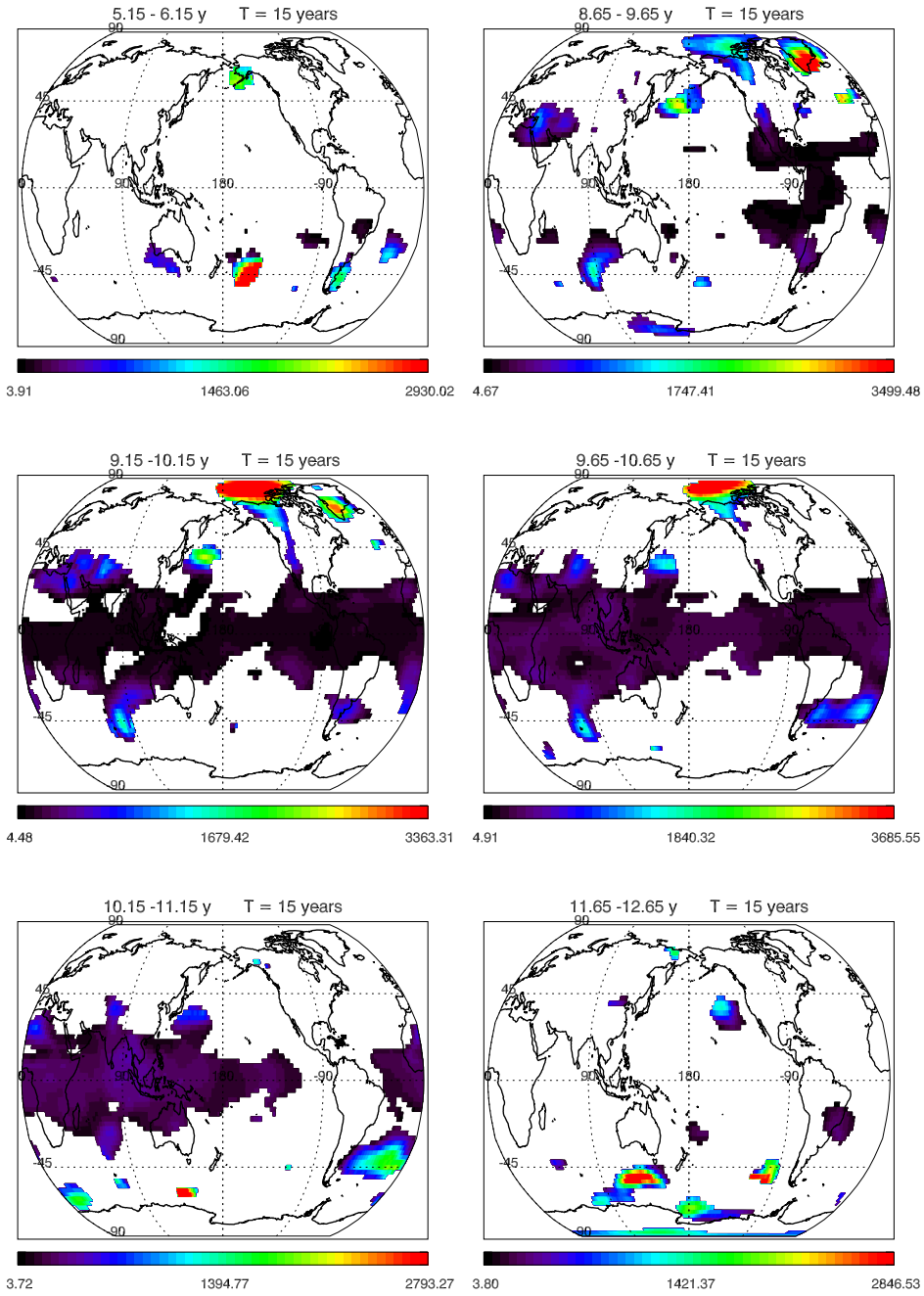

Figure *A.14:* Geographical regions of distinct oscillations in the geopotential heights field at 500 hPa lasting 15 years at least (the colored scale represents the wavelet power)

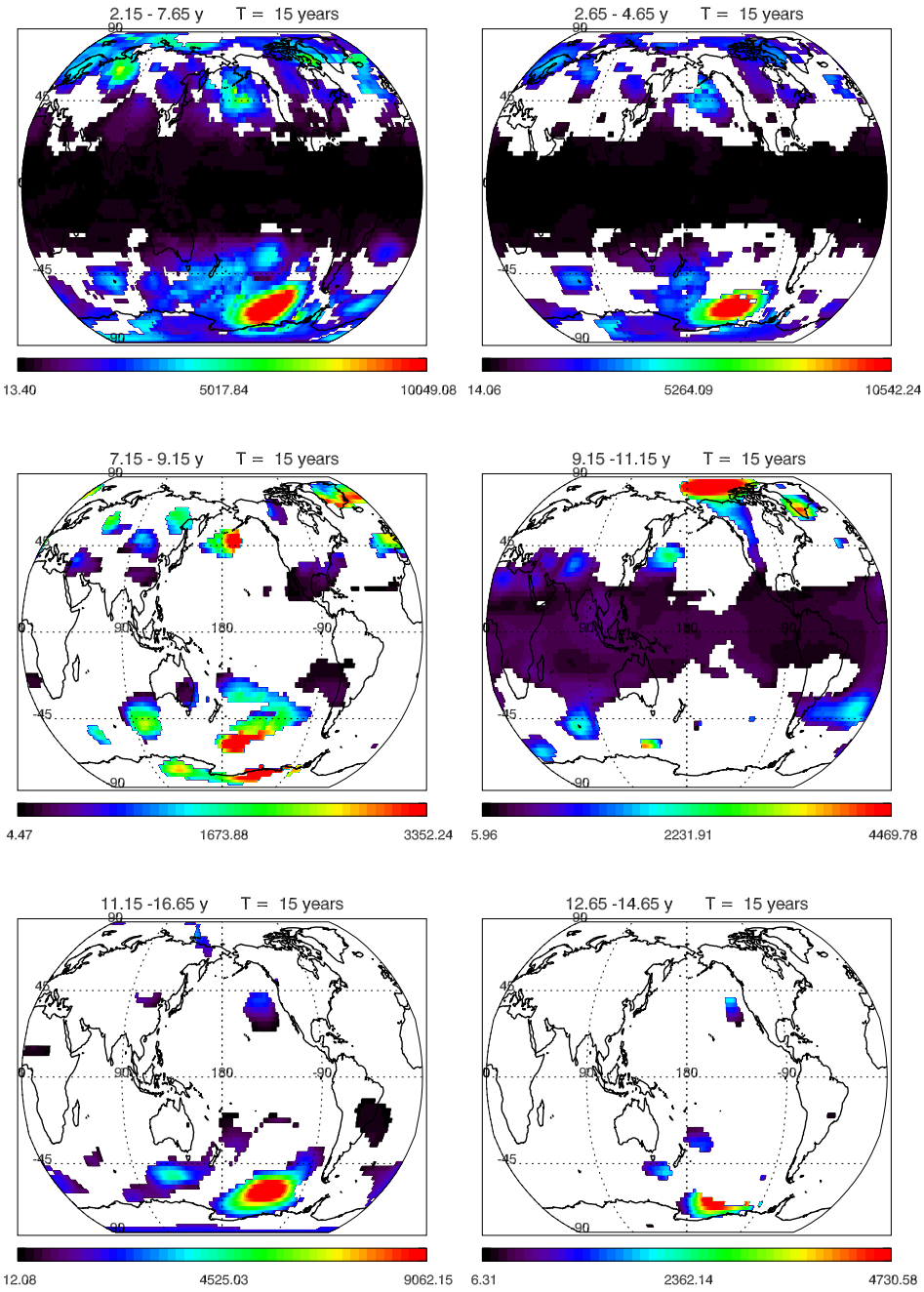

Figure *A.15:* Geographical regions of distinct oscillations in the geopotential heights field at 500 hPa lasting 15 years at least (the colored scale represents the wavelet power)

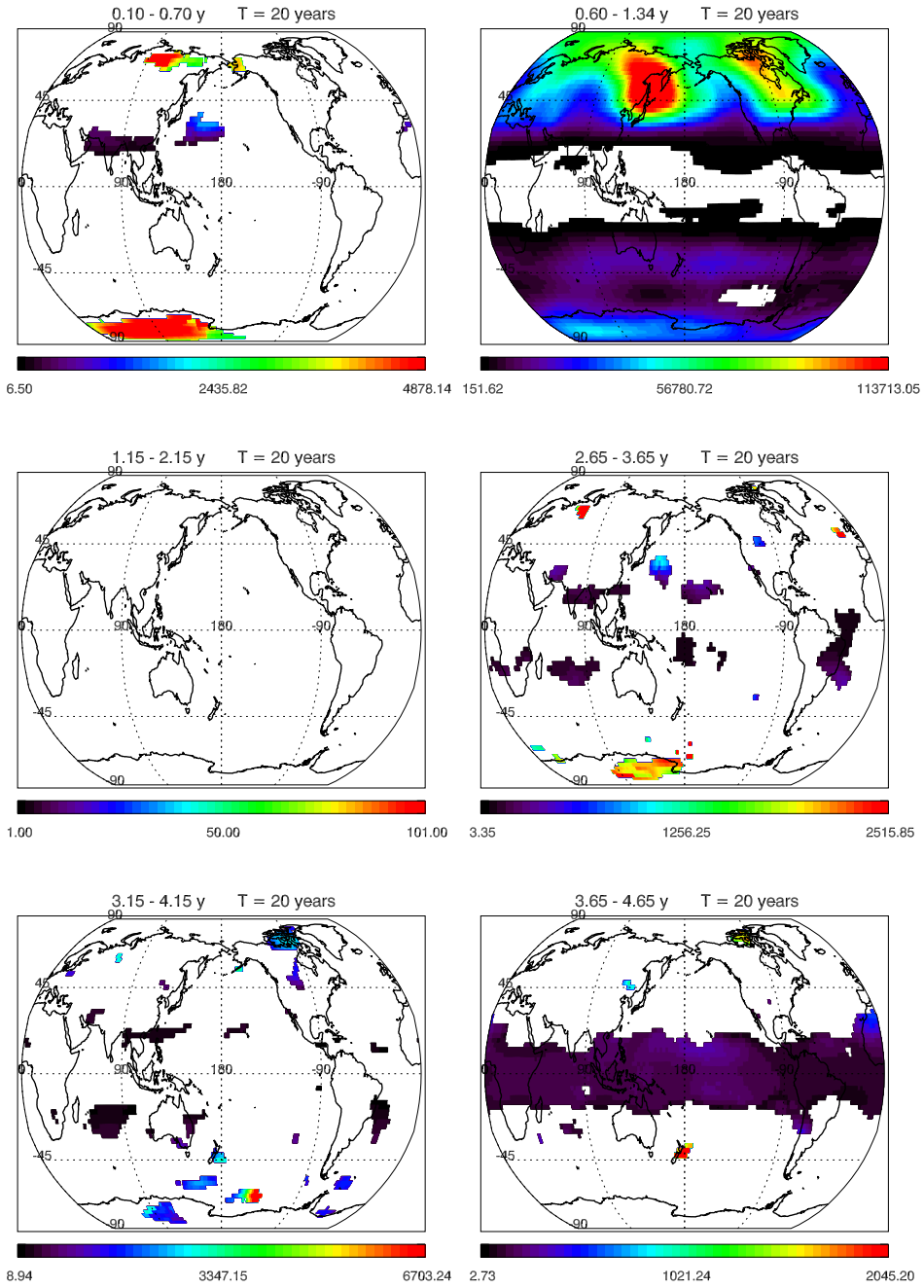

Figure *A*.**16:** Geographical regions of distinct oscillations in the geopotential heights field at 500 hPa lasting 20 years at least (the colored scale represents the wavelet power)

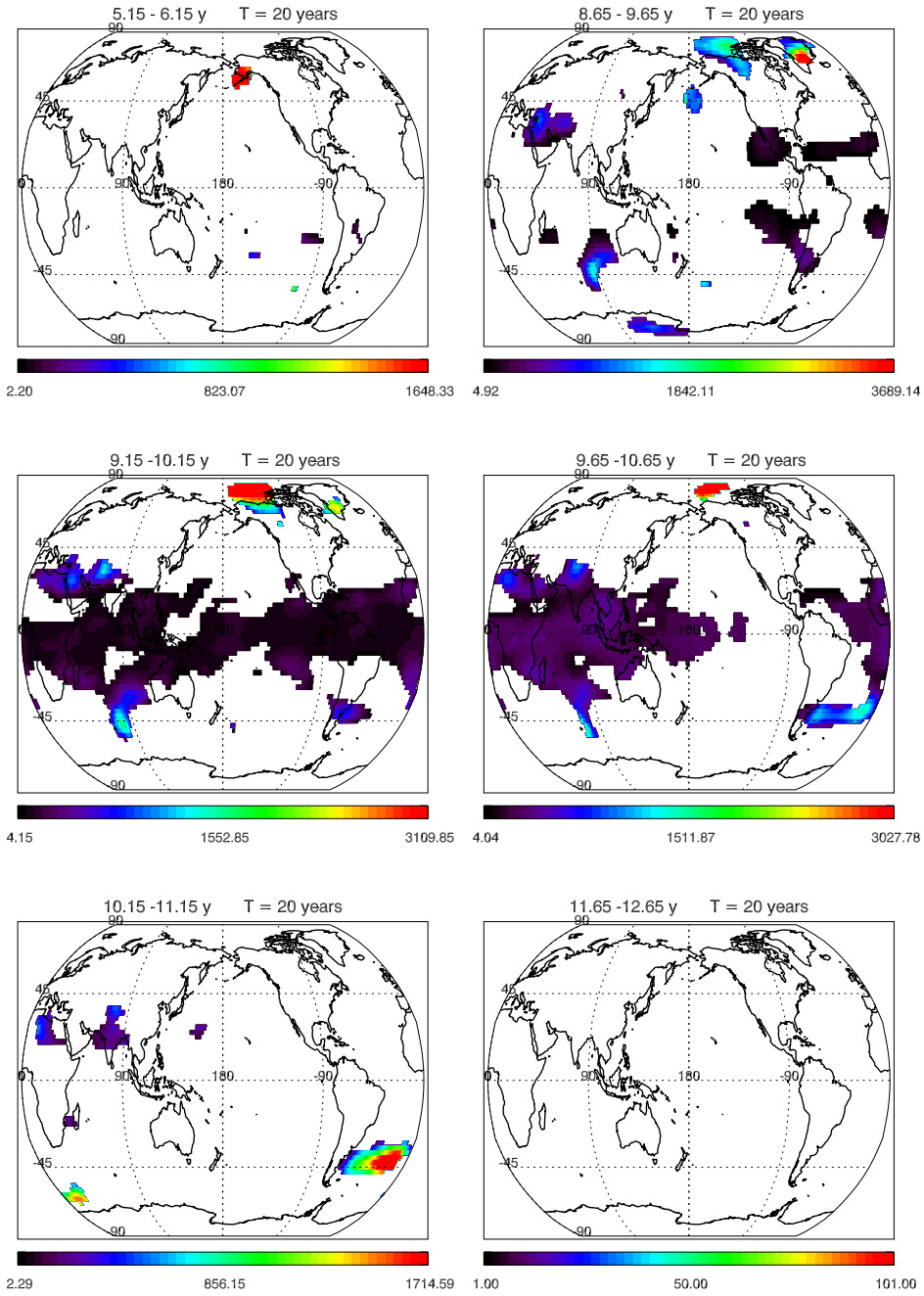

Figure *A*.**17:** Geographical regions of distinct oscillations in the geopotential heights field at 500 hPa lasting 20 years at least (the colored scale represents the wavelet power)

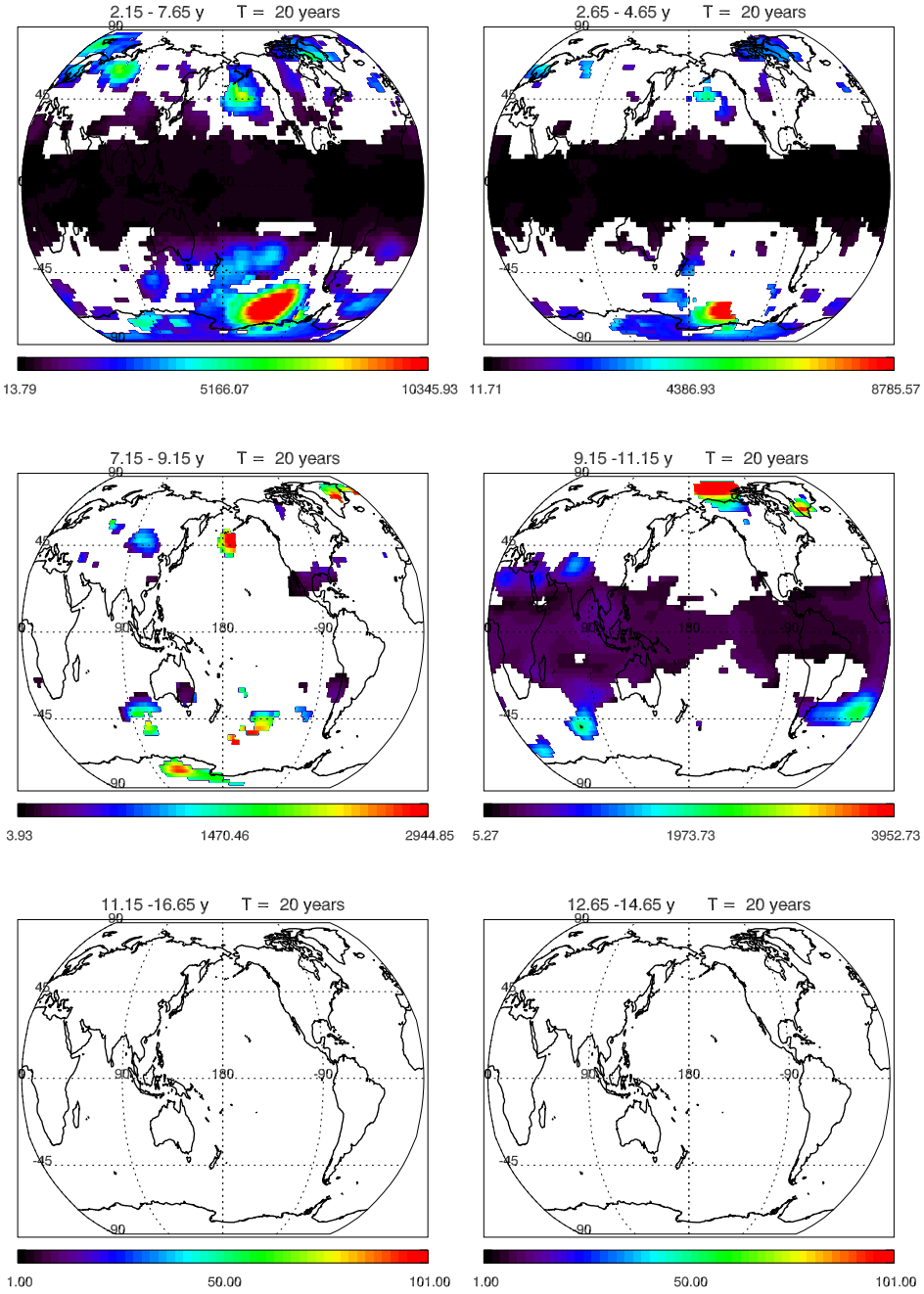

Figure *A.18:* Geographical regions of distinct oscillations in the geopotential heights field at 500 hPa lasting 20 years at least (the colored scale represents the wavelet power)

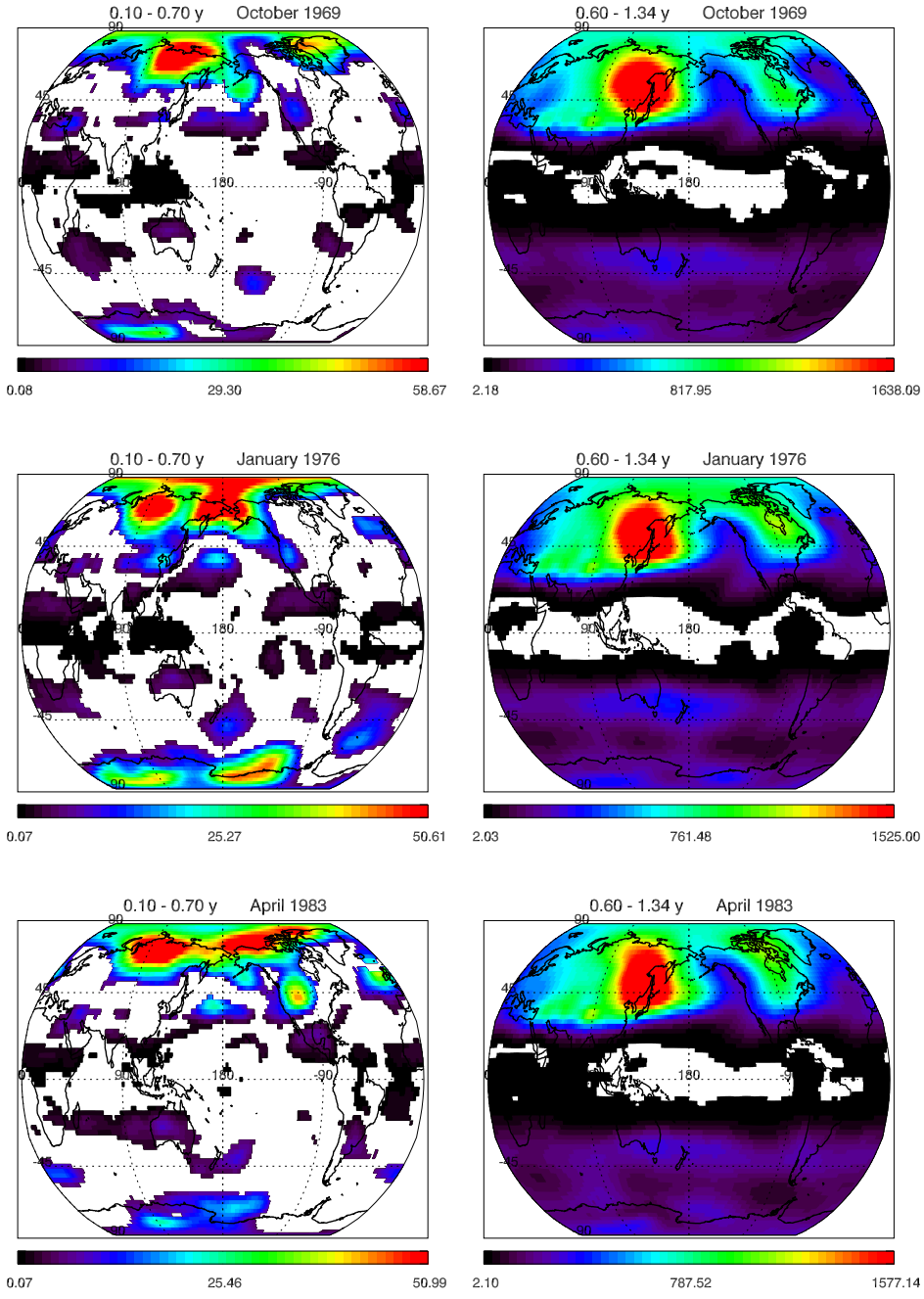

Figure *A*.**19:** Temporal evolution of geographical regions of different oscillations in the temperature field at 500 hPa (the colored scale represents the wavelet power)

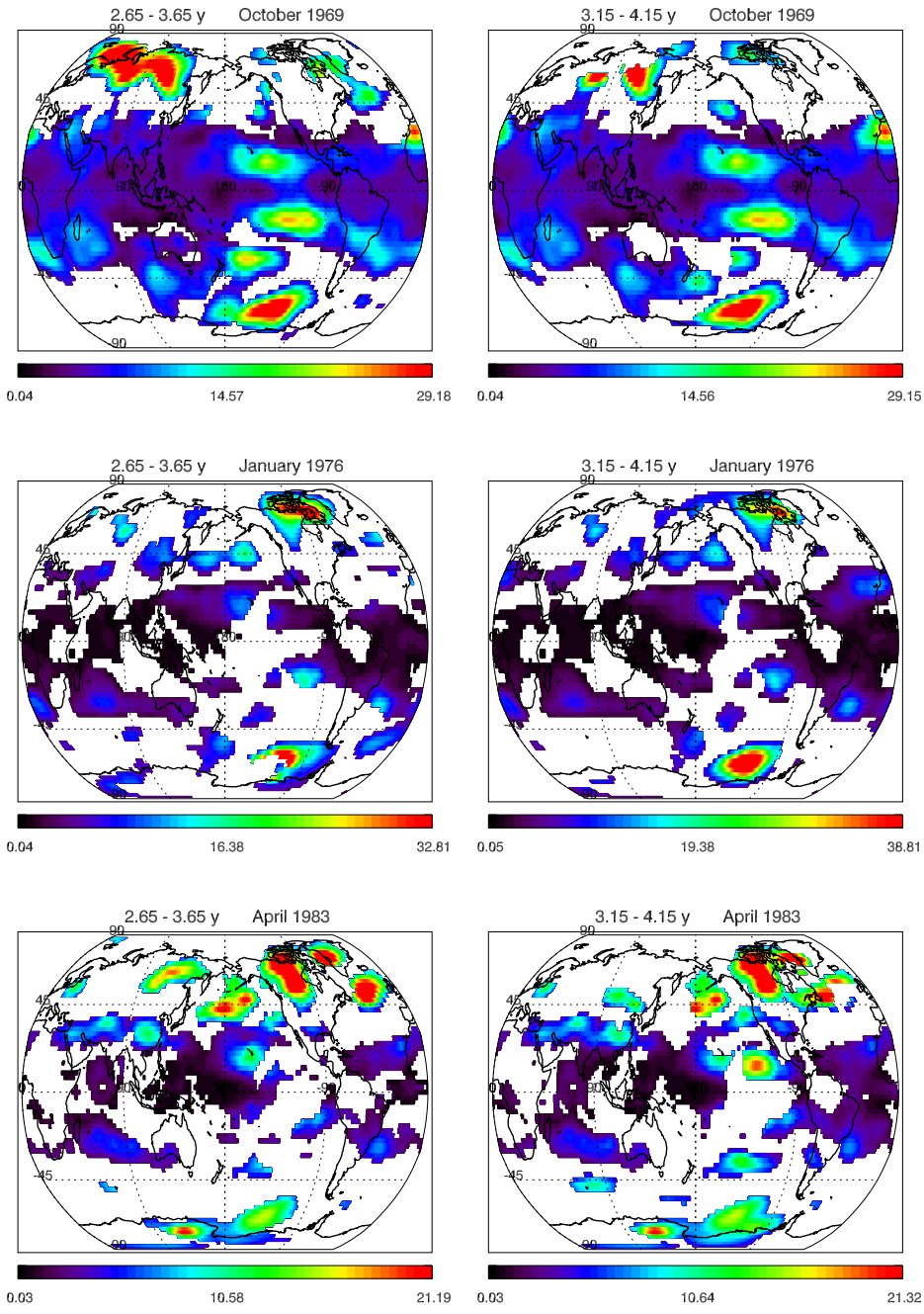

Figure *A*.20: Temporal evolution of geographical regions of different oscillations in the temperature field at 500 hPa (the colored scale represents the wavelet power)

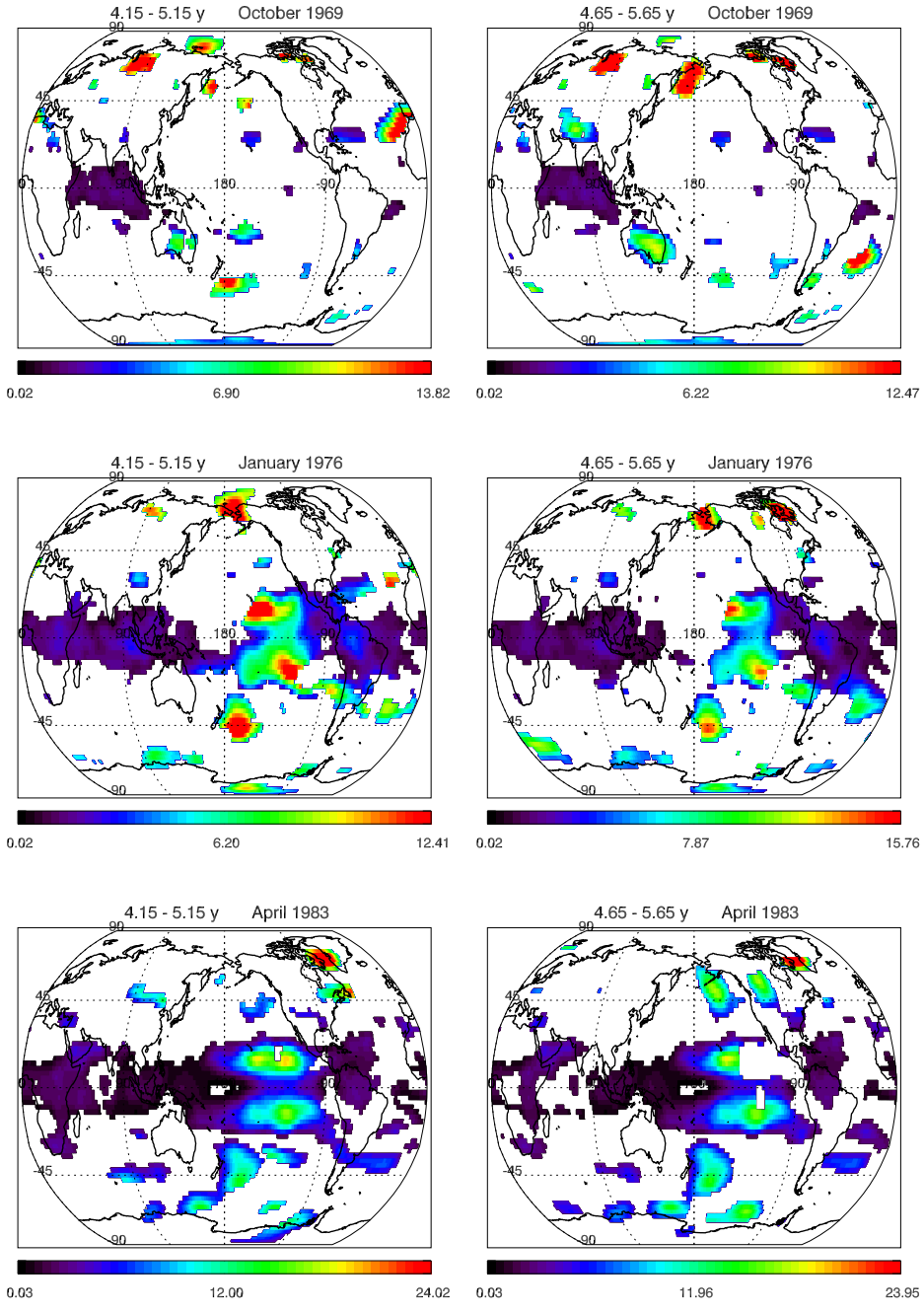

Figure *A*.**21:** Temporal evolution of geographical regions of different oscillations in the temperature field at 500 hPa (the colored scale represents the wavelet power)

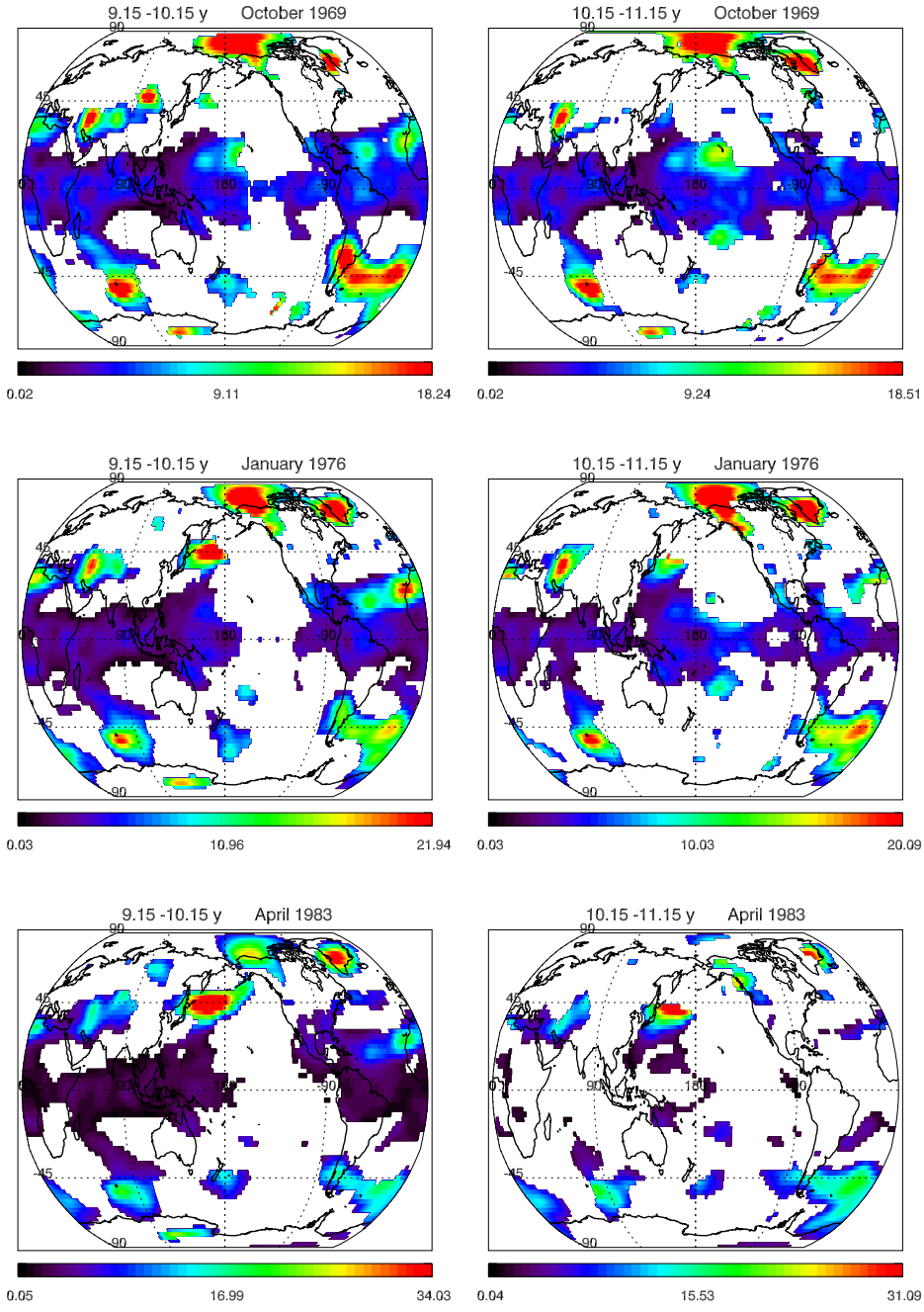

Figure *A*.**22:** Temporal evolution of geographical regions of different oscillations in the temperature field at 500 hPa (the colored scale represents the wavelet power)

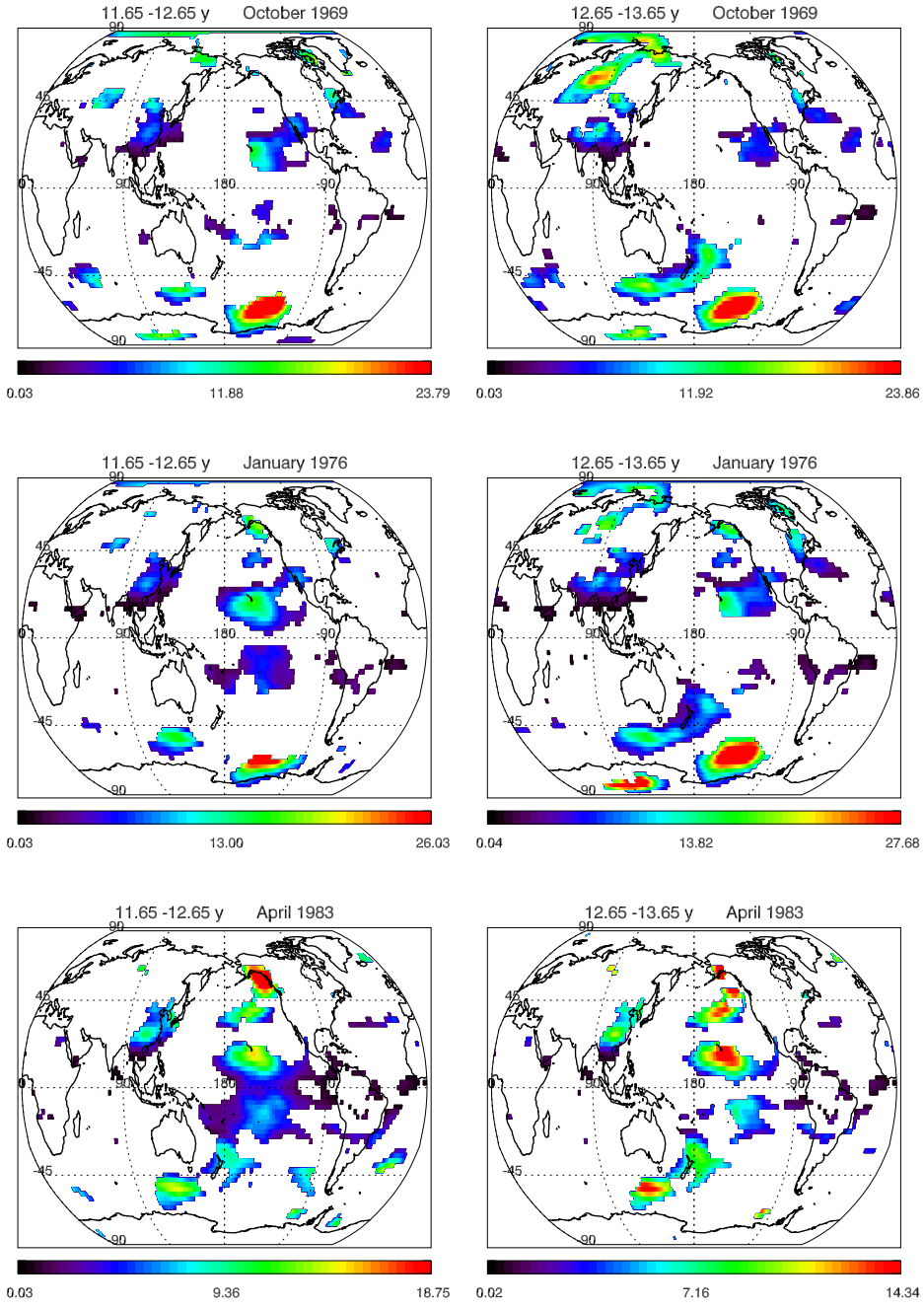

Figure *A*.23: Temporal evolution of geographical regions of different oscillations in the temperature field at 500 hPa (the colored scale represents the wavelet power)

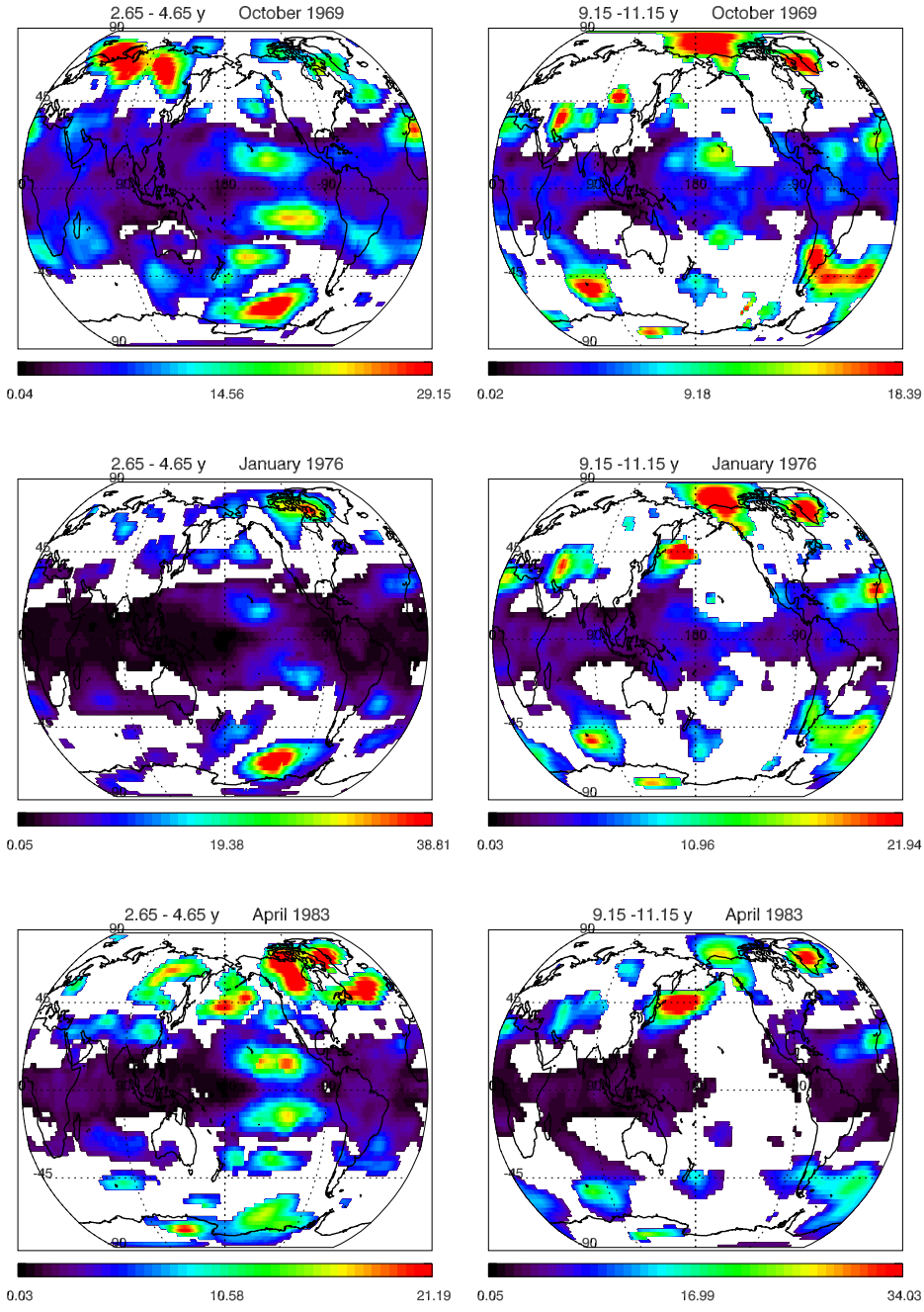

Figure *A*.**24:** Temporal evolution of geographical regions of different oscillations in the temperature field at 500 hPa (the colored scale represents the wavelet power)

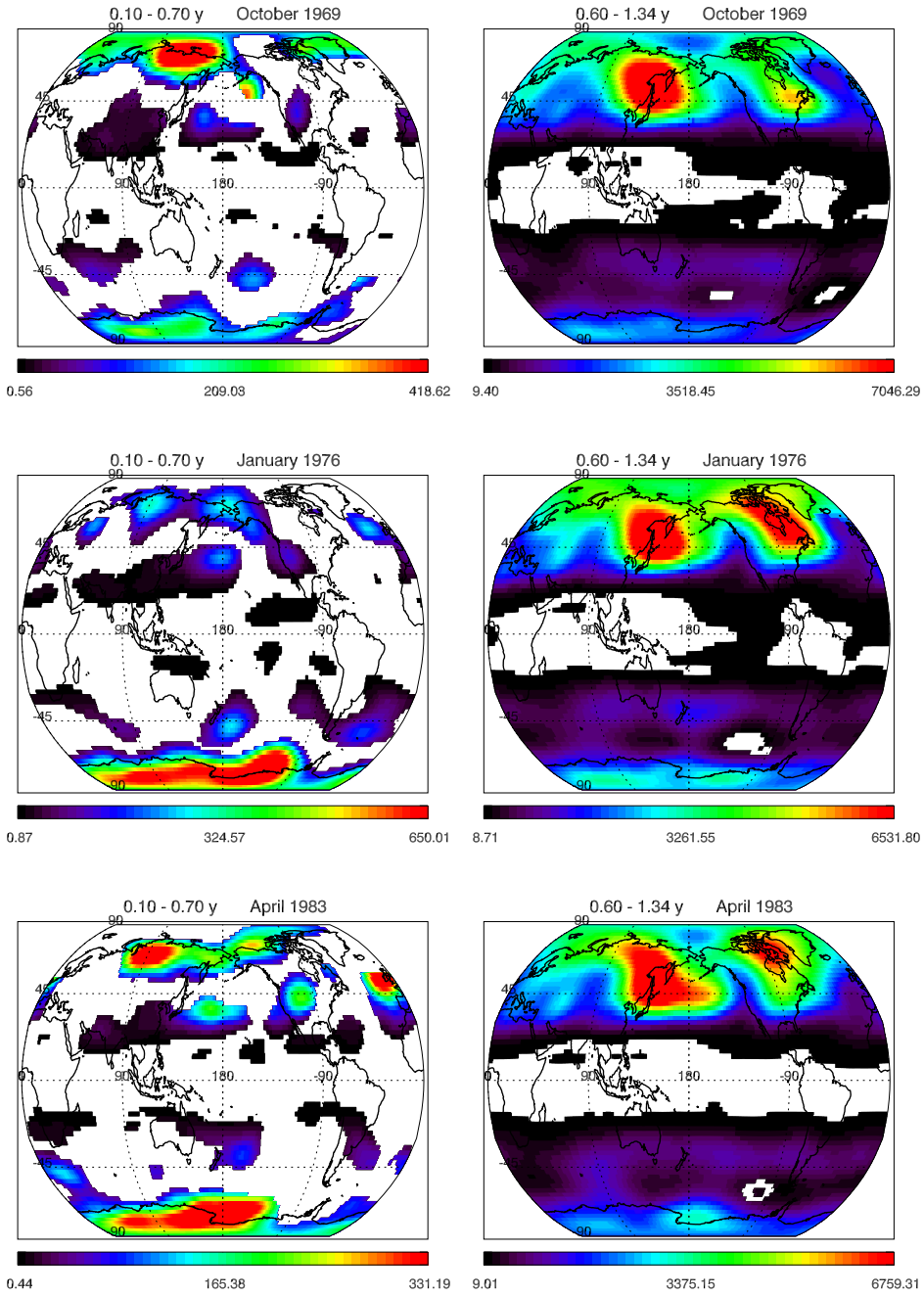

Figure *A*.**25:** Temporal evolution of geographical regions of different oscillations in the geopotential heights field at 500 hPa (the colored scale represents the wavelet power)

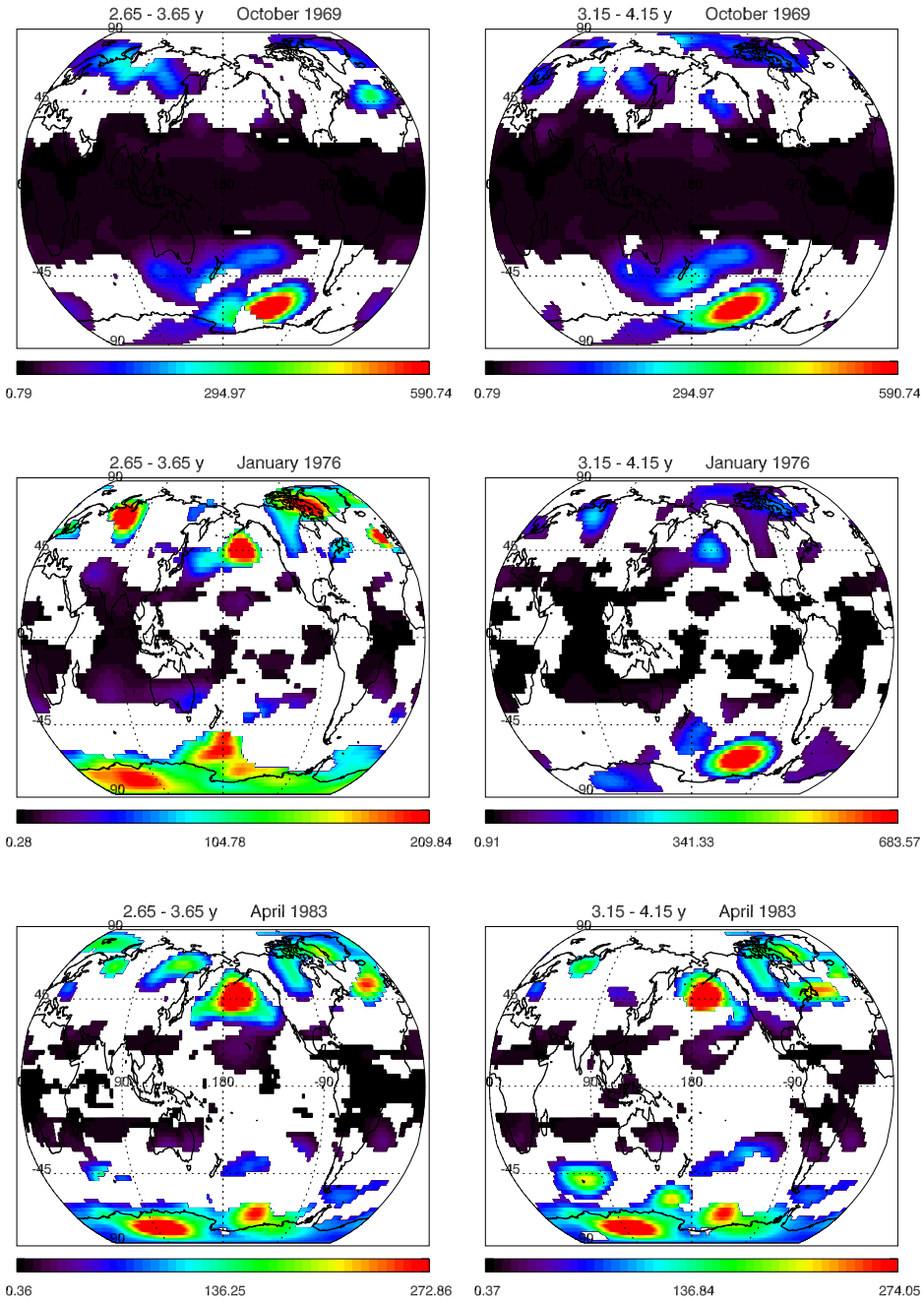

Figure *A*.**26:** Temporal evolution of geographical regions of different oscillations in the geopotential heights field at 500 hPa (the colored scale represents the wavelet power)

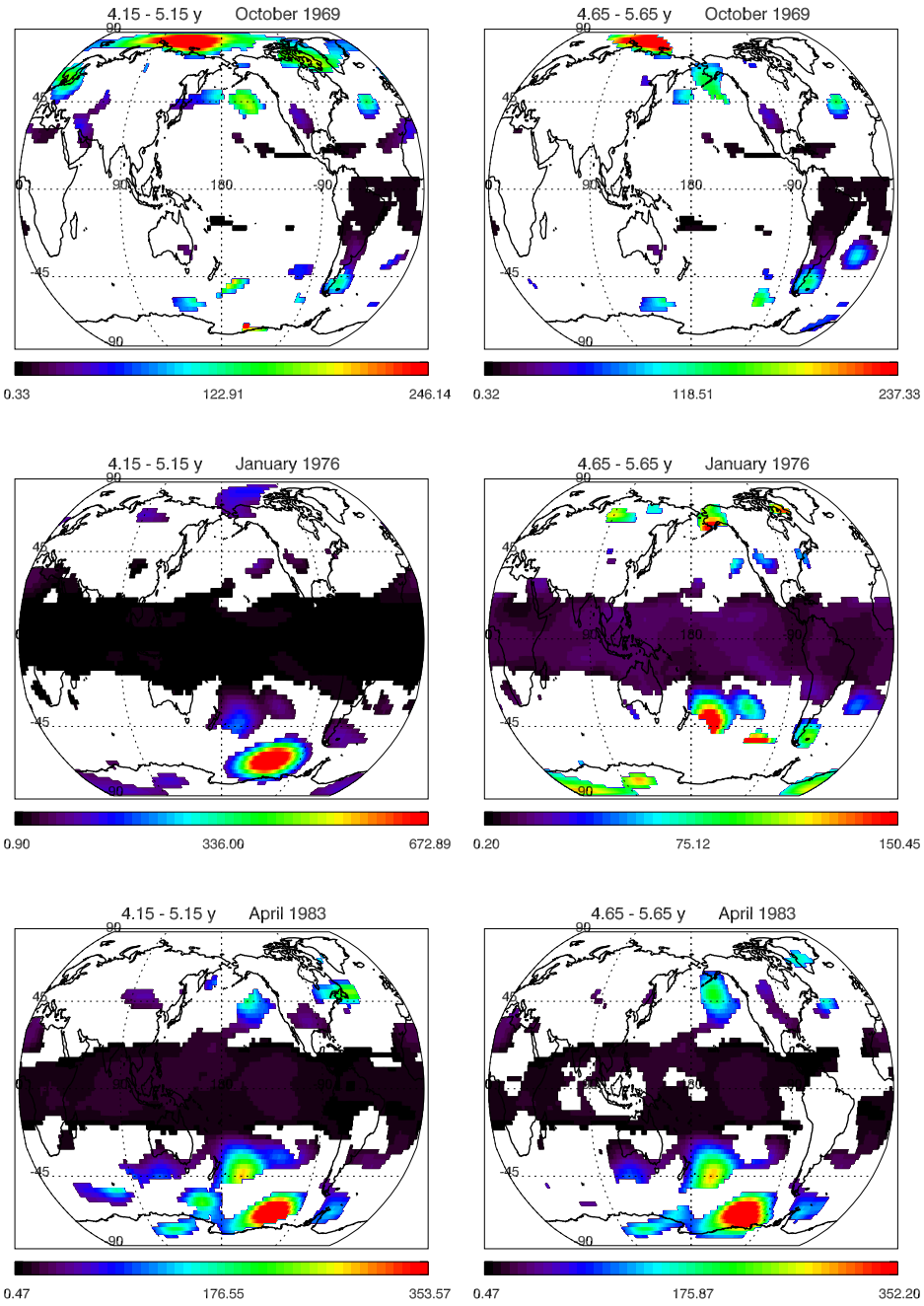

Figure *A*.**27:** Temporal evolution of geographical regions of different oscillations in the geopotential heights field at 500 hPa (the colored scale represents the wavelet power)

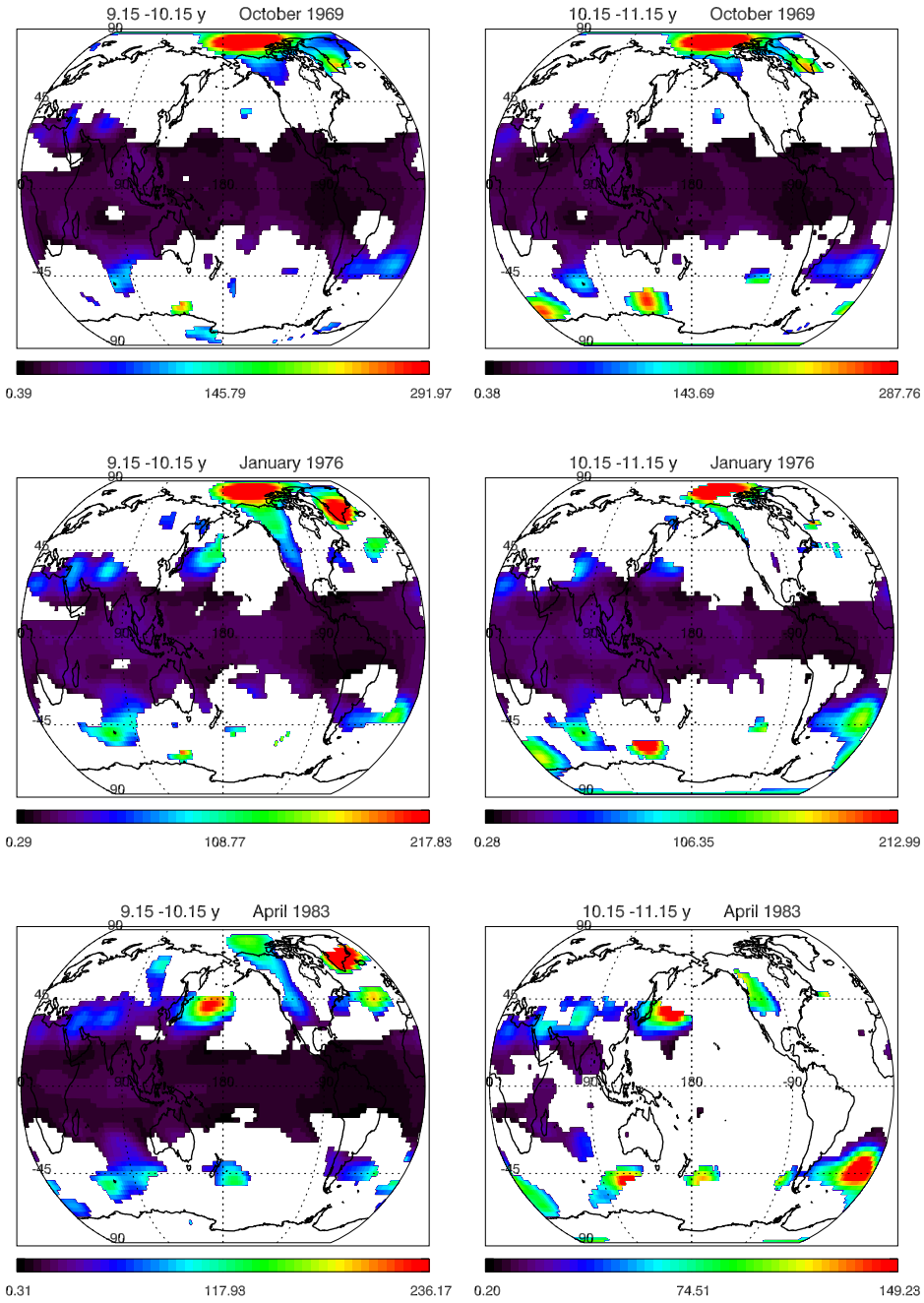

Figure *A*.**28:** Temporal evolution of geographical regions of different oscillations in the geopotential heights field at 500 hPa (the colored scale represents the wavelet power)

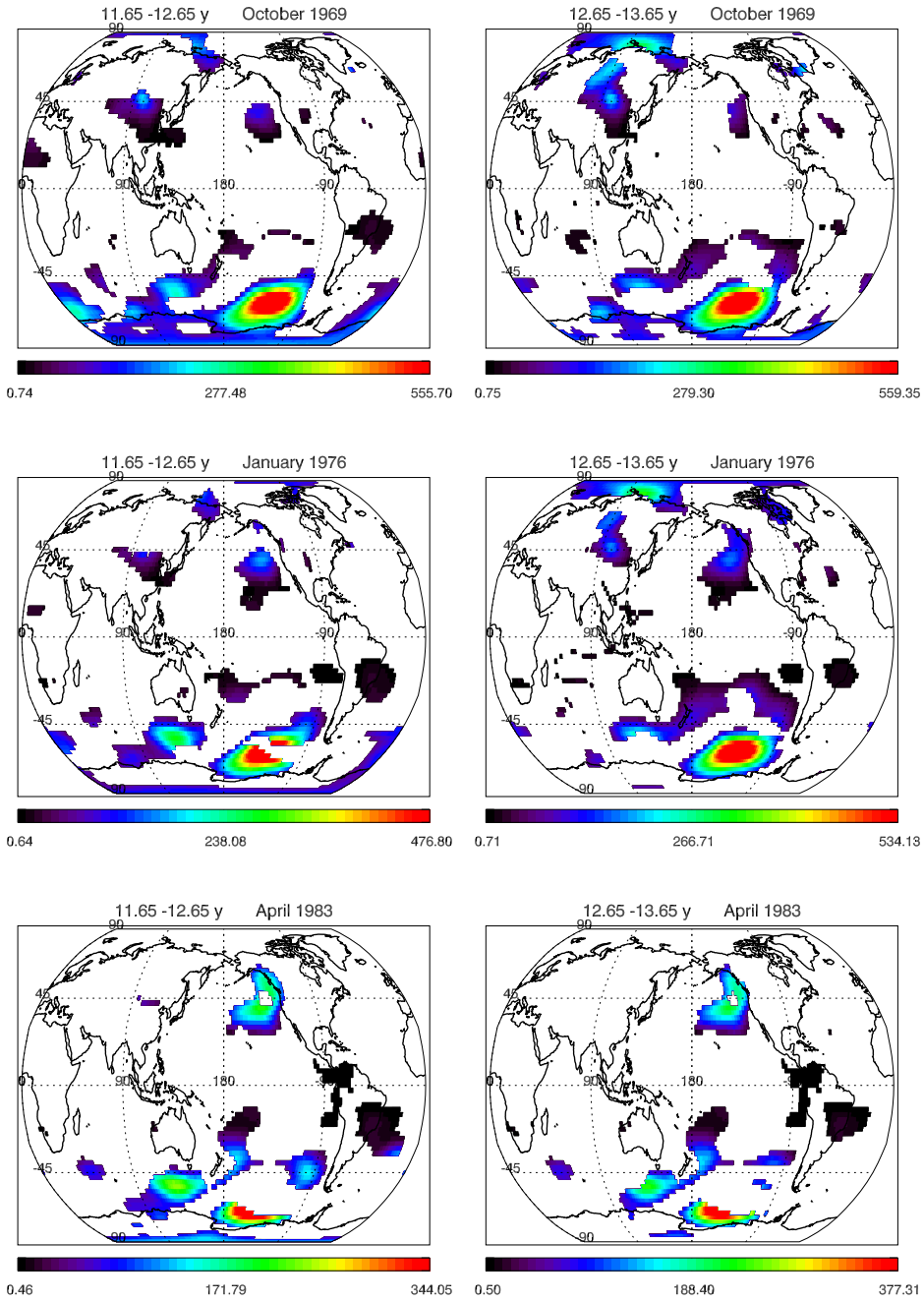

Figure *A*.**29:** Temporal evolution of geographical regions of different oscillations in the geopotential heights field at 500 hPa (the colored scale represents the wavelet power)

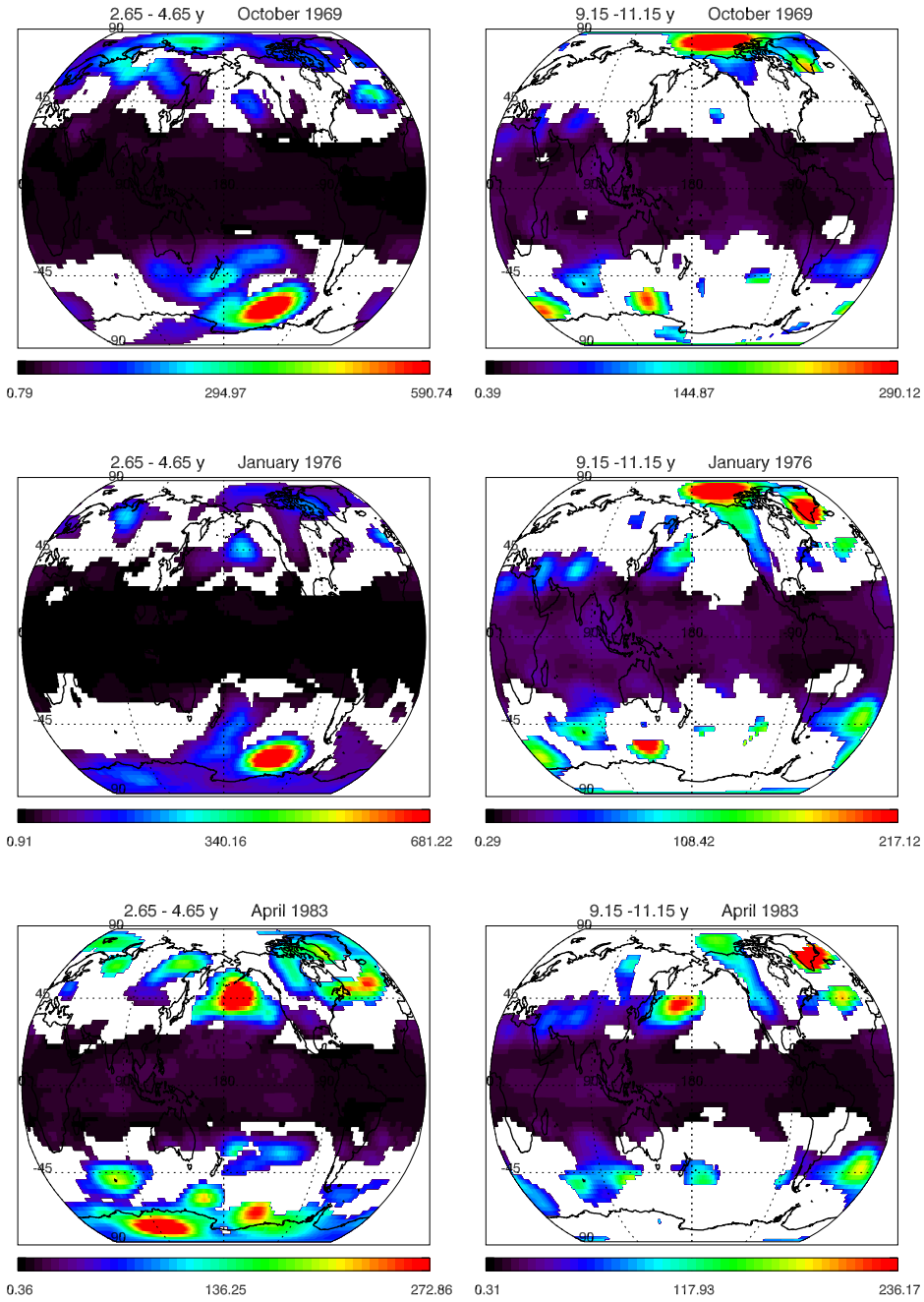

Figure *A*.**30:** Temporal evolution of geographical regions of different oscillations in the geopotential heights field at 500 hPa (the colored scale represents the wavelet power)

Appendix B

The pseudo-2D wavelet transform produced a great number of results only the most striking of which are illustrated in this paper. All the results are, however, included in the attached CD.

The study outcome included in the CD is divided into two main folders and several subfolders. The main folders are named HGT (containing the results of the geopotential heights field analysis) and TMP (containing the results of the temperature field analysis). These folders include folders $contiX$ and $evol$. The first one contains results of the procedure searching for the long-lasting periodicities and the X in the folder name stands for the specific time T in years. The folder $evol$ contains results describing the temporal evolution of the particular period ranges. The individual results in the $contiX$ folders are named as X_conti_K or X_conti2_K. The X has the same meaning as it has in the name of the folder. The K represents in the first case the individual Γ_p ranges and in the second case (X_conti2_K) it denotes the Γ'_p ranges. The results describing the temporal evolution of the particular period ranges are named as day_K_D or $day2\_K\_D$. The K has the same meaning as it has in the previous case. The D is equal to 1, 2 or 3 respectively and represents results describing the periodicities state in October 1969, January 1976 and in April 1983, respectively. The final subfolders also include, besides the results, the folders named www. These contain files needed for displaying the results in a web gallery.

The root folder contains also file $index.html$ which represents a web page guide throughout all results.

Bibliography

Barnston, A. G., Livezey, R. E. (1987): Classification, Seasonality and Persistence of Low-Frequency Atmospheric Circulation Patterns. *Mon. Wea. Rev*, **115**, 1083-1126.

van den Berg, J. C. (1999): Wavelets in Physics. Cambridge University Press, Cambridge, 1999, 454 pp.

Brassington, G.B. (1997): The Modal Evolution of the Southern Oscillation, *Journal of Climate*, 5, **10**, 1021–1034.

van den Broeke, M. R. (1998): The semiannual oscillation and Antarctic climate, part 1: Influence on near-surface temperatures (1957–1979), *Antarctic Science*, **10**, 175–183.

van den Broeke, M. R. (1998): The semiannual oscillation and Antarctic climate, part 2: Recent changes, *Antarctic Science*, **10**, 184–191.

van den Broeke, M. R. (1998): The semiannual oscillation and Antarctic climate, part 4: A note on sea ice cover in the Amundsen and Bellingshausen Seas, *International Journal of Climatology*, **20**, 455–462.

van den Broeke, M. R. (1998): The semiannual oscillation and Antarctic climate, part 5: Impact on the annual temperature cycle as derived from NCEP re-analysis, *Climate Dynamics*, **16**, 369–377.

Buttkus, B. (2000): Spectral analysis and filter theory in applied geophysics, Springer, 2000, 667 pp.

Chen, T. C., Wu, K. D. (1992): Semi-annual oscillation of the global divergent circulation, *Tellus*, **44A**, 357–365.

Chen, T. C., Yen, M. C., van Loon, H. (1996): An Observational Study of the Tropical-Subtropical Semiannual Oscillation, *Journal of Climate*, **9**, 1993–2002.

Chen, W., Takahashi, M., Graf, H. F. (2003): Interannual variations of stationary planetary wave activity in the northern winter troposphere and stratosphere and their relations to NAM and SST, *Journal of Geophysical Research-Atmospheres*, D24, **108**, 4797.

Cullather, R. I., Lynch, A. H. (2003): The annual cycle and interannual variability of atmospheric pressure in the vicinity of the North Pole, *International Journal of Climatology*, 23, **10**, 1161–1183.

Dima, M., Rimbu, N., Stefan, S., Dima, I. (2001): Quasi-Decadal Variability in the Atlantic Basin Involving Tropics-Midlatitudes and Ocean-Atmosphere Interactions, *Journal of Climate*, 5, **14**, 823–832.

Dima, M., Stefan, S., Dima, V., Borsan, D. (2001): Interdecadal Variability Generated by Interaction between Pacific and Atlantic Oceans, *Geophysical Research Letters*, 23, **28**, 4459–4463.

Dima, M., Rimbu, N., Dima, I. (2002): Arctic Oscillation variability generated through inter-ocean interactions, *Geophysical Research Letters*, 14, **29**, 22(1)–22(4).

Dunkerton, T. J., Delisi, D. P. (1985): Climatology of the equatorial lower stratosphere, *Journal of the Atmospheric Sciences*, **42**, 376–396.

Drinkwater, M. R., Venegas S. (2001): Interannual Variations in Antarctic Atmosphere-Ice-Ocean Coupling, *Earth Observation Quarterly*, **69**, 13–17.

Garric, G., Huber, M. (2003): Quasi-decadal variability in paleoclimate records: Sunspot cycles or intrinsic oscillations?, *Paleoceanography*, 3, **18**, 13(1)–13(8).

Heddinghaus, T. R., Kung, E. C. (1980): An Analysis of Climatological Patterns of the Northern Hemispheric Circulation, *Monthly Weather Review*, 1, **108**, 1–17.

Holton, J. R., Lindzen, R. S. (1972): An updated theory for the Quasi-Biennial cycle of the tropical stratosphere, *Journal of the Atmospheric Sciences*, **29**, 1076–1080.

Jiang, N., Neelin, J. D., Ghil, M. (1995): Quasi-quadrennial and quasibiennial variability in the equatorial Pacific, *Climate Dynamics*, **12**, 101–112.

Kalnay et al. (1996): The NCEP/NCAR 40-Years Reanalysis Project, *Bulletin of the American Meteorological Society*, **77**, 437–471.

Kijewski, T., Kareem, A. (2003): Wavelet Transforms for System Identification in Civil Engineering, *Computer Aided Civil and Infrastructure Engineering*, **18**, 339–355.

Kistler et al. (2001): The NCEP-NCAR 50-Year Reanalysis: Monthly Means CD-Rom and Documentation, *Bulletin of the American Meteorological Society*, **82**, 247–267.

Lanzante, J. R. (1985): Some Singularities and Irregularities in the Seasonal Progression of the 700 mb Height Field, *Journal of Applied Meteorology*, 22, **6**, 967–981.

Lanzante, J. R. (1985): Further Studies of Singularities Associated with the Semiannual Cycle of 700 mb Heights, *Monthly Weather Review*, 113, **8**, 1372–1378.

van Loon, H. (1967): The Half-Yearly Oscillations in Middle and High Southern Latitudes and the Coreless Winter, *Journal of the Atmospheric Sciences*, 24, **5**, 472–486.

Mizoguchi, K., Meyers, S. D., Basu, S. K., O'Brien, J. J. (1999): Multi- and Quasi-Decadal Variations of Sea Surface Temperature in the North Atlantic, *Journal of Physical Oceanography*, **29**, 3133–3144.

Moron, V., Vautard, R., Ghil, M. (1998): Trends, interdecadal and interannual oscillations in global sea-surface temperatures, *Climate Dynamics*, **14**, 545–569.

Metelka, L. (1997): Analýza Sekulárních Řad Klimatologických Charakteristik. PhD thesis, Charles University, 1997, 64 pp.

Percival, D. B. (2002): Wavelets, *Encyclopedia of Environmetrics*, **4**, 2338–2351.

Percival, D. B., Walden, A. T. (2000): Wavelet Methods for Time Series Analysis. Cambridge University Press, Cambridge, 2000, 595 pp.

Pišoft, P. (2002): Wavelet Analysis of Meteorological Time Series. Diploma thesis, Charles University, 2002, 84 pp.

Polikar, R. (1994): Wavelet Tutorial
http://engineering.rowan.edu/~polikar/WAVELETS/WTtutorial.html

Rasmusson, E. M., Wang, X., Ropelewski, C.F. (1990): The biennial component of ENSO variability, *Journal of Marine System*, **1**, 71–96.

Reed, R. G., Campbell, W. J.,Rasmussen, L. A., Rogers, D. G. (1961): Evidence of downward-propagating annual wind reversal in the equatorial stratosphere, *Geophysical Research Letters*, **66**, 813–818.

Reuter, E., Borgheim, E. (1936): Die synoptische Darstellung der 1/2 jahrigen Druckwelle, *Veroff. Geophys.Inst. Univ. Leipzig*, **7**, 257–295.

Ribera, P., Mann, M.E. (2002): Interannual variability in the NCEP Reanalysis 1948-1999, *Geophysical Research Letters*, 10, **29**, 132(1)–132(4).

Ribera, P., Mann, M. E. (2003): ENSO related variability in the Southern Hemisphere, 1948-2000, *Geophysical Research Letters*, 1, **30**, 6(1)–6(4).

Scaife, A. A., Butchart, N., Warner, C. D., Stainforth , D., Norton, W. A., Austin, J. (2000): Realistic Quasi-Biennial Oscillations in a simulation of the global climate, *Geophysical Research Letters*, **27**, 3481–3484.

Schwerdtfeger, W., Prohaska, F. (1956): The Semi-Annual Pressure Oscillation, Its Cause and Effects, *Journal of Meteorology*, 13, **2**, 217–218.

von Storch, H., Zwiers, F. W. (1999): Statistical Analysis in Climate Research. Cambridge University Press, Cambridge, 1999, 484 pp.

Tennant, W. (2004): Considerations when using pre-1979 NCEP/NCAR reanalyses in the southern hemisphere, *Geophysical Research Letters*, 11, **31**, L11112.

Terray, L., Cassou, C. (2002): Tropical Atlantic sea surface temperature forcing of quasi-decadal variability over the North Atlantic European region, *Journal of Climate*, **22**, 3170–3187.

Torrence, C., Compo, G. P. (1998): A Practical Guide to Wavelet Analysis, *Bulletin of the American Meteorological Society*, **79**, 61–78.

Walland, D., Simmonds, I. (1999): Baroclinicity, Meridional Temperature Gradients, and the Southern Semiannual Oscillation, *Journal of Climate*, 12, **12**, 3376–3382.

White, G. H., Wallace, J. M. (1978): The Global Distribution of the Annual and Semiannual Cycles in Surface Temperature, *JMonthly Weather Review*, 6, **106**, 901–906.

Wikle, C. K., Chen, T. (1996): On the Semiannual Variation in the Northern Hemisphere Extratropical Height Field, *Journal of Climate*, 9, **9**, 2250–2258.

Yuan, A.L (1999): The Quasi-quadrennial Oscillation and the Causes of Inter-El Niño Variability, proceed. of Workshop on the Impacts of the 1997/99 ENSO, 5–7 October 1999, Central Weather Bureau, Taipei, Taiwan.

Zhang, X, Sheng, J.,Shabbar, A. (1998): Modes of interannual and interdecadal variability of Pacific SST, *Journal of Climate*, **11**, 2556–2569.